Structure and Properties of the Electrospun PLLA/PDLA Blend Nanofibers

Masaki Yamamoto

Kyoto Institute of Technology

2015

TABLE OF CONTENTS

Structure and Properties of the Electrospun PLLA/PDLA Blend Nanofibers

GENERAL INTRODUCTION

CHAPTER 1 Effect of the Solution-electrospinning Conditions on the Higher-order Structure and the Stereocomplex Formation of the PLLA/PDLA Blend Nanofibers

CHAPTER 2 Structure of Melt-Electrospun PLLA/PDLA Blend Fibers

CHAPTER 3 Effect of the Take-up Velocity on the Higher-order Structure of the Melt-electrospun PLLA/PDLA Blend Fibers

General Introduction

1. Bio-based polymers

Polymeric materials synthesized from petroleum-based resources have been used in the daily life and industrials. Recently, there is an increased interest in the bio-based polymers based on the renewable resource. However, these bio-based polymers have not been widely spread yet as general-purpose plastics because of the problems such as the insufficient physical property, molding productivity, and the production cost. Therefore, bio-based polymers still hold a small fraction of the total global plastic market. Currently, biopolymers share less than 1% of the total plastics market.[1]

The first-generation technologies on the bio-based polymers mainly focused on the materials synthesized from food resources such as corn, rice, and other carbohydrate feedstocks. The major bio-based plastic feedstocks are still sugar-based, derived primarily from plants such as corn or sugar cane at present. Recently, the focus is shifting to the second and the third generations which give less impact to the food resources than utilization of corn and other first generation feedstocks.[2-4] The bio-based technology focuses on the realization of a sustainable society by utilizing renewable feedstocks hopefully non-food resources such as waste biomass and cellulose.

The current bio-based industry started making bio-versions of existing monomers and polymers.[5] Performance of these existing products has been well known, and it is relatively easy to replace the existing product with similar performance of bio-versions. Many developments are currently underway to develop various polyamides, polyesters, and other polymeric materials for automotive, electronics, and biomedical applications.

Bio-based polymer can be roughly divided into three types as follows: 1. Naturally occurring polymers including polysaccharides such as starch, cellulose, and alginates and proteins, 2. Bacterial polymers such as polyhydroxyalkanoates and bacterial cellulose, and 3. Polymers synthesized from bio-based monomers. One of the typical synthetic polymers is poly(lactic acid) (PLA). PLA is synthesized by chemical polymerization of lactic acid obtained by lactate fermentation after saccharization by fermentation hydrolysis of starch in the plants such as corn and potatoes.

2. Poly(lactic acid)

Poly(lactic acid) (PLA), one of the typical bio-based materials has been applied in the

medical and agricultural fields. In addition, PLA has been expected as an alternative to some petroleum-based plastics because of its fairly high melting point among various aliphatic polyesters and a good mechanical property. Although PLA has been known since 1845, it has not been commercialized until early 1990. The monomer, lactic acid (2-hydroxy propionic acid) $HOCHCH_3COOH$, was first discovered from sour milk in 1780s.[6] Lactic acid is naturally occurring organic acid that can be produced not only by the fermentation process and also by the chemical synthesis.[7]

Fig. 1 shows various synthesis routes of PLA.[8-13] Currently, ring-opening polymerization patented by Cargill Inc. in 1992[8] seems to be the typical method for obtaining high molecular weight PLA. Although direct polycondensation which does not pass through lactide is the least expensive route, it is very difficult to obtain a solvent-free high molecular weight PLA. Therefore, chain coupling agents and adjuvants are required and thereby the cost is high and the polymerization process is also complicative.[10-13]

Since two different stereoisomers of lactic acid exist, variety of the molecular structures of PLA can be prepared.[11, 14-17] These include the homo poly(L-lactic acid) (PLLA), homo poly(D-lactic acid) (PDLA) and the copolymers of L- and D-lactic acids with various L/D ratios (PDLLA). Fig. 2 shows the chemical structures of PLLA and PDLA. Although PLLA and PDLA are crystalline polymers, PDLLAs whose L/D ratio is in between 0.25 and 0.75 are amorphous polymers. Lactic acid has one methine carbon between ester bonds and thereby molecular mobility is rather poor. This low mobility of the PLA chains makes the crystallization rate significantly low[18], although the crystallization promotes in the case of fibers and films which form the quadratic kernel by orientational crystallization upon drawing. Therefore, the production rate of the injection molded parts has been limited in order to obtain PLA products with a sufficient thermal resistance comparable with that of the general-purpose plastics.

The mechanical and thermal properties of the PLA strongly depend on the morphology and crystal structure.[19-23] The main crystalline form of PLLA and PDLA is a homo-chiral crystal (HC), One of the crstyalline structure of HC is a pseudo-orthorhombic of 10_3 helix, and cell dimensions are a = 1.07 nm, b = 0.595 nm, and c = 2.78 nm, $\alpha = \beta = \gamma = 90^o$ reported by De Santis et al.[24] and is called α-form. The melting point of α-form crystal is around 180°C. Recently, Zhang et al.[25] reported that α-form of HC transforms to α'-form upon annealing at a temperature lower than 110°C. α'-form is an orthorhombic of 10_3 helix with some distortion. Pan et al.[26] reported the cell dimension of α'-form, a = 1.072 nm and b = 0.594 nm,

respectively, while that of α-form, a = 1.058 nm and b = 0.595 nm, respectively and c of these forms are almost the same. Thus, the unit cell of α-form is a slightly smaller than that of α'-form due to the more ordered and denser packing of polymer chains in α-crystal. The melting point of α'-form crystal is 5°C higher than that of α-form when it is crystallized at a temperature lower than 150°C.[27] However, when α-form is crystallized at a temperature higher than 150°C, the melting temperatures of α'-form crystals is almost the same as that of α-form. Interestingly, the small exothermal peak is observed around the melting peak when PLLA crystallized below 120°C. Zhang et al.[27] reported that peak corresponds to the disorder-to-order (α'-to-α) phase transition, in which the chain packing of the crystal lattice becomes more compacted.

In addition to α and α'-forms, PLA can crystallizes into β-form. The first study of the β-form was done by Eling et al.[22] who reported that β-formation occurs in some drawing condition.[28-30] In general, when the amorphous PLLA is drawn above the glass transition temperature and succeedingly annealed around the crystallization temperature, α-crystal or α'-crystal is formed. However, when a semicrystalline PLLA is drawn to a high draw ratio near the melting temperature, α-crystal and α'-crystal are transformed to the β-form crystal. Hoogsteen et al. reported that β-crystal is orthorhombic (containing 6 chains) of 3_1 helix, and cell dimensions are a = 1.03 nm, b = 1.82 nm, and c = 0.90 nm, α = β = γ = 90°.[29] The melting point of β-form crystal is around 170°C and it is 10°C lower than that of α-form crystal.

Recently, Cartier et al.[31] reported that a specific PLLA crystal can be obtained by the epitaxial growth on the hexamethylbenzene substrate called γ-form crystal. Two chains are antiparallel in the crystal unit cell of the γ-form. γ-crystal is orthorhombic of 3_2 helix, and cell dimensions are a = 0.995 nm, b = 0.625 nm, and c = 0.88 nm, α = β = γ = 90°.[31]

Table 1 shows these crystal structures of PLLA. As mentioned above, PLLA can crystallize into various forms and the crystalline form reflects the mechanical and thermal properties. In any cases, PLLA and PDLA show the melting temperatures around 180°C and it decreases with the fraction of the enantiomeric monomer in PLLA and PDLA.

3. Poly(lactic acid) Stereocomplex

As is described above, PLA can crystallize in various forms and the thermal property changes depending on the crystalline forms. The melting points to these crystalline forms are fairly high among various aliphatic polyesters. However the thermal resistance of the PLA

with various crystalline forms is not always sufficient for some applications such as textile fibers. The fundamental solution to this rather poor thermal resistance may be a utilization of the stereocomplex which forms in the equal blend of poly(L-lactic acid) (PLLA) and poly(D-lactic acid) (PDLA), an enantiomer of PLLA.

Fig. 3 shows the crystal structures of PLLA homo-chiral and PLLA/PDLA stereocomplex. In the stereocomplex crystal, a pair of different polymer chains constructs a special crystalline structure in which each component polymer chain has a conformation different from that in the homo-crystal. One of the well-known example of the stereocomplex is that forms in the mixture of isotactic and syndiotactic PMMAs first reported by Fox et al. in 1950s.[32] The first study of stereocomplex PLA was reported by Ikada et al. in 1980s.[33] Since the lactic acid has an asymmetric carbon, there exist two enantiomers, L- and D-lactic acids. These L- and D-lactic acids are polymerized into poly(L-lactic acid) (PLLA) and poly(D-lacti caicd) (PDLA), respectively. When these PLAs are mixed, stereocomplex crystal (SC) forms due to their mutual strong interaction. It has been known that the melting point of SC is 230°C about 50°C higher than that of PLLA and PDLA homo-chiral crystal (HC).

The SC has a different crystal structure from that of HC. The SC is triclinic (*P*1) with cell dimensions: a = 0.916 nm, b = 0.916 nm, c (chain axis) = 0.870 nm, α = 109.2º, β = 109.2º, γ = 109.8º reported by Okihara et al.[34] PLLA and PDLA segments are contained as a pair and packed laterally in parallel fashion taking a 3_1 helical conformation in the unit cell. So the PLLA and PDLA are slightly more extended than those of 10_3 helix in the HC.

The SC forms most effectively in an equal blend of PLLA and PDLA, and the formation of SC decreases when the ratio of PLLA/PDLA is close to 100/0 or 0/100.[33] Several reports[35-38] have indicated that both SC and HC of each component co-exist in the PLLA/PDLA blends prepared by the simple mixing. Takasaki et al.[37] reported on the development of SC in the PLLA/PDLA blend fibers obtained by the high-speed melt spinning process. They showed that the PLLA/PDLA blend fibers taken-up at high velocities are highly oriented and highly crystallized containing both α-form of HC and SC. However the fiber contains mainly SC after drawing and subsequent annealing at 190°C. Furuhashi et al.[39] also reported the relations among the processing conditions, crystalline structures, thermal properties, and mechanical properties of PLLA/PDLA melt-spun fibers. Masaki et al.[40] took a special blending technique and prepared the PLLA/PDLA blend in which only SC forms. They reported that the melt-spun fibers drawn and annealed at an optimum condition have SC as a unique crystalline component and show an excellent thermal stability. They also

demonstrated the much higher crystallization rate of the stereocomplex than that of HC.[40]

The stereocomplexation phenomenon can be utilized in order to obtain PLA products with an excellent thermal resistance. For example, it has been reported that the fabrics made of the stereocomplex fiber stands for ironing even at 200°C.[41]

4. Electrospinning

4.1 Solution-electrospinning

Fig. 4 shows the general schematic diagram of the electrospinning set-up. Electrospinning is a facile method of producing fibers of nano-order diameters from polymer solution. Electrospinning system consists of an extrusion device, a high voltage generator, and a metal target. A high voltage is applied between the polymeric liquids and the metal target. When electrostatic force exceeds the surface tension of the polymeric liquid, the liquid jets are drawn from the spinneret and carried to the metal target. The solvent in the solution jet vaporizes from the spinline and the fine fibers accumulated on the target.

A sharp conical shape of charged solution called “Taylor cone” is formed at the exit of the metal spinneret. Taylor reported the first study of the fundamental jet forming process of the electrospinning in 1960s.[42] He also determined that an angle of 49.3^{o} is required to balance the surface tension of the polymer solution and the charged electrostatic force.[43] Several authors[44-47] have reported the configuration of Taylor cone and behavior of the solution jet. These reports have indicated the relation between the morphology of the fiber and the configuration of Taylor cone. The configuration of Taylor cone was determined by various factors in the electrospinning process such as the surface tension of the droplet, the solution concentration, the applied voltage, the nozzle-target distance, and so on. Fig. 5 shows the principle diagram of the relation between Taylor cone and the surface tension of the polymer solution.

In 1930s, the first patent of electrospinning as a viable fiber spinning technique was filed by Formhals et al.[48] He patented his invention relating to the electrospinning process and the apparatus for producing artificial filaments. He also patented to refine some problems in completely drying the fibers after spinning.[49]

Many applications of electrospun nanofibers are expected in various fields. Nanofibers are obtained with this simple method although productivity is low. Electrospun nanofiber shows unique properties such as large surface area to volume ratio, highly porous structure, high transparency due to the fiber diameter thinner than wavelength of light around 400 nm,

and so on. These effects are applicable to the products as a filter with a high adsorptive property, a cell culture membrane, an electrolyte membrane of fuel battery, and a transparency organic EL film.

The morphology of the fiber, fiber diameter, and the amount of the nanofiber obtained by the electrospinning process are determined by various solution properties and the electrospinning conditions such as polymer molecular weight, concentration of the solution, viscosity of the solution, vapor pressure of the solvent, applied voltage, distance between the nozzle and the target, and so on. The viscosity of the solution depends on the polymer molecular weight, the solubility of the polymer to the solvent and the concentration of the solution. In the case of low molecular weight or low concentration of the solution, the viscosity is low and thereby the fiber diameter decreases and the beads formation tends to occur. On the other hand, the viscosity is high in the case of high molecular weight or high concentration of the solution and thereby the fiber diameter increases and the beads do not form. In order to obtain thinner fibers without forming beads, it is important to investigate the suitable viscosity by choosing the polymer molecular weight, the solvent and the concentration of the solution.

The higher the applied voltage, the stronger the electrostatic force. The distance between the nozzle and the target also affect the electric field. The shorter the nozzle-target distance, the stronger the electric field. However, the nozzle-target distance is too short, the solvent does not vaporize sufficiently and the fiber diameter becomes non-uniform. The solvent should not be too volatile. The highly volatile solvents evaporate immediately after extrusion of the solution from the spinneret and the solidification of the polymer at the tip of the nozzle occurs.

As mentioned above, various factors influence the electrospinning conditions and the morphology of the nano-fibers. In order to obtain the good nano-fibers effectively, it is necessary to examine these factors and to investigate the best electrospinning condition carefully.

4.2 Melt-electrospinning

Most of the studies on the electrospinning have been relating to the solution type and only a few studies on the melt-type electrospinning have been made so far. In 1980s, the first study of electrospinning from molten polymer was reported by Larrondo and Manley.[50-52] They obtained the polyethylene and polypropylene melt-electrospun fibers with diameters

larger than 50 μm with the melt-electrospinning process. Lyons et al.[53] obtained the melt-electrospun polypropylene fibers by grounding the metallic nozzle of the screw extruder and applying a positive charge to the metal target. They investigated the relation between melt-electrospinning condition and the fiber diameter. They obtained the melt-electrospun thin fibers by decreasing molecular weight, increasing the electric field strength, and decreasing the amount of the polymer supply to form a small Taylor cone.

Recently, laser electrospinning method has been proposed. This is a novel method to rapidly and uniformly heat polymers by irradiating CO_2 laser beam. Ogata et al.[54-56] succeeded to melt-electrospun poly(ethylene-co-vinyl alcohol) copolymer, PLLA, and PET into fibers with diameters less than 1μm by using a laser heating method.

The melt-electrospinning apparatus is complicated as compared with that of the solution electrospinning. The comparatively high applied voltage and short nozzle-target distance are required for the melt-electrospinning process due to the high melt viscosity. Therefore, the dielectric breakdown often occurs. In addition, the thermal degradation of the polymers may occur. When the laser output is high and the extrusion rate is low, polymer is irradiated with a high thermal laser and the thermal degradation occurs. Takasaki et al.[57] investigated the change in molecular weight of the fiber in the laser melt-electrospinning process combined with air blowing. They reported that the thermal degradation the melt-electrospun fiber was suppressed with increasing air flow rate because the fiber temperature was decreased by the cooling effect of air blowing.

Serious disadvantage of the melt-electrospinning process is inability to make the fiber with a nano-order scale diameter as compared with the solution type electrospinning of the. Several authors[57-59] have been trying to make the sub-micron order melt-electrospun fiber by using techniques such as the blowing of the heated air, utilization of the heat gun and heat chamber. Therefore, melt-electrospun fiber is not extended sufficiently, since the molten polymer jet from the extrudate is immediately quenched to the room temperature. Most of studies regarding the melt electrospinning have not successed to obtain the thin fiber less than 1 μm yet.

On the other hand, the melt-electrospinning method is expected in the future as this process can be carried out solvent free and its solvent free process is considered to be environmentally friendly. In addition, it is possible to make thin fiber of the polymer which does not dissolve in any solvents. Therefore, the melt-electrospinning process may be suitable for the wide variety of industrial applications.

5. Purpose of study

It is possible to make electrospun stereocomplex PLA fibers either from PLLA/PDLA blend solution or melt.[60] Various trials have been made to produce thermally resistant PLA fibers obtained by the melt-spinning and the solution-spinning methods.[35-38, 61] Recently, the studies on the production of PLLA/PDLA blend electrospun nanofibers have been reported.[62-64]

It is the purpose of this study to investigate the effect of the spinning condition on the morphology, the higher-order structure and the stereocomplex formation of the electrospun PLLA/PDLA blend fibers. The electrospinning was carried out by two methods, the solution and melt electrospinning processes. The electrospun fibers were collected on both a fixed target and a rotating target in this study. The effect of the taking-up by the rotating target was also examined.

References

1. S. Doug, *Bioplastics: technologies and global markets*, BCC research reports PLS050A.
2. R. Hatti-Kaul, U. Törnvall, L. Gustafsson and P. Börjesson, *Trends in Biotechnology*, **25**, 119 (2007).
3. K. Lewis, R. Narayan, E. Simon, *The Society of the Plastics Industry, Bioplastics Council*, August (2013).
4. R. Mülhaupt, *Macromolecular Chemistry and Physics*, **214**, 159 (2013).
5. R. P. Babu. K. O'Connor, and R. Seeram, *Progress in Biomaterials*, **2**,8 (2013).
6. C. W. Scheele, *Allgemeine Literatur-Zeitung*, **1**, 627 (1788).
7. R. Datta, S. -P. Tsai, P. Bonsignore, S. -H. Moon, J. R. Frank, *FEMS Microbiology Reviews*, **16**, 221 (1995).
8. Cargill Inc., *US Patent*, 5142023 (1992).
9. Mitsui Toatsu Chemicals Inc., *EP Patent*, 572675A1 (1993).
10. R. Dunsing and H. R. Kricheldorf, *Polymer Bulletin*, **14**, 491 (1985).
11. J. W. Leenslag, A. J. Pennings, *Die Makromolekulare Chemie*, **188**, 1809 (1987).
12. S. -H. Hyon, K. Jamshidi, and Y. Ikada, *Biomaterials*, **18**, 1503 (1997).
13. R. Auras, B. Harte, S. Selke, *Macromolecular Bioscience*, **4**, 835 (2004).
14. T. M. Ovitt and G. W. Coates, *Journal of the American Chemical Society*, **121**, 4072 (1999).
15. A. G. Andreopoulos, E. Hatzi, M. Doxastakis, *JOURNAL OF MATERIALS SCIENCE: MATERIALS IN MEDICINE*, **10**, 29 (1999).
16. T. M. Ovitt and G. W. Coates, *Journal of the American Chemical Society*, **124**, 1316 (2002).
17. S. Inkinen, M. Hakkarainen, A. -C. Albertsson, A. Södergãrd, *Biomacromolecules*, **12**, 523 (2011).
18. S. C. Schmidt, M. A. Hillmyer, *Journal of Macromolecular Science: Part B: Polymer Physics*, **39**, 300 (2001).
19. G. Perego, G. D. Cella, and C. Bastioli, *Journal of Applied Polymer Science*, **59**, 37 (1996).
20. L. Fambri, A. Pegoretti, R. Fenner, S. D. Incardona, and C. Migliaresi, *Polymer*, **38**, 79 (1997).
21. H. Okuzaki, I. Kubota, T. Kunugi, *Journal of Macromolecular Science: Part B: Polymer Physics*, **37**, 991 (1999).

22. R. G. Alamo, M. -H. Kim, M. J. Galante, J. R. Isasi, L. Mandelkern, *Macromolecules*, **32**, 4050 (1999).
23. C. D. Rosa, M. C. Gargiulo, F. Auriemma, O. R. de Ballesteros, A. Razavi, *Macromolecules*, **35**, 9083 (2002).
24. P. De Santis, A. J. Kovacs, *Biopolymer*, 6, 199 (1968).
25. J. Zhang, Y. Duan, H. Sato, H. Tsuji, I. Noda, S. Yan, Y. Ozaki, *Macromolecules*, **38**, 8012 (2005).
26. P. Pan, B. Zhu, W. Kai, T. Dong, Y. Inoue, *Journal of Applied Polymer Science*, **107**, 54 (2008).
27. J. Zhang, K. Tashiro, H. Tsuji, and A. J. Domb, *Macromolecules*, **41**, 1352 (2008).
28. B. Eling, S. Gogolewski, A. J. Pennings, *Polymer*, **23**, 1587 (1982).
29. W. Hoogsteen, A. R. Postema, A. J. Pennings, G. ten Brinke, P. Zugenmaier, *Macromolecules*, **23**, 634 (1990).
30. D. Sawai, K. Takahashi, T. Imamura, K. Nakamura, T. Kanamoto, S. -H. Hyon, *Journal of Macromolecular Science: Part B: Polymer Physics*, **40**, 95 (2002).
31. L. Cartier, T. Okihara, Y. Ikada, H. Tsuji, J. Puiggali, B. Lotz, *Polymer*, **41**, 8909 (2000).
32. T. G. Fox, B. S. Garrett, W. E. Goode, S. Gratch, J. F. Kincaid, A. Spell, J. D. Stroupe, *Journal of the American Chemical Society*, **80**, 1768 (1958).
33. Y. Ikada, K. Jamshidi, H. Tsuji, S. -H. Hyon, *Macromolecules*, **20**, 904 (1987).
34. T. Okihara, M. Tsuji, A. Kawaguchi, K. Katayama, *Journal of Macromolecular Science: Physics*, **B30(1&2)**, 119 (1991).
35. H. Tsuji, S. -H. Hyon, Y. Ikada, *Macromolecules*, **24**, 5651 (1991).
36. H. Tsuji, Y. Ikada, *Macromolecules*, **26**, 6918 (1993).
37. M. Takasaki, H. Ito, T. Kikutani, *Journal of Macromolecular Science, Part B Physics*., **42**, 403 (2003).
38. J. Zhang, K. Tashiro, H. Tsuji, A. J. Domb, *Macromolecules*, **40**, 1049 (2007).
39. Y. Furuhashi, Y Kimura, N. Yoshie, H. Yamane, *Polymer*, **47**, 5965 (2006).
40. D. Masaki, Y. Fukui, K. Toyohara, M. Ikegame, B. Nagasaka, and H. Yamane, *Sen'i Gakkaishi*, **64**(8), 212 (2008).
41. M. Ikegame, H. Kurihara, K. Toyohara, *WO Patent*, 2008120807 A1 (2008).
42. G. Taylor, *Proceedings of the Royal Society of London, Series A*, **280**, 383 (1964).
43. G. Taylor, *Proceedings of the Royal Society of London, Series A*, **313**, 453 (1969).
44. J. Doshi, D. H. Reneker, *Industry Applications Society Annual Meeting*, **3**, 1698 (1993).

45. J. M. Deitzel, J. Kleinmeyer, D. Harris, and N. C. Beck Tan, *Polymer*, **42**, 261 (2001).
46. Y. M. Shin, M. M. Hohman, M. P. Brenner, and G. C. Rutledge, *Polymer*, **42**, 9955 (2001).
47. A. L. Yarin, S. Koombhongse, and D. H. Reneker, *Journal of Applied Physics*, **90**, 4836 (2001).
48. A. Formhals, *US Patent*, 1975504 (1934).
49. A. Formhals, *US Patent*, 2160962 (1939).
50. L. Larrondo and R. St. John Manley, *Journal of Polymer Science, Part B Polymer Physics*, **19**, 909, (1981).
51. L. Larrondo and R. St. John Manley, *Journal of Polymer Science, Part B Polymer Physics*, **19**, 921, (1981).
52. L. Larrondo and R. St. John Manley, *Journal of Polymer Science, Part B Polymer Physics*, **19**, 933, (1981).
53. J. Lyons, C. Li, and F. Ko, *Polymer*, **45**, 7597 (2004).
54. N. Ogata, G. Lu, T. Iwata, S. Yamaguchi, K. Nakane, and T. Ogihara, *Journal of Applied Polymer Science*, **104**, 1368 (2007).
55. N. Ogata, S. Yamaguchi, N. Shimada, G. Lu, T. Iwata, K. Nakane, and T. Ogihara, *Journal of Applied Polymer Science*, **104**, 1640 (2007).
56. N. Ogata, N. Shimada, S. Yamaguchi, K. Nakane, and T. Ogihara, *Journal of Applied Polymer Science*, **105**, 1127 (2007).
57. M. Takasaki, K. Hara, Y. Ohkoshi, T. Fujii, H. Shimizu, M. Saito, *Polymer Engineering and Science*, pen.23811 (2013).
58. P. D. Dalton, D. Grafahrend, K. Klinkhammer, D. Klee, M. Möller, *Polymer*, **48**, 6823 (2007).
59. E. Zhmayev, D. Cho, Y. L. Joo, *Polymer*, **51**, 4140 (2010).
60. Japan Patent Kokai 2008-115503 (2008).
61. H. Tsuji, Y. Ikada, S. -H. Hyon, Y. Kimura, T. Kitao, *Journal of Applied Polymer Science*, **51**, 337 (1994).
62. H. Tsuji, M. Nakano, M. Hashimoto, K. Takashima, S. Katsura, A. Mizuno, *Biomacromolecules*, **7**, 3316 (2006).
63. D. Ishii, T. H. Ying, A. Mahara, S. Murakami, T. Yamaoka, W. -K. Lee, T. Iwata, *Biomacromolecules*, **10**, 237 (2009).
64. O. Monticelli, M. Putti, L. Gardella, D. Cavallo, A. Basso, M. Prato, S. Nitti, *Macromolecules*, **47**, 4718 (2014).

Table 1 Crystal structures of PLLA.

Crystalline form	Unit cell	Cell dimensions	Helical conformation
α	Pseudo-orthorhombic	a = 1.07, b = 0.595, c = 2.78 nm $\alpha = \beta = \gamma = 90^o$ (De Santis et al.)	10_3 helix
α	Pseudo-orthorhombic	a = 1.058, b = 0.595, c = 2.89 nm $\alpha = \beta = \gamma = 90^o$ (Pan et al.)	10_3 helix
α'	Pseudo-orthorhombic	a = 1.072, b = 0.594, c = 2.89 nm $\alpha = \beta = \gamma = 90^o$	10_3 helix
β	Orthorhombic (containing 6 chains)	a = 1.03, b = 1.82, c = 0.90 nm $\alpha = \beta = \gamma = 90^o$	3_1 helix
γ	Orthorhombic	a = 0.995, b = 0.625, c = 0.88 nm $\alpha = \beta = \gamma = 90^o$	3_2 helix

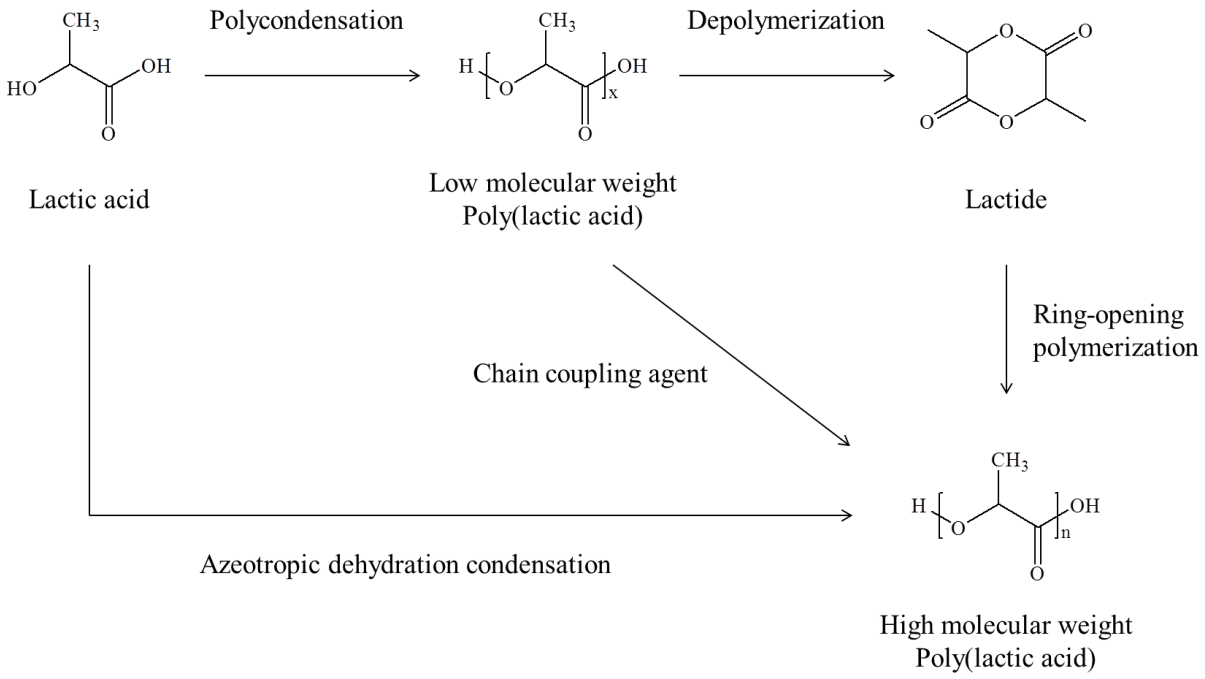

Fig. 1 Synthesis method of PLA.

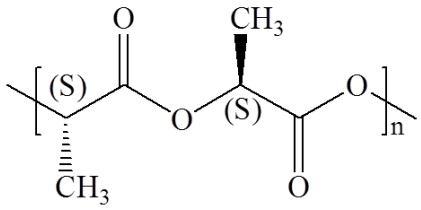

Poly(L-lactic acid)

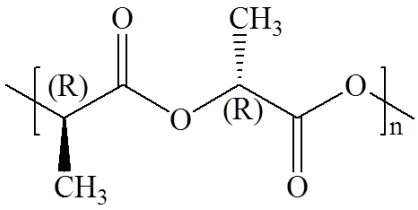

Poly(D-lactic acid)

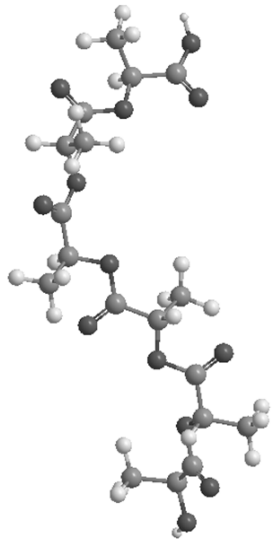

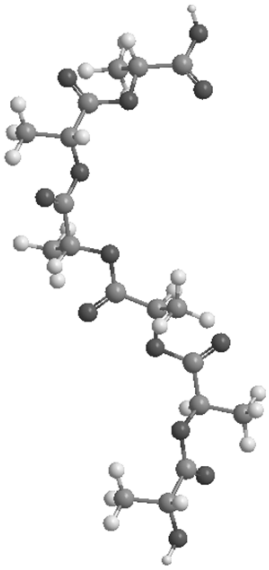

Fig. 2 Chemical structures of PLLA and PDLA.

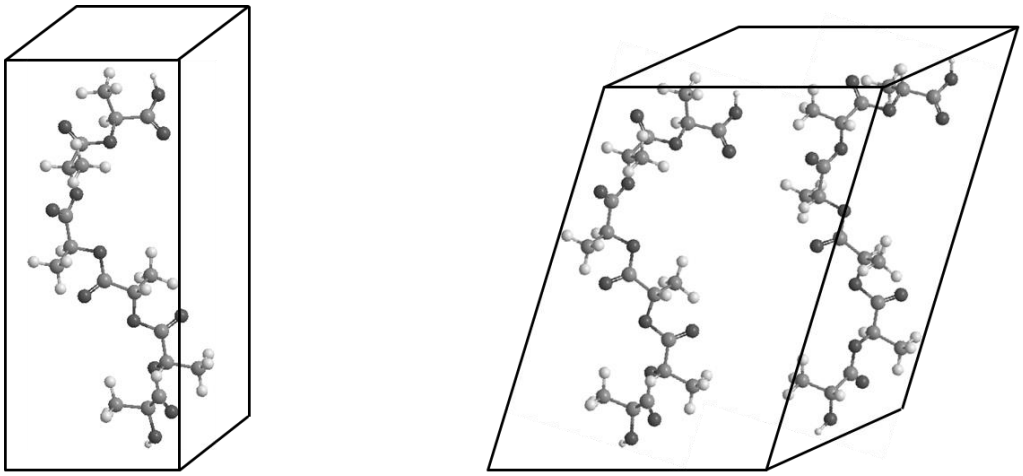

Homo-chiral crystal	Stereocomplex crystal
Pseudo-orthorhombic	Triclinic (*P*1)
a = 1.07, b = 0.595, c = 2.78 nm	a = 0.916, b = 0.916, c = 0.870 nm
$\alpha = \beta = \gamma = 90^{o}$	$\alpha = 109.2, \beta = 109.2, \gamma = 109.8^{o}$
10_3 helix	3_1 helix
Tm = 180°C	Tm = 230°C

Fig. 3 Crystal structures of PLLA homo-chiral and PLLA/PDLA stereocomplex crystals.

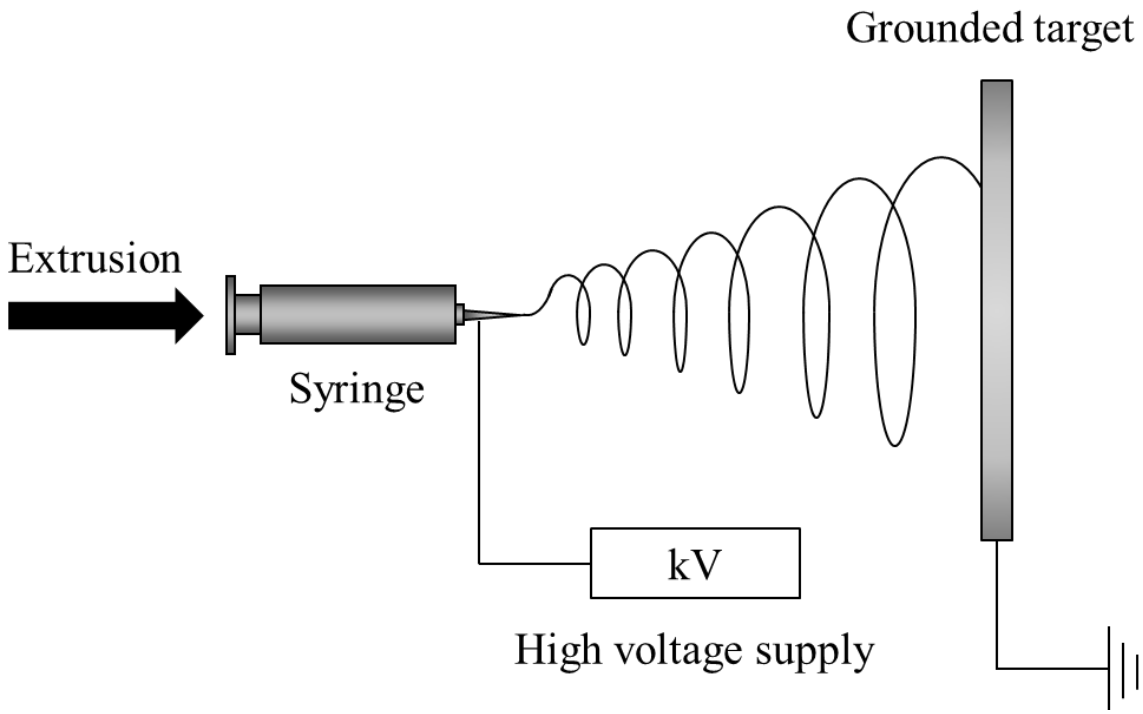

Fig. 4 Schematic diagram of the electrospinning set-up.

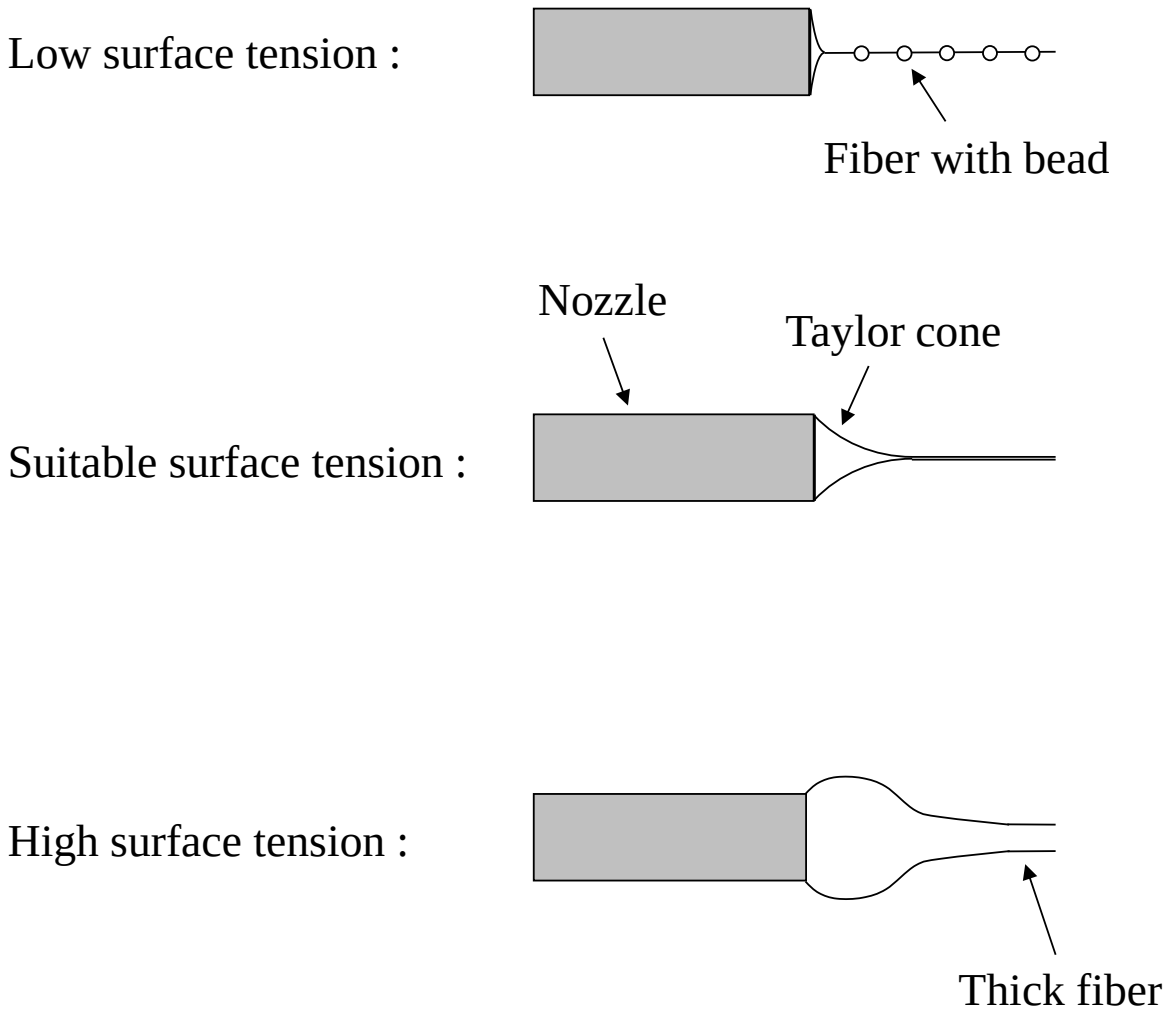

Fig. 5 Principle diagram of the relation between Taylor cone and the surface tension of polymer solution.

Chapter 1

Effect of the Solution-electrospinning Conditions on the Higher-order Structure and the Stereocomplex Formation of the PLLA/PDLA Blend Nanofibers

1. Introduction

Bio-based polymers include the naturally occurring polymers with and without chemical modification, the polymers chemically synthesized from various naturally occurring resources and those synthesized by microorganisms. Among these bio-based polymers, thermoplastic aliphatic polyester such as poly(lactic acid) (PLA) has been attracting much industrial attention. However PLA has its intrinsic problems which may be a major obstacle to the practical applications. A major obstacle of PLA is its low thermal resistance, especially when it is to be used as textile fibers. The fundamental solution to this problem may be a utilization of the stereocomplex (SC) which forms in the equal blend of poly(L-lactic acid) (PLLA) and poly(D-lactic acid) (PDLA), an enantiomer of PLLA.[1]

The α-form of PLLA, a homo-chiral crystal (HC) is crystallized in a pseudo-orthorhombic unit cell with parameters for a = 1.07 nm, b = 0.595 nm, c (fiber axis) = 2.78 nm, and $\alpha = \beta = \gamma = 90°$.[2] Two 103 helices are contained in the unit cell of HC. On the other hand, the SC shows different crystal structure from that of HC. The SC system is triclinic (P1) with cell dimensions: a = 0.916 nm, b = 0.916 nm, c (chain axis) = 0.870 nm, $\alpha = 109.2°$, $\beta = 109.2°$, and $\gamma = 109.8°$.[3]

Various trials have been made to obtain highly thermally stable PLA fibers. However the most researches indicated that both HC and SC tend to co-exist in the PLLA/PDLA blends prepared by the simple mixing. Takasaki et al. reported on the development of SC in the PLLA/PDLA blend fibers by a high-speed melt spinning process.[4] They showed that the highly oriented and highly crystallized fibers containing the α-form of HC and SC were obtained at a take-up velocity. In the high-speed spinning, higher tensile stress is applied to the spin-line and the orientation-induced crystallization is promoted. Annealing of the fibers at a temperature between the melting temperatures of HC and SC yielded the fiber structure mainly consisting of highly oriented SC. Masaki et al. prepared the PLLA/PDLA blend in which only SC forms by a special blending technique.[5] They reported that the melt-spun fibers drawn and annealed have SC as a unique crystalline component and showed an

excellent thermal stability.

Electrospinning is a facile method to produce fibers of nano-order diameters. Electrospinning system consists of an extrusion device, a high voltage generator, and a metal target. A high voltage is applied between the polymer solution and the metal target. When the electrostatic force exceeds the surface tension of the polymer solution, the solution jets blast off and are carried to the metal target. Many researches have prepared the electrospun PLA nanofibers applied for the medical devices and cellular tissue engineering.[6-11] Tsuji et al. studied the effect of the electrospinning condition on the structure of the PLLA/PDLA blend nanofibers and reported that the formation of SC is promoted with the increase in the applied voltage.[12] Present authors also studied the effect of the molecular weight of PLLA and PDLA, the solution concentration and the spinning conditions on the SC formation behavior in the electrospun nanofibers.[13]

It is a purpose of this chapter to investigate the effect of the spinning condition on the morphology, the higher-order structure and the SC formation of the electrospun PLLA/PDLA blend nanofibers taken-up on a rotating target.

2. Experimental

2.1 Materials

The materials used are PLLA (M_w = 2.90 x 10^5, and M_n = 1.18 x 10^5) and PDLA (M_w = 2.83 x 10^5, and M_n = 1.17 x 10^5). Equal amounts of PLLA and PDLA were dissolved in $CHCL_3$ and 1,1,1,3,3,3-hexafluoro-2-propanol (HFIP) (9:1 wt) mixed solvent at a concentration of 6 wt% and the solution was used as a spinning dope.

2.2 Electrospinning

Fig. 1-1 shows the electrospinning set-up used in this study. A metallic nozzle with an inner diameter of 0.2 mm was used. The solution was extruded at a constant rate of 1.0 μL/min by using a micro-feeder pump (Furue Science). The electrospinning conditions were set at the applied voltages of 2.5 and 10 kV by using a high voltage supply device (Model-600F, Pulse Electronic Engineering) and the distances between the nozzle and the metal target were set at 5 and 20 cm. The electrospinning was carried out by three conditions, (1) a low applied voltage and a short nozzle-target distance, 2.5 kV and 5 cm (2) a high applied voltage and a short nozzle-target distance, 10 kV and 5 cm and (3) a high applied voltage and a long nozzle-target distance, 10 kV and 20 cm. The uniaxially aligned

electrospun fibers were obtained by using a rotating metal target. For comparison, some of the fibers were collected on a fixed flat target. The nanofibers prepared were annealed for 1 min at 140°C keeping the fiber length constant.

2.3 Measurements and observations

Morphology was observed by using a scanning electron microscope (SEM) (VE-7800, KEYENCE). The electro-spun sample was placed on a sample holder with an adhesive carbon tape and coated with gold. Thermal analyses were carried out by using a DSC (DSC3100SA, Bruker axs) under a nitrogen atmosphere. The heating rate was set at 10°C/min. Wide-angle X-ray diffraction (WAXD) patterns and spectra were obtained at room temperature using a nickel-filtered CuKα radiation of the wave-length 0.1542 nm, from a CN4037A1 (Rigaku) sealed beam X-ray generator operating at 40 kV and 20 mA. The distance between sample and camera was 63 mm. Small-angle X-ray scattering (SAXS) patterns and spectra were obtained on the PILATUS 1M (DECTRIS) detector using a radiation of the wave-length 0.15 nm from BL-15A beam line at the High Energy Accelerator Research Organization (Tsukuba, Japan). The distance between sample and camera was set at 2.5 m.

3. Results and discussion

3.1 Morphology

SEM images and the average fiber diameter of PLLA/PDLA blend nanofibers taken-up at various velocities are shown in Figs. 1-2(a)~(c), and 3(a)~(c), respectively. The diameter distributions are also added to Fig. 1-3. The fibers collected on the fixed target and on the target rotating at velocities up to 100 m/min were randomly accumulated without showing any particular orientation and the diameter distributions were broad. Although the fiber obtained on the target rotating at 300 m/min when the nozzle-target distance 5 cm and the applied voltage 2.5 kV was more or less aligned, the diameter distribution was still broad. The diameter distribution tended to be much narrower and the fibers were more oriented to the take-up direction with increasing take-up velocity. This may suggest that the velocity of the solution jet carried by the electrostatic force may be lower than 300 m/min so that the fibers were further elongated when the take-up velocity was higher than 300 m/min.

When the applied voltage was increased to 10 kV keeping the nozzle-target distance at 5 cm, the velocity of the solution jet was considered to be much higher and thinner fibers were obtained. However, because of the short nozzle-target distance, the fiber reached to the target

without being stretched sufficiently. Therefore, some thick fibers were formed and the diameter distribution was still broad, when the take-up velocity was low.

When the nozzle-target distance was increased to 20 cm keeping the voltage at 10 kV, the distribution of the fiber diameter was narrower, and only thin fibers were obtained irrespective of the take-up velocity. The fibers collected on the target rotating at 1,130 m/min were very thin and nozzle-target distance. The influences of the taken-up velocity on the fiber diameter and its distribution were rather small.

These results indicate that the high applied voltage contributes to the intensity of the electrostatic force which determines the velocity of the solution jet at the spinneret. On the other hand, the distance between the nozzle and target determines the amount of extensional deformation applied to the fiber. When the applied voltage is low and the nozzle-target distance is short, the fibers were not stretched sufficiently resulting in the thick fibers with a broad diameter distribution.

3.2 Formation of SC crystal

3.2.1 Thermal Analyses

DSC thermograms of as-spun nanofibers taken-up at various velocities are shown in Figs. 1-4(a)~(c) and the melting peak area of SC was plotted in Fig. 1-5 as a function of the take-up velocity. The fibers collected on the fixed target and taken-up at a velocity lower than 300 m/min at an applied voltage 2.5 kV and nozzle-target distance 5 cm showed the melting peak of HC and SC around 174°C and 222°C, respectively. However, the melting peak of HC disappeared completely at higher taken-up velocities. Meanwhile, the crystallization temperature decreased with increasing taken-up velocities. In particular, the fiber taken-up at velocities higher than 600 m/min showed a crystallization temperature about 30°C lower than that of the fiber collected on a fixed target. Although the peak area of SC was the smallest, it increased significantly with increasing take-up velocity.

When the fiber obtained on the fixed target at an applied voltage 10 kV keeping the nozzle/target distance at 5 cm, the DSC curve showed a smaller melting peak of HC. However, the fibers obtained on the rotating target showed only the melting peak of SC. The melting peak area of SC was intermediate and increased with the taken-up velocity gradually. The melting peak areas of SC were larger at all the take-up velocity. The temperature of crystallization peak did not change with the taken-up velocity, comparing with the fibers obtained at the applied voltage and the nozzle-target distance, 2.5 kV and 5 cm, respectively.

When the nozzle-target distance was increased to 20 cm keeping the applied voltage at 10 kV, the melting peak of HC completely disappeared irrespective of the taken-up velocity. Although the melting peak area of SC was the highest, it increased slightly.

Fig. 1-6 shows the melting peak area of SC plotted against the fiber diameter. Open symbols in this figure indicate the data for the fibers collected on a fixed target. It is clear that the SC formation was promoted with the decrease in the fiber diameter. In our electrospinning process, three factors, the applied voltage, the nozzle-target distance and the take-up velocity, influence the fiber diameter. Among these factors, increases in the applied voltage and the nozzle-target distance reduced the fiber diameter and promoted the SC formation. Tsuji et al. reported that the orientation caused by high voltage or electrically induced high extensional force during electrospinning enhances the formation and growth of SC and suppresses the formation of HC.[12] The electrically induced high extensional force increased the surface area of the molecular chains and thereby elevated the interaction between PLLA and PDLA chains, resulting in rapid stereocomplex crystallization. Further the increase in the take-up velocity promoted the SC formation. The mechanical extension gives the high extensional stress on the fiber and this stress may promote the SC formation.

3.2.2 Higher-order structure

3.2.2.1 Crystalline forms

Since all of the as spun fibers obtained in this study were in an amorphous state, WAXD analyses were carried out for the annealed fibers to determine the crystalline structure. Figs. 1-7(a)~(c) and 1-8(a)~(c) show the WAXD patterns and the equatorial spectra of the annealed fibers taken-up at various velocities. The Miller indices are indicated in a WAXD pattern in Fig. 1-7(d).

Oriented PLLA fibers generally show a strong equatorial diffraction at a 2θ value around 17° identified as the α-form of PLLA crystallized in a pseudo-orthorhombic unit cell of dimensions a = 1.07 nm, b = 0.595 nm, and c = 2.78 nm, which contains two 10_3 helices.[2] On the other hand, the oriented stereocomplex fibers show three equatorial diffractions at 2θ values around 12°, 21°, and 24° for the PLA stereocomplex crystallized in a triclinic unit cell of dimensions a = 0.916 nm, b = 0.916 nm, c = 0.870 nm, α = 109.2°, β = 109.2°, and γ = 109.8°, in which L-lactide and D-lactide segments are packed parallel taking a 3_1 helical conformation.[3] These three diffractions are indexed as (100)/(010)/(-110), (110)/(-120)/(-210), and (200)/(020)/(-220) of SC.[3, 14]

When the applied voltage and the nozzle-target distance were set at 2.5 kV and 5 cm, respectively, the fibers collected on the fixed target showed a reflection of HC at 16.7° and the reflections of SC at 12°, 20.5°, and 23.8°. These reflections were observed in the shape of a ring indicating almost no crystalline orientation to any particular directions. On the other hand, the fibers obtained on the rotating target showed arc-like reflections at lower take-up velocities and these reflections changed to spot-like at velocities higher than 900 m/min. The intensity of the reflection of SC increased and that of HC decreased significantly with increasing take-up velocity. Especially, when the taken-up velocities were higher than 900 m/min, the reflection of HC completely disappeared. These results may suggest that the rapid mechanical stretching of the fiber promotes the formation of SC. Similar results were reported by Takasaki et al. who reported the development of SC in the PLLA/PDLA blend high-speed melt-spun fibers. They observed that the formation of SC was promoted with the increase in the take-up velocity suppressing the formation of HC in the fiber.[4] In their case, the fiber crystallized in the spin-line, while the electrospun PLA fiber prepared in this study was frozen into amorphous state. Consideration of these differences may suggest that the high-speed extension in the electrospinning process produces the pre-structure which easily crystallizes into SC. Even when the applied voltage was increased to 10 kV keeping the nozzle-target distance at 5 cm, the fiber collected on the fixed target showed the reflections of both HC and SC. However, the fibers collected on the rotating target did not show any reflections of HC but only the reflections of SC. The ring-like reflections of SC turned to be arc-like and the intensity increased as the take-up velocity increased. This tendency was more pronounced when the nozzle-target distance was increased to 20 cm. These results suggest that the fiber sufficiently extended at a high rate forms of SC more efficiently.

3.2.2.2 Crystalline Orientation

So far the results obtained by DSC measurements and WAXD analyses clearly indicated that the formation of SC was more pronounced in the thinner fibers. The solution jets driven by a strong electrically induced force and further extended by the mechanical force given by the rotating target resulting in thinner fibers. Now it may be interesting to determine the orientation of SC and to examine the relation between the crystalline orientation and the degree of SC formation.

Hermans et al. reported the concept of the orientation factor by which the axis orientation of a crystalline fiber is evaluated quantitatively for the first time.[15] Stein reported

the degree of orientation of each crystal axis about the reference axis Z. Stein showed that the crystalline orientation factor (f_c) of axis c as follows:[16]

$$f_c = \frac{1}{2}\left(3 < cos^2\varphi_{c,Z} > -1\right) \quad (1)$$

Angle φ is inclination to the crystal face over a fiber axis, and $<cos^2\varphi_{c,Z}>$ is a degree of the inclination of the crystal axis c to the fiber axis Z. Hermans[17] and Wilchinsky[18] reported that the value of $<cos^2\varphi_{c,Z}>$ was shown from inclination of a crystal axis (φ) and X-ray intensity distribution. They show that $<cos^2\varphi_{c,Z}>$ as follows:

$$< cos^2\varphi_{c,Z} >= \frac{\int_0^{\pi/2} I(\varphi) sin\varphi cos^2\varphi d\varphi}{\int_0^{\pi/2} I(\varphi) sin\varphi d\varphi} \quad (2)$$

The crystalline orientation factor (f_c) for SC was analyzed with the cell dimensions, a = 0.916 nm, b = 0.916 nm, c = 0.870 nm, α = 109.2°, β = 109.2°, and γ = 109.8° and the intensity distribution of reflections at 2θ around 12° and 20.5° indexed as (1 0 0)/(0 1 0)/(-1 1 0), and (1 1 0)/(-1 2 0)/(-2 1 0) and (-2 0 1)/(0 -2 1)/(1 -2 1) and (-1 0 2)/(0 -1 2)/ (-1 -1 2), respectively.[3]

Fig. 1-9 shows the c-axis orientation factor of the fibers as a function of fiber diameter. The fibers collected at the lower take-up velocities were manually aligned without applying any tension in the fiber direction. Unfortunately, the fibers on the fixed target were randomly accumulated completely so that the determination of the orientation factor was not possible. It should be noted that the orientation factor was determined form the reflections of SC in the annealed fibers and reflects the orientation of the molecules which were transformed into SC. The orientation factor almost linearly increased with the decreasing fiber diameter. If the orientation factors are extrapolated to the diameter of the fibers collected on the fixed target, they tend to approach to zero indicating that the fibers collected on the fixed target have a very low molecular orientation. It is interesting to note that the orientation factors were in the order of 2.5 kV/5 cm > 10 kV/5 cm > 10 kV/20 cm comparing at a constant fiber diameter. This dependence is in the opposite order of the fiber diameter. These results may be explained as follows. In the electrospinning process, a jet of the solution is driven to the target by the applied electric charge. The higher applied voltage induces the higher electrically force which draws thinner jets from the Taylor cone of the solution at a higher velocity. However the

molecular orientation caused in the stretched solution readily relaxes. Then all the part of the jet is carried to the target by the electric charge so that the molecules in the jet are not extended in this process significantly and the jet or nanofiber collected on the fixed target has almost no molecular orientation. When the jet was further extended by the rotating target mechanically, the force applied to the jet just arrived at the target can be transported to the capillary tip through the molecular entanglement. Because of the extensional force transported through the molecular entanglement stretches the molecules resulting in the molecular orientation to the fiber axis. The taking-up of the thicker fiber by the rotating target in the short nozzle-target distance greatly increases the molecular orientation. When the applied voltage is high, larger amount of electrical charge produces the thinner solution jets and carries them to the target at higher velocities. The mechanical taking-up at a lower velocity does not enhance the molecular orientation significantly and the orientation factors get close to unity as the take-up velocity increases. Because of the mechanism described above, the fiber with a larger diameter tended to have a higher orientation factor when it was stretched by the rotating target.

Now the relation between the molecular orientation and the extent of the SC formation has to be examined. The peak area of SC determined by using the DSC was plotted against the orientation factor as shown in Fig. 1-10. The relation seems to indicate that the amounts of SC in the annealed fiber linearly increase with the orientation factor. However there is a fairly large variation depending on the set of the applied voltage and the nozzle-target distance. These results suggest that the SC formation and the suppression of HC formation may be enhanced when the crystallization of the PLLA and PDLA mixture occurs in the extremely narrow space of the nanofibers.

3.2.2.3 Crystallite size

The crystallite size, *D*, was calculated by well-known Scherrer's equation[18] :

$$\mathrm{D} = \frac{K\lambda}{B\cos\theta}$$

K is a constant related to the crystallite shape, normally taken as 0.9, λ is the X-ray wavelength, and *B* is the width of the diffraction peak profile at half maximum height. The crystallite size of SC was analyzed with the intensity distribution of a reflection at 2θ around 12° indexed as (100)/(010)/(-110). It should be noted that these planes are parallel to the

c-axis and the crystallite size determined correspond to the dimension in the direction perpendicular to the c-axis.

Fig. 1-11 shows the crystallite size of SC plotted against the diameter of the fibers obtained at various electrospinning conditions. Crystallite size decreased with increasing fiber diameter in all electrospinning conditions. This result seems to be reasonable since the molecular chains tend to orient to the fiber direction as the fiber diameter becomes smaller so that the crystal tends to have less space to grow in the radial direction. Here it should be noted that the tendencies of changes in the crystallite size are different for the fibers obtained at different conditions. The crystallite sizes are in order of 2.5 kV/5 cm < 10 kV/5 cm < 10 kV/20 cm comparing at a constant fiber diameter. This result is similar to the relation between orientation factor and fiber diameter. The orientation factors are in order of 2.5 kV/5 cm > 10 kV/5 cm > 10 kV/20 cm comparing at a constant fiber diameter. In other words, the crystallite size of highly oriented fiber is smaller at a constant fiber diameter. However the size of the crystallite in the fiber obtained at 2.5 kV/5 cm decreased gradually, while that of the fiber obtained at 10 kV/20 cm decreased more drastically.

Fig. 1-12 shows the relation between the DSC peak area of SC and the crystallite size of SC. The degree of SC increased with decreasing crystallite size. As the fiber diameter decreased, the formation of HC was restrained while that of SC seems to be promoted. This may be due to the difference in the enthalpy of fusion of SC and HC, the enthalpy of fusion of HC is much lower than that of SC.[19, 20] It has been known that the crystal can start to grow only when it has a size large enough for the bulk free energy of fusion to exceed the interfacial free energy.[21] As the fiber diameter becomes smaller, HC may not have enough space to have an enough size, while SC can start growing from much smaller nucleus. Presence of the very small SC crystallite was reported by Yamane et al. who studied the effect of the addition of the small amount of PDLA on the melt rheology and the crystallization behavior of the PLLA matrix.[22] They demonstrated that the presence of the very small SC crystallites dispersing in the PLLA matrix act as the crosllinking points and show crystal nucleating effect.

3.2.2.4 Crystalline periodicity

Figs. 1-13 and 1-14 show SAXS patterns and the meridional spectra of the annealed fibers. The long period, *L*, was calculated using the Bragg's low[23] as follows:

$$L = \frac{2\pi}{q}$$

Where q is the scattering vector defined by

$$q = \frac{4\pi \sin\theta}{\lambda}$$

and was obtained from meridional spectra. λ is the x-ray wavelength and θ is one half of the scattering angle (2θ).

The relation between the long period and fiber diameter is shown in Fig. 1-15. The fibers collected on the fixed target did not show the reflection based on the long period at each electrospinning condition indicating that the fiber does not have a lamellar structure. On the other hand, the fibers taken-up on the rotating target showed the meridional reflections slightly and these reflections shifted to larger q with increasing take-up velocity. In other words, the long period of SC decreased with decreasing fiber diameter. The tendencies of changes in the long period are different for the fibers obtained at different conditions. Again the long periods are in order of 2.5 kV/5 cm < 10 kV/5 cm < 10 kV/20 cm comparing at a constant fiber diameter.

Meanwhile, triangular streak was observed in the equatorial direction and this streak turned to be sharper with increasing take-up velocity. Since this equatorial streak was disappeared when the fiber was immersed in isopropanol, it is considered as the surface scattering of fiber bundle.

Fig. 1-16 shows the melting peak area of SC plotted against the long period. It is clear that the SC formation was promoted with the decrease in the long period. This result was similar to the relation between the formation of SC and the crystallite size. Both the crystallite size and the long period decreased with decreasing fiber diameter. Hoffman et al. showed that the melting point of the crystal increases linearly with the decrease in the reciprocal of the lamellar thickness.[24] Although the long periods determined in this study include both the thicknesses of the lamellae and the amorphous area, they should be strongly related to the lamellar thickness. It has been known that the melting points of the HC and SC are usually observed at around 170°C and 230°C, respectively. As the lamella of HC and SC reduce their thickness, the melting points of these should decrease in some extent. The disappearance of HC in the fibers taken-up at high velocities may be due to the fact that the thin lamella of HC

have a melting point lower than the annealing temperature, 140°C.

4. Conclusion

The effects of the solution-type electrospinning condition on the higher-order structure and the stereocomplex (SC) formation of the PLLA/PDLA blend nanofiber taken-up on the rotating target were investigated. Measurements of the orientation factor of the fibers indicated that the nanofibers collected on the fixed target were not stretched significantly between the nozzle and the target. However the fibers taken-up on the rotating target were stretched between the nozzle and target and showed a high crystalline orientation to the fiber direction. Although the molecular orientation function of the nanofibers has some correlation to the amount of SC, the decrease in the fiber diameter seems to promote the SC formation more directly. These results suggest that the SC formation may be enhanced and the HC formation may be suppressed when the crystallization of the PLLA and PDLA mixture occurs in the extremely narrow space of the nanofibers. As the fiber diameter decreased significantly, the crystal does not have enough space and has to reduce its lateral size and lamellar thickness. It can be speculated that the HC with a very small size may not be able to exist as a crystal because of the lower enthalpy of fusion and a melting point lower than the annealing temperature.

References

1. Y. Ikada, K. Jamshidi, H. Tsuji, S. -H. Hyon, *Macromolecules*, **20**, 904 (1987).
2. P. De Santis, A. J. Kovacs, *Biopolymer*, **6**, 299 (1968).
3. T. Okihara, M. Tsuji, A. Kawaguchi, K. Katayama, *Journal of Macromolecular Science: Physics*, **B30(1&2)**, 119 (1991).
4. M. Takasaki, H. Ito, T. Kikutani, *Journal of Macromolecular Science: Part B Physics*, **42**, 403 (2003).
5. D. Masaki, Y. Fukui, K. Toyohara, M. Ikegame, B. Nagasaka, and H. Yamane, *Sen'i Gakkaishi*, **64**(8), 212 (2008).
6. M. Bognitzki, W. Czado, T. Frese, A. Schaper, M. Hellwig, M. Steinhart, A. Greiner, J. H. Wendorff *Advanced Materials*, **13**, 70 (2001).
7. X. Zong, K. Kim, D. Fang, S. Ran, B. S. Hsiao, B. Chu, *Polymer*, **43**, 4403 (2002).
8. J. Zeng, X. Chen, Q. Liang, X. Xu, X. Jing, *Macromolecular Biosci*ence, **4**, 1118 (2004).
9. S. R. Bhattarai, N. Bhattarai, P. Viswanathamurthi, H. K. Yi, P. H. Hwang, H. Y. Kim, *Journal of Biomedical Materials Research Part A*, **78**, 247 (2006).
10. A. S. Asran, M. Salama, C. Popescu, G. H. Michler, *Macromolecular Symposia*, **294**, 153 (2010).
11. H. Ma, J. Hu, P. X. Ma, *Functional Materials*, **20**, 2833 (2010).
12. H. Tsuji, M. Nakano, M. Hashimoto, K. Takashima, S. Katsura, A. Mizuno, *Biomacromolecules*, **7**, 3316 (2006).
13. M. Yamamoto, Master thesis, Kyoto Institute of Technology (2011).
14. P. H. Hermans, P. Plazek, *Kolloid-Zeitschrift*, **88**, 68 (1939).
15. R. S. Stein, *Journal of Applied polymer Science*, **31**, 327 (1958).
16. P. H. Hermans, "Contribution to the Physics of Cellulose Fibers," Elsevier, Amsterdam, 1946, Appendix III (J. J. Hermans).
17. Z. W. Wilchinsky, "Advances in X-Ray Analysis," **Vol. 6**, Plenum Press, New York, 231

(1963).

18. P. Scherrer, *Göttinger Nachrichten Gesell.*, **2**, 98 (1918).

19. E. W. Fischr, H. J. Sterzel, G. Wegner, *Kolloid-Zeitschrift und Zeitschrift für Polymere*, **251**, 980 (1973).

20. Loomis GL, Murdoch JR, Gardner KH, *Polymer Preprints*, **31**, 55 (1990).

21. J. D. Hoffman, G. T, Davis, J. I. Lauritzen Jr., "Treatise on Solid State Chemistry, Vol. 3, Crystalline and noncrystalline Solids", N. B. Hannay, ed., Plenum, New York (1976).

22. H. Yamane, K. Sasai, *Polymer*, **44**, 2569 (2003).

23. W. L. Bragg, *Proceedings of the Cambridge Philosophical Society*, **17**, 43 (1913).

24. J. D. Hoffman, J. J. Weeks, *Journal of Research of the National Bureau of Standards, Section A: Physics and Chemistry*, **66** ,13 (1962).

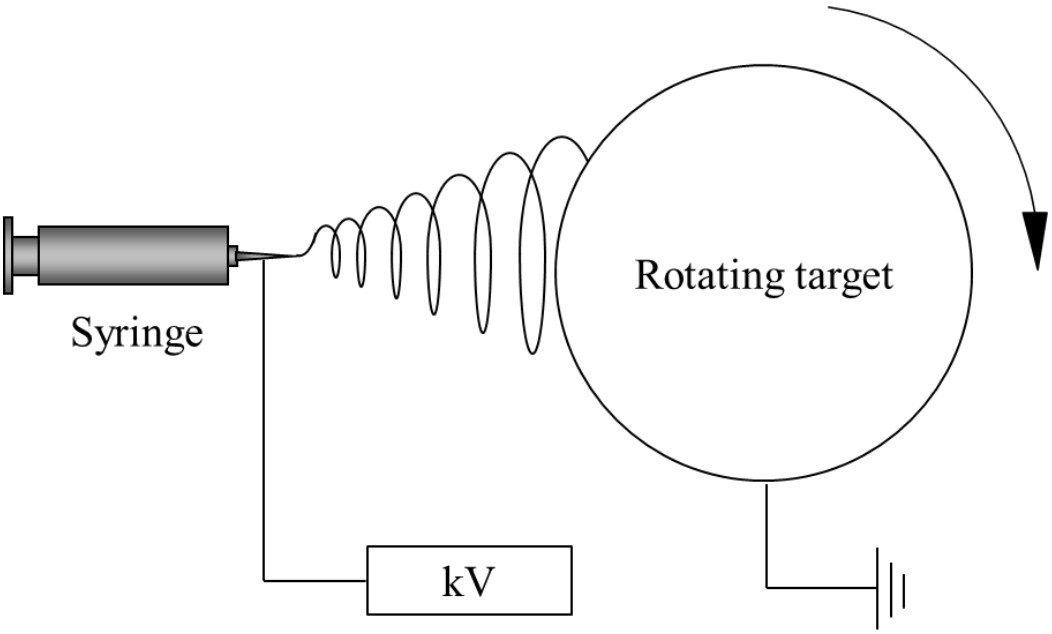

Fig. 1-1 Electrospinning set-up used in this study.

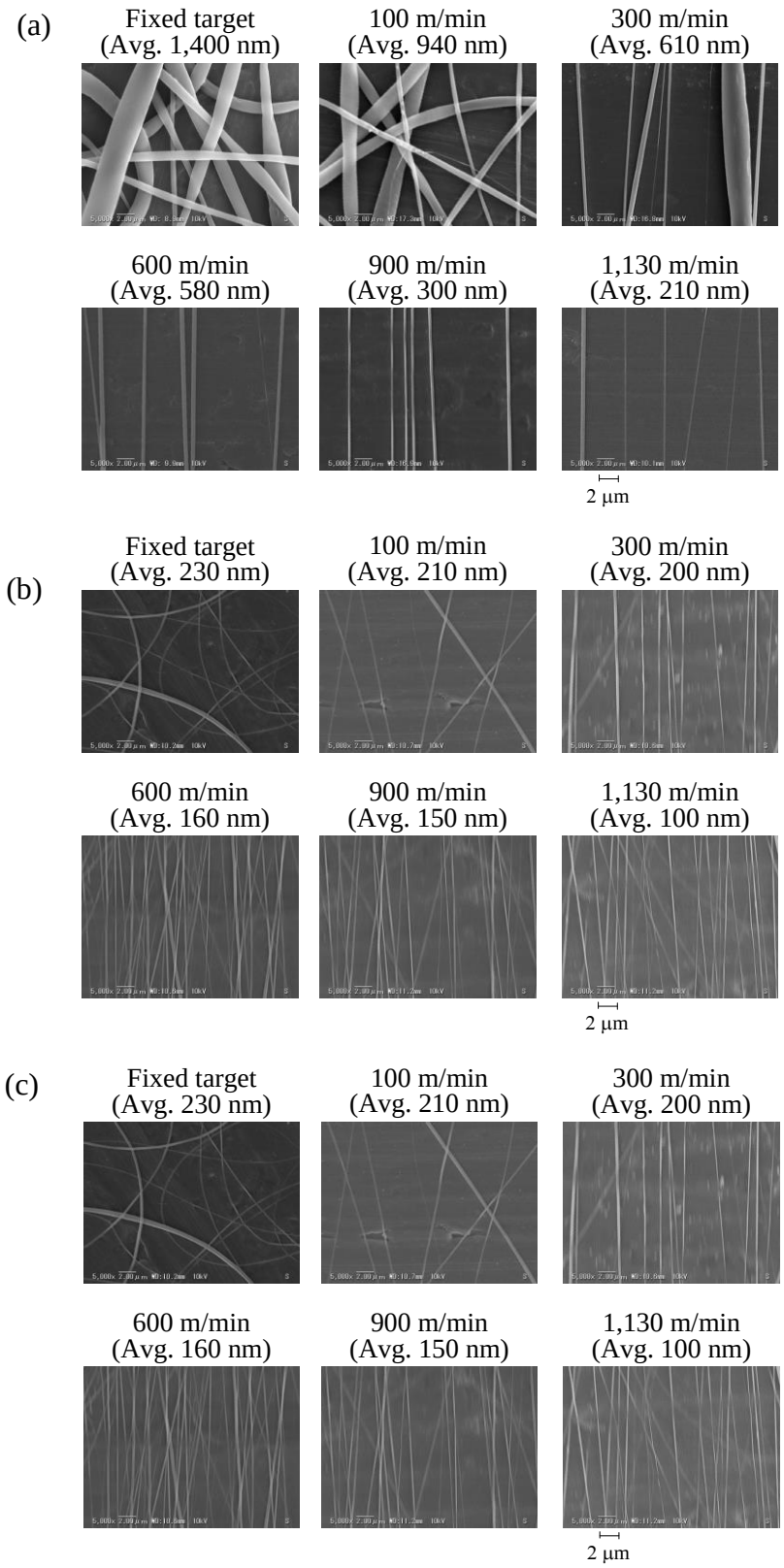

Fig. 1-2 SEM images of PLLA/PDLA blend nanofibers taken-up at various velocities. Spinning conditions are (a) 2.5 kV/5 cm, (b) 10 kV/5 cm, and (c) 10 kV/20 cm.

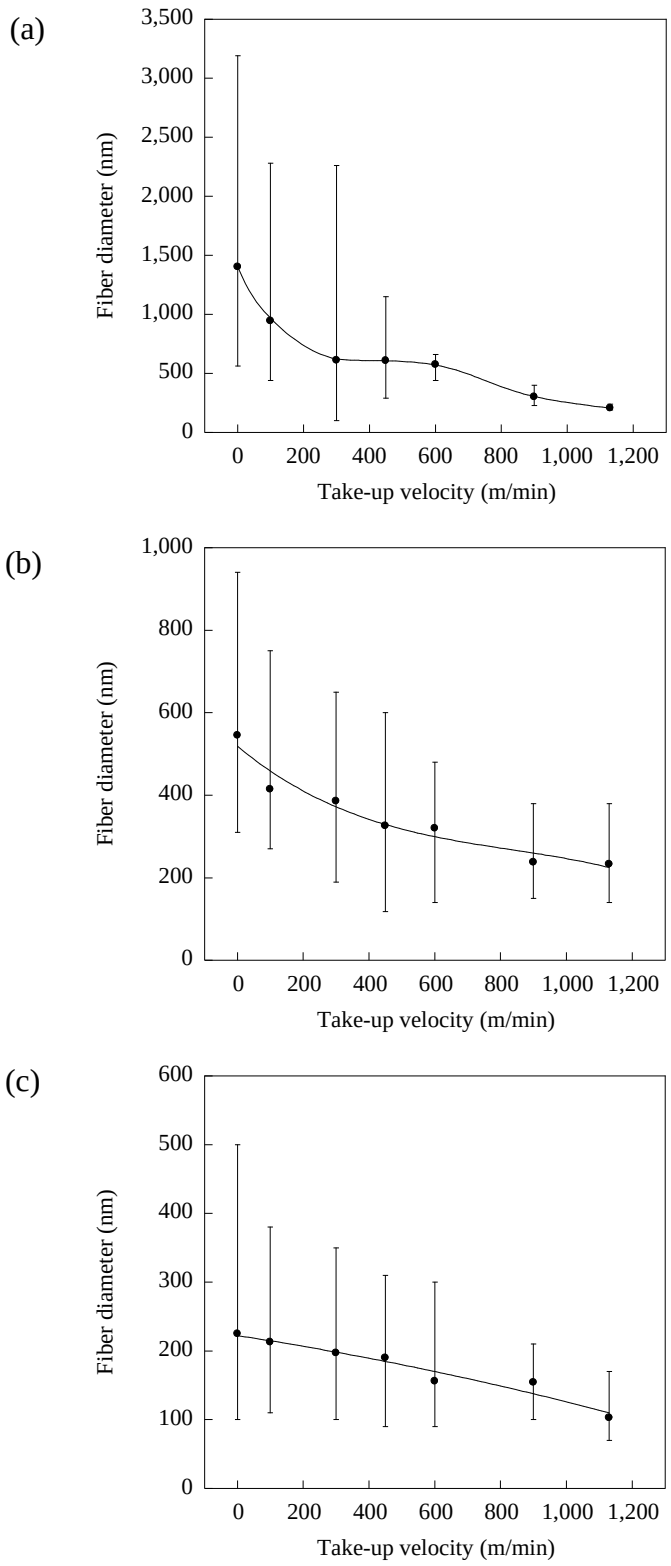

Fig. 1-3 Diameters of PLLA/PDLA blend nanofibers taken-up at various velocities. Spinning conditions are (a) 2.5 kV/5 cm, (b) 10 kV/5 cm, and (c) 10 kV/20 cm.

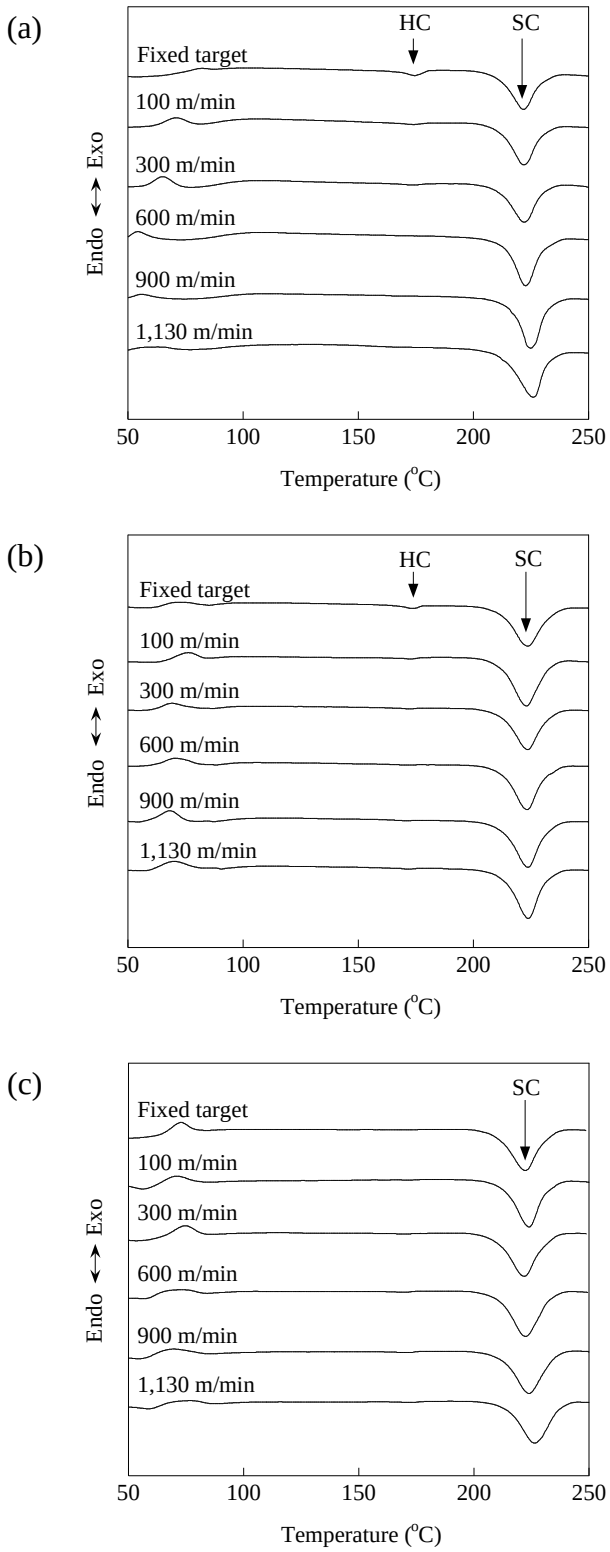

Fig. 1-4 DSC thermograms of PLLA/PDLA blend nanofibers taken-up at various velocities. Spinning conditions are (a) 2.5 kV / 5 cm, (b) 10 kV / 5 cm, and (c) 10 kV / 20 cm.

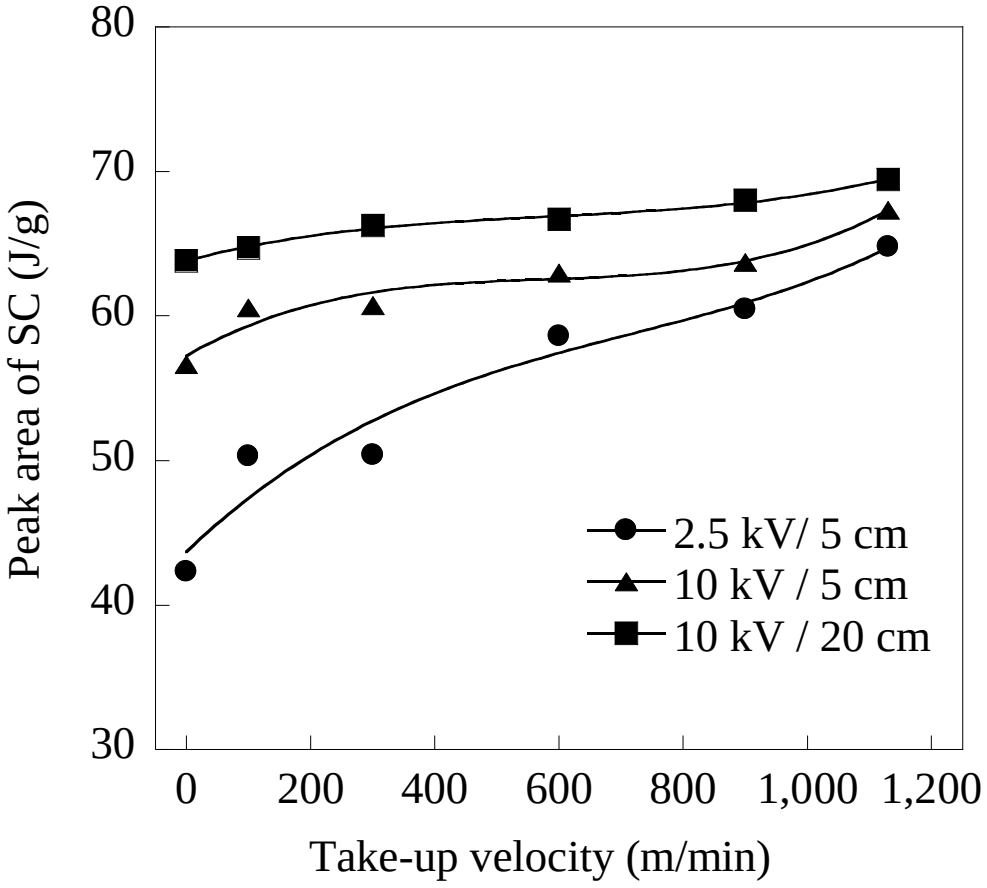

Fig. 1-5 Melting peak area of SC plotted as a function of the take-up velocity.

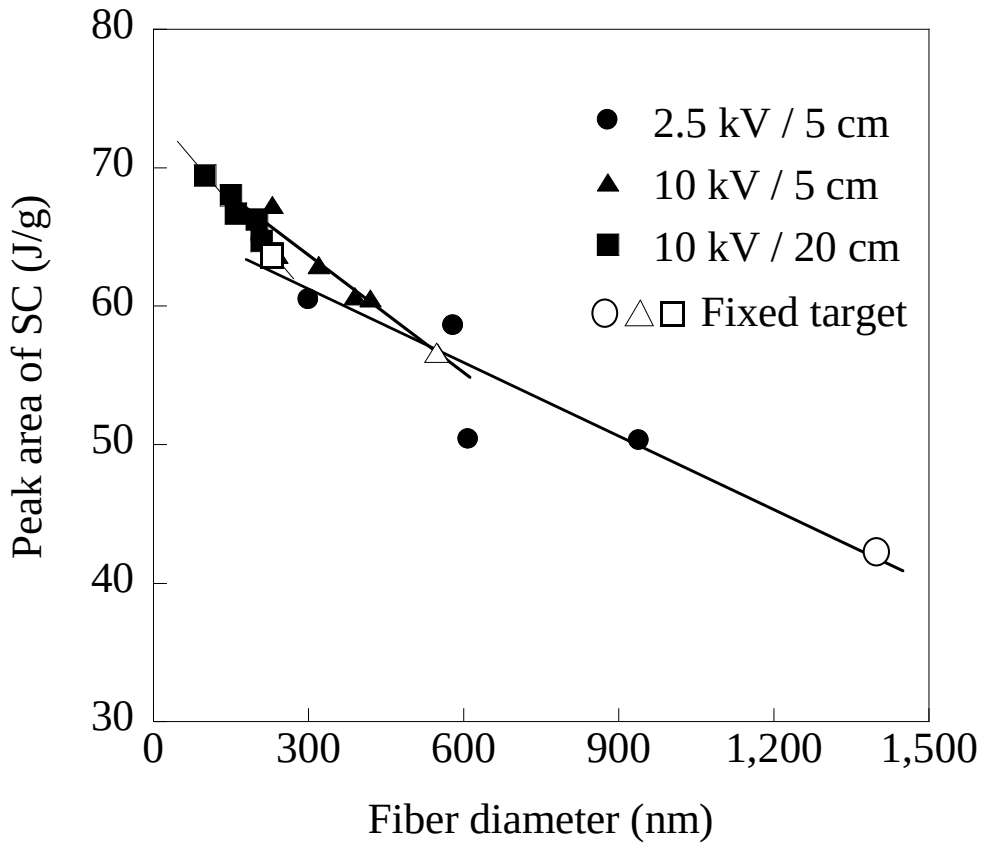

Fig. 1-6 Melting peak area of SC plotted against the fiber diameter.

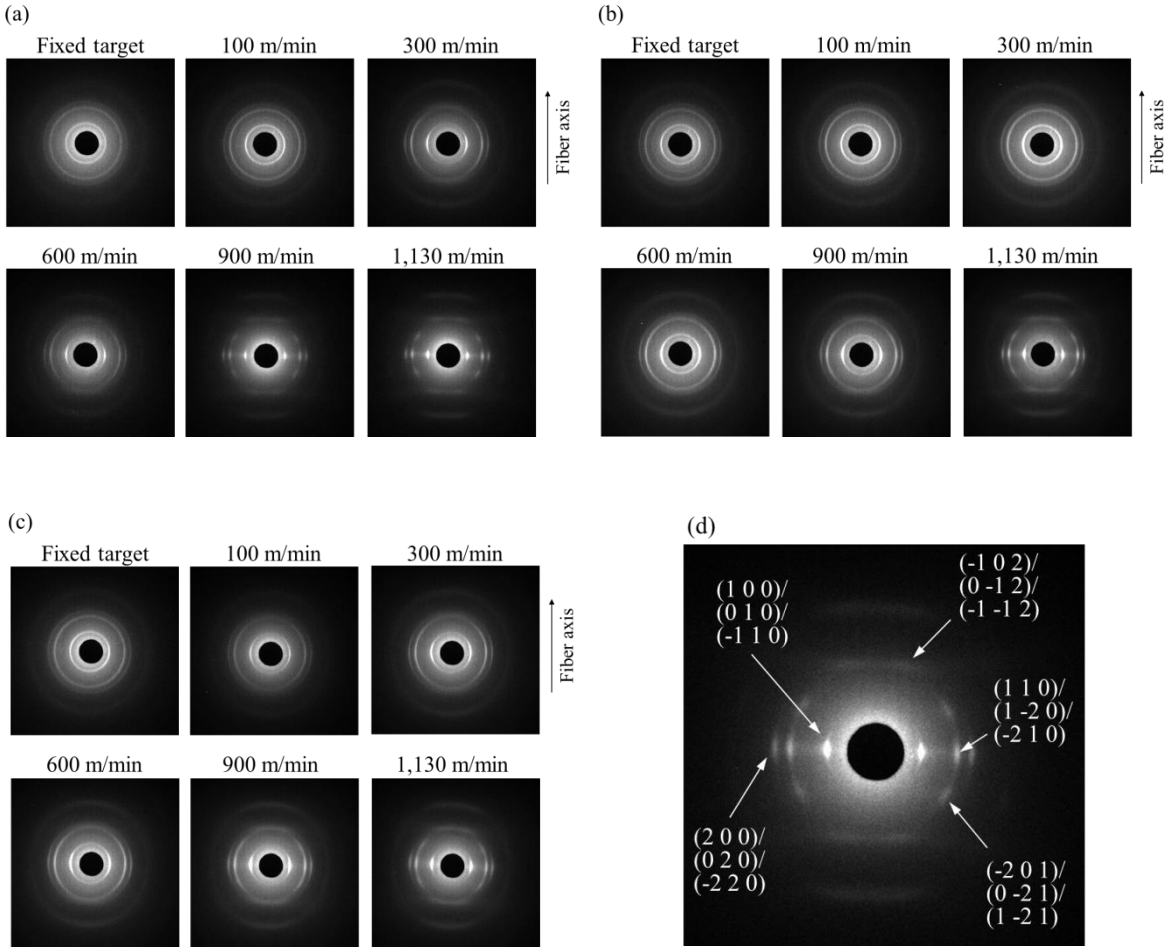

Fig. 1-7 WAXD patterns of PLLA/PDLA blend nanofibers annealed at 140°C for 1 min. Spinning conditions are (a) 2.5 kV / 5 cm, (b) 10 kV / 5 cm, and (c) 10 kV / 20 cm. The Miller indices are indicated in a WAXD pattern in (d).

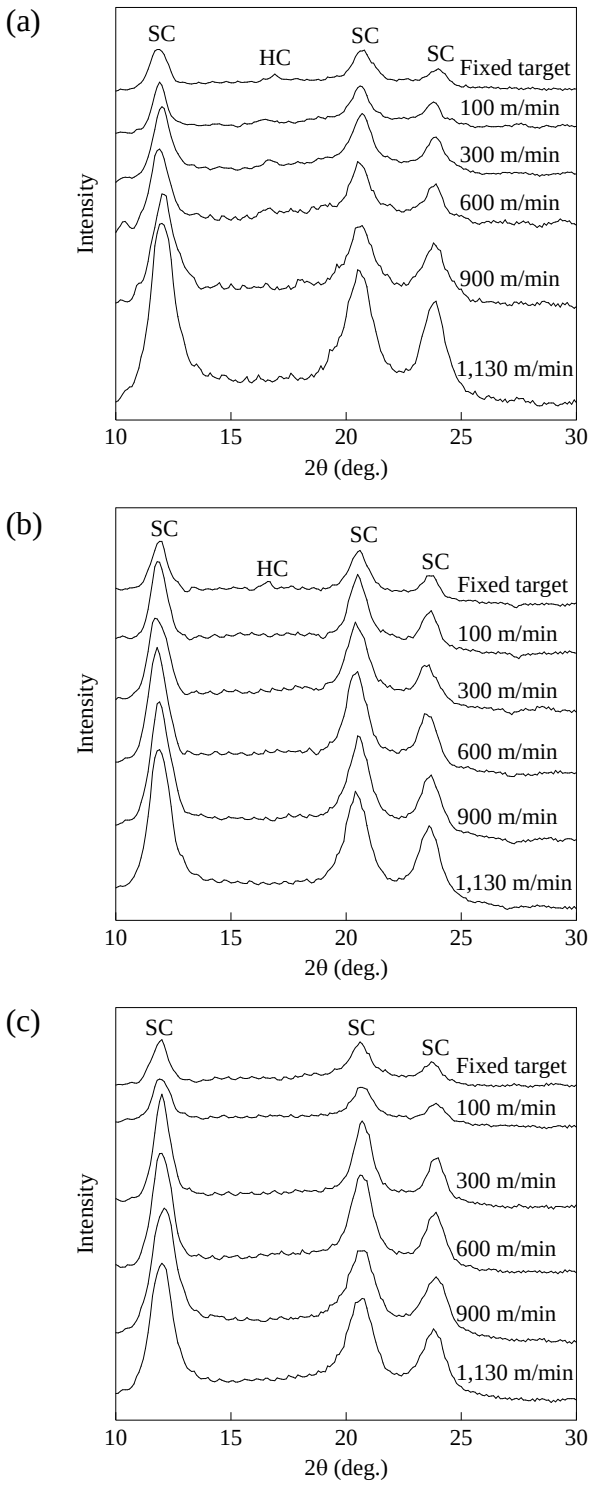

Fig. 1-8 WAXD spectra of PLLA/PDLA blend nanofibers taken-up at various velocities annealed at 140°C for 1 min. Spinning conditions are (a) 2.5 kV / 5 cm, (b) 10 kV / 5 cm, and (c) 10 kV / 20 cm.

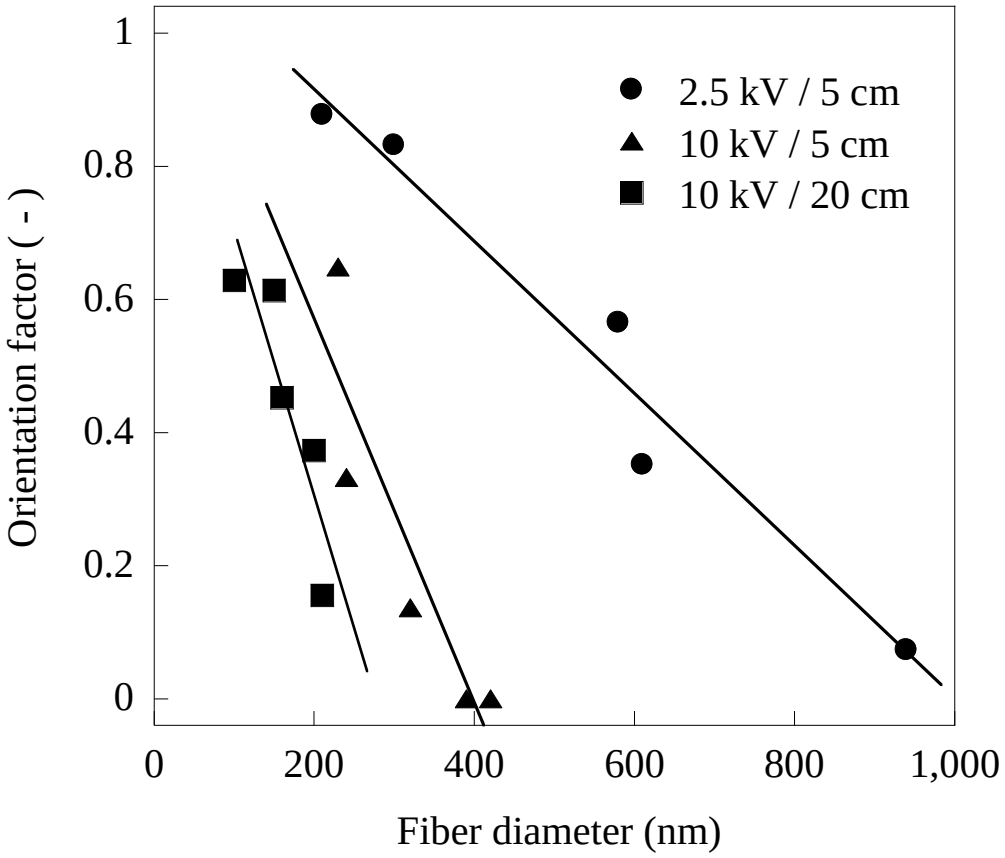

Fig. 1-9 Orientation function as a function of the fiber diameter for the nanofibers obtained at various conditions.

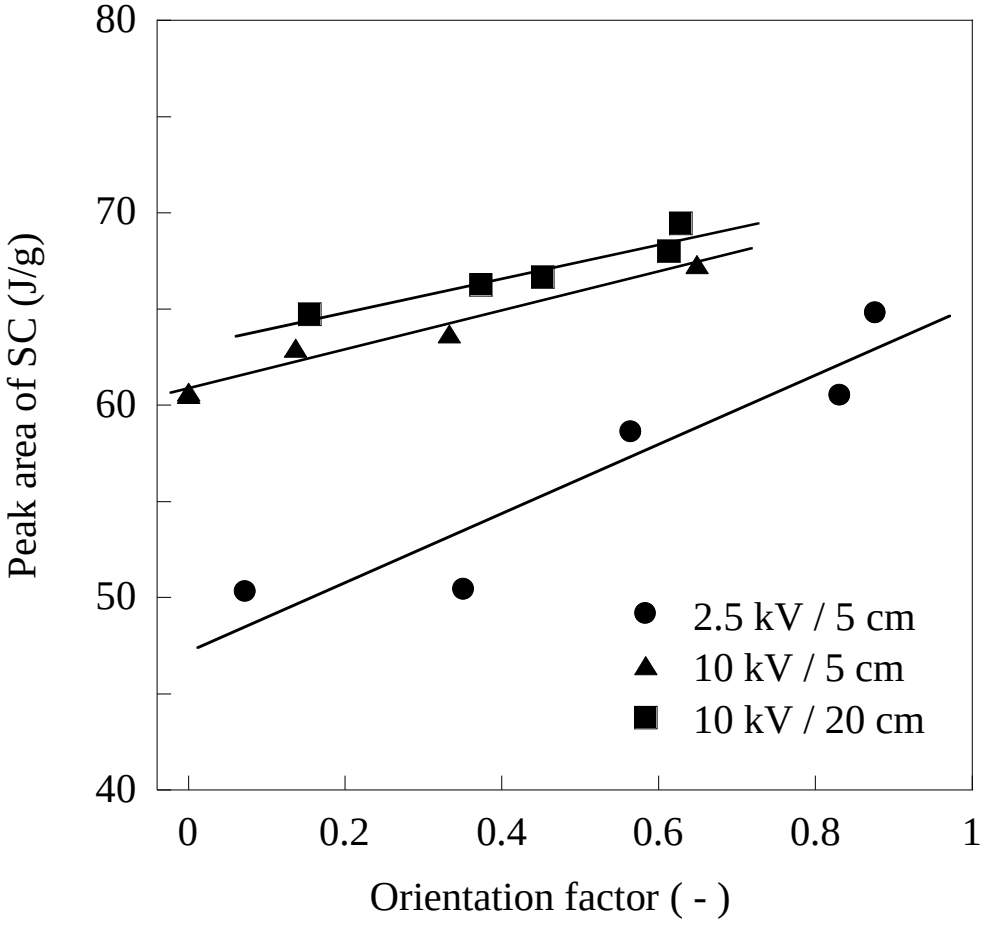

Fig. 1-10 Peak area of SC as a function of the orientation factor of the nanofibers obtained at various conditions.

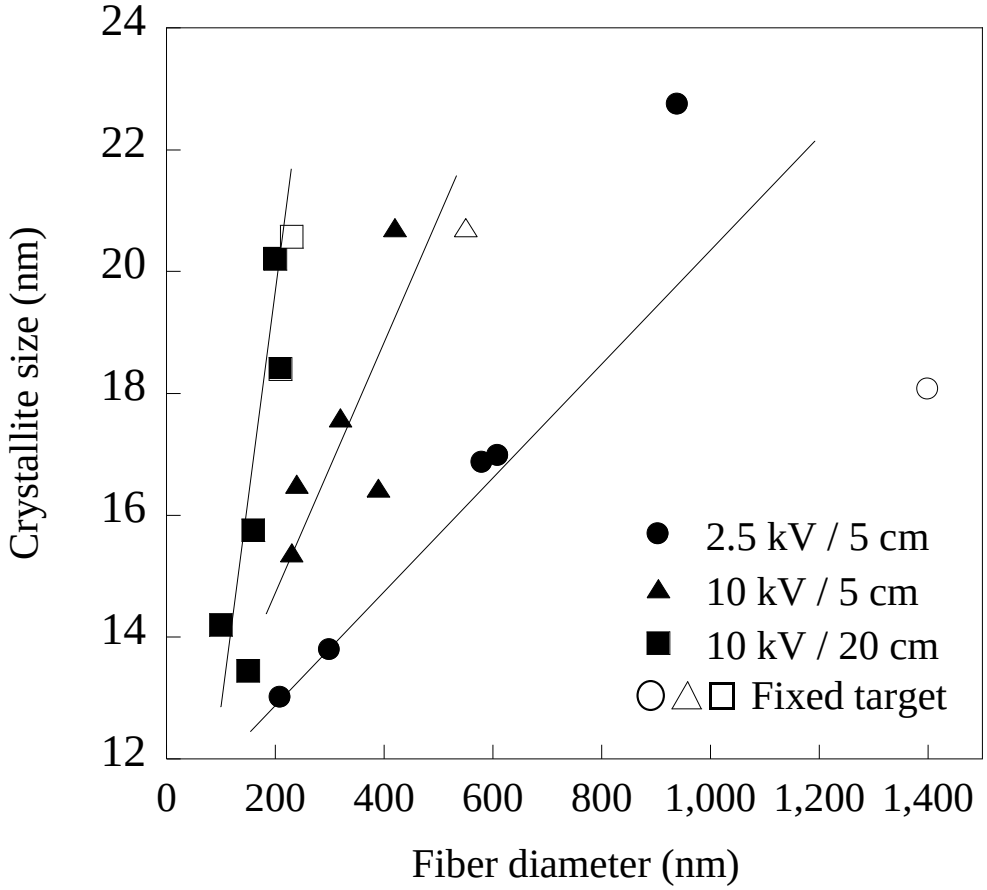

Fig. 1-11 Crystallite size as a function of the fiber diameter for the nanofibers obtained at various conditions.

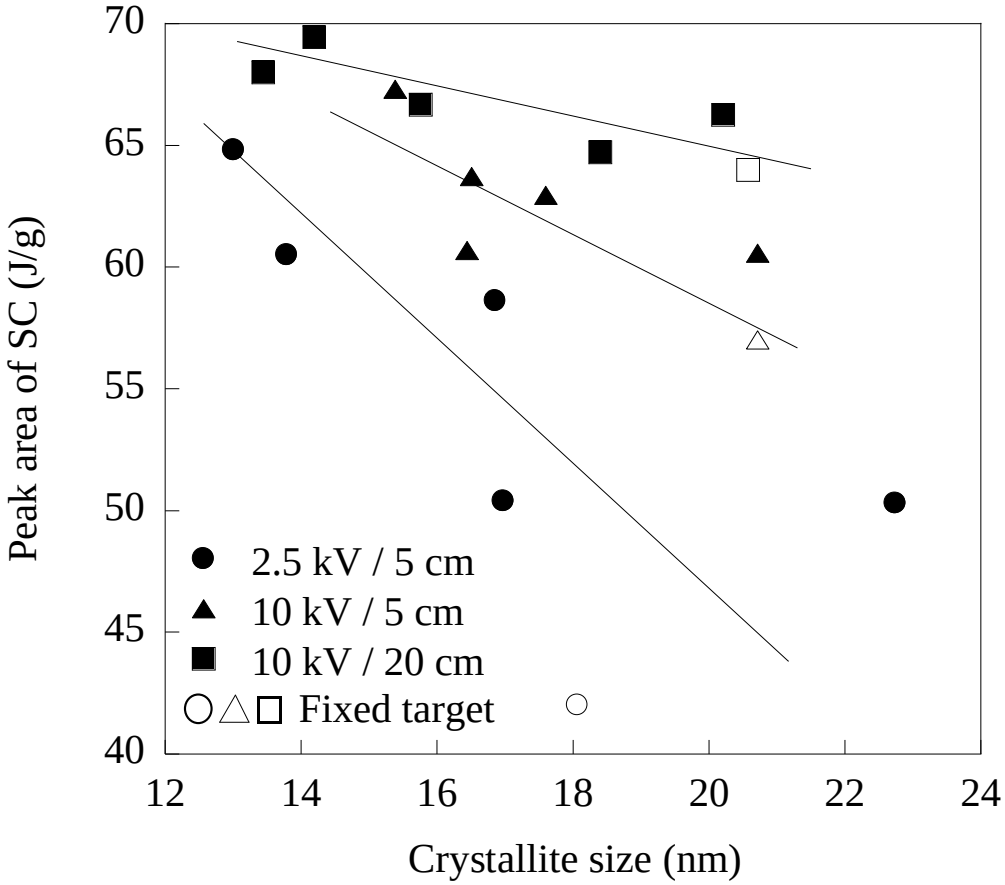

Fig. 1-12 Peak area of SC as a function of the crystallite size of the nano fibers obtained at various conditions.

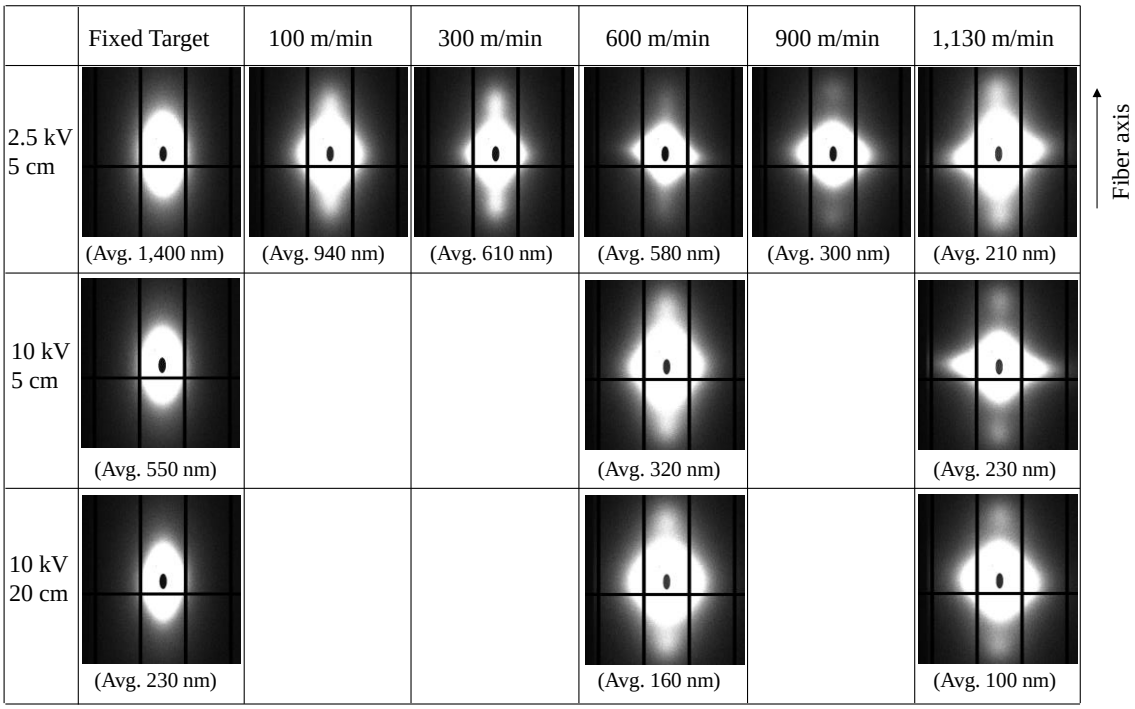

Fig. 1-13 SAXS patterns of PLLA/PDLA blend nanofibers annealed at 140°C for 1 min.

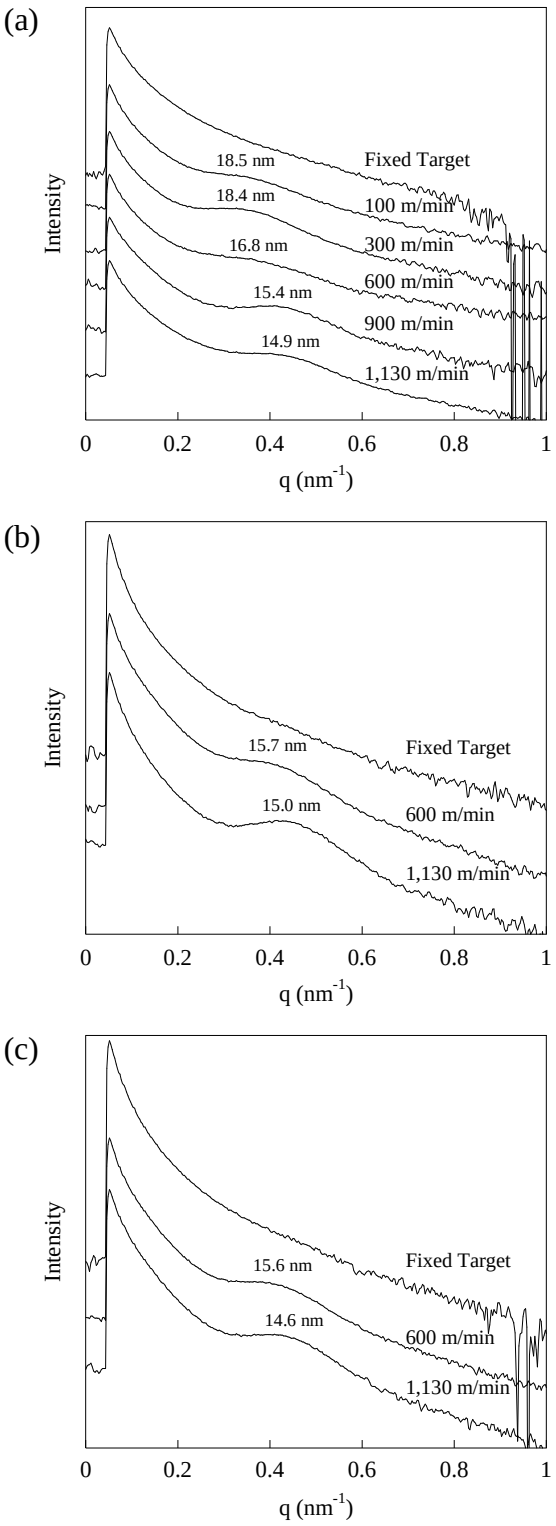

Fig. 1-14 SAXS spectra of PLLA/PDLA blend nanofibers taken-up at various velocities annealed at 140°C for 1 min. Electrospinning conditions are (a) 2.5 kV / 5 cm, (b) 10 kV / 5 cm, and (c) 10 kV / 20 cm.

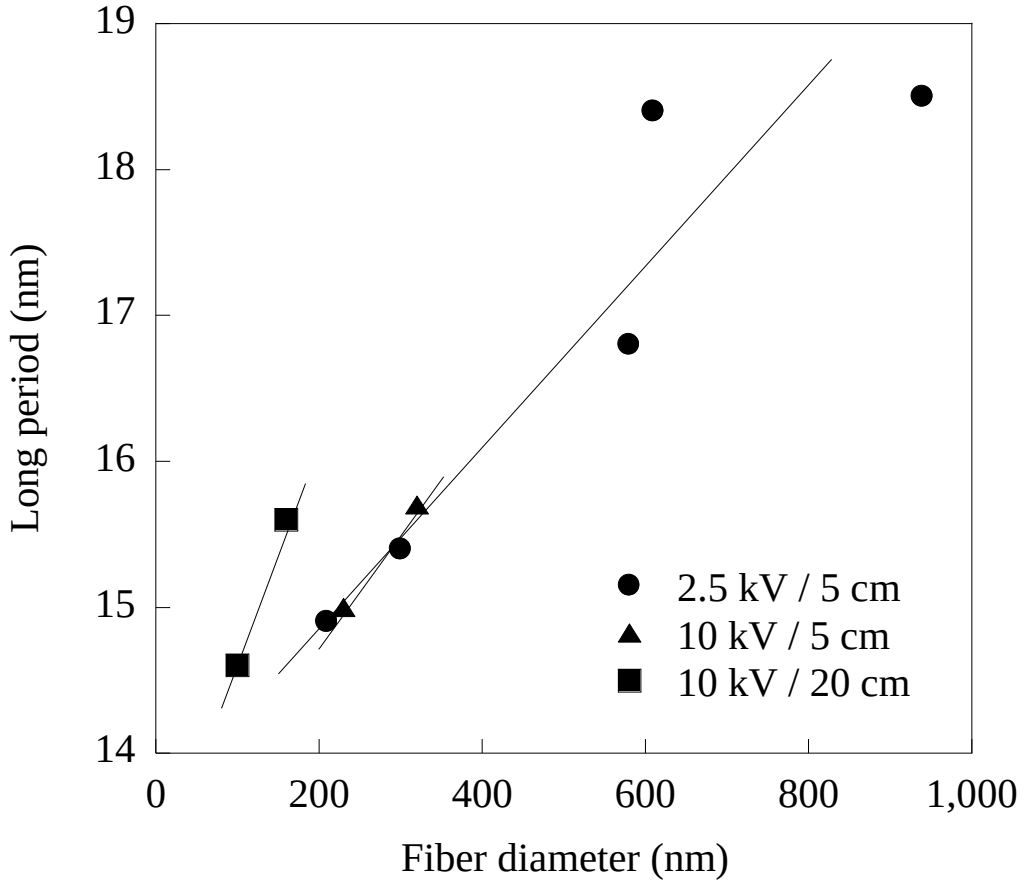

Fig. 1-15 Long period as a function of the fiber diameter for the nanofibers obtained at various conditions.

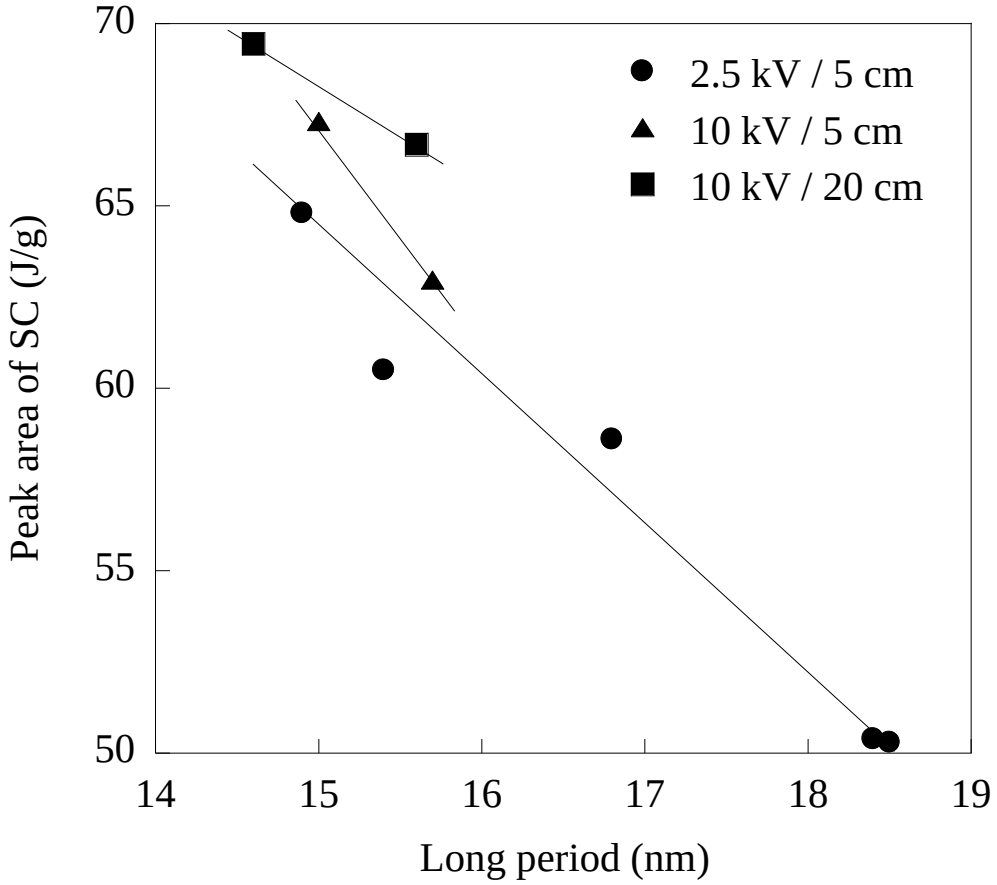

Fig. 1-16 Peak area of SC as a function of the long period of the nano fibers obtained at various conditions.

CHAPTER 2

Structure of Melt-Electrospun PLLA/PDLA Blend Fibers

1. Introduction

Poly(L-lactic acid) (PLLA) is one of the aliphatic polyesters and has a fairly high melting point among them. However its thermal resistance is not high enough to be utilized for textile fibers, structural materials and other applications which require high thermal resistance. One of the fundamental solutions to this poor thermal resistance is to utilize the stereocomplex (SC) formation in the equal blend of PLLA and poly(D-lactic acid) (PDLA), an enantiomer of PLLA reported by Ikada et al.[1] It has been known that the SC has a melting point about 50°C higher than the homo-chiral crystal (HC) of PLLA.[1] De Santis et al.[2] and Hoogsteen et al.[3] reported that the α-form HC is a pseudo-orthorhombic unit cell of dimensions a = 1.07 nm, b = 0.595 nm, and c = 2.78 nm, $\alpha = \beta = \gamma = 90^{o}$, which contains two 10_3 helices. On the other hand, PLA stereocomplex crystalizes in a triclinic unit cell of dimensions a = 0.916 nm, b = 0.916 nm, and c = 0.870 nm, $\alpha = 109.2^{o}$, $\beta = 109.2^{o}$, $\gamma = 109.8^{o}$, in which L-lactide and D-lactide segments are packed parallel taking a 3_1 helical conformation reported by Okihara et al.[4]

Most of studies on the nanofibers prepared by electrospinning have been a solution type. However, only a few studies on the melt-type electrospinning have been made so far. Lyons et al.[5] obtained the melt-electrospun polypropylene fibers by grounding the metallic nozzle of the screw extruder grounded and applying a positive charge to the metal target and investigated the relation between melt-electrospinning condition and fiber diameter. Reneker et al.[6] obtained the polyimide, polypropylene, and polyethylene naphthalate fibers with 1 to 3 μm in diameter by the melt-electrospinning in vacuo.

Although the melt-electrospinning apparatus is complicated and it is difficult to make the fiber with nano-order scale diameter as compared with the electrospinning of the solution type, this process can be carried out solvent free. It is possible to make electrospun stereocomplex PLA fibers either from PLLA/PDLA blend solution or melt.[7] We have reported that the amorphous PLLA fiber was obtained on the fixed target by melt-electrospinning with CO_2 laser and its minimum diameter was 2 μm. Observation with a polarized microscope revealed that the melt-electrospun fiber oriented to the fiber axis.[8] In addition, the fibers taken up by a rotating target were annealed and the crystalline orientation was analyzed by the wide angle

X-ray diffraction (WAXD) method.

In this chapter, PLLA/PDLA blend fibers were obtained by the melt-electrospinning method using the same spinning condition taken for the PLLA fibers reported previously[8] and studied the effect of spinning condition on the fiber diameter and the fiber structure. Further the effect of the annealing was also investigated.

2. Experimental

2.1 Materials

The materials used are PLLA (Mw = 2.90 x 10^5, and Mw/Mn = 2.5) and PDLA (Mw = 2.83 x 10^5, and Mw/Mn = 2.4). Equal amounts of PLLA and PDLA were dissolved in $CHCL_3$/HFIP (9:1) mixed solvent at a concentration of 5 wt% and cast into films of 0.2 mm thick. In addition, PLLA/PDLA blend prepared by the method reported Masaki et al.[9] was also cast into films of 0.2 mm thick. These films were annealed for 5 min at 130°C and cut into ribbons of 1 mm wide.

2.2 Melt-electrospinning

The melt-electrospinning was carried out by using a melt-electrospinning system. This system consist of a CO_2 laser heating device (PIN-011, Onizuca Co. Ltd), a polymer ribbon supplier, high-voltage supplier (Model-600F, Pulse Electronic Engineering), and a metal target. The ribbon-shaped sample was supplied at a constant rate of 0.1 mm/s from metallic pipe. The tip of the ribbon was heated and melted instantaneously with carbon dioxide laser radiated from 4 directions. The melt-electrospinning condition was set at an applied voltage of 20 kV and the distance between the nozzle and the metal target of 5 cm. The laser outputs were set at 10, 14, and 20 W. Unfortunately the temperature of the polymer melt at the point of laser irradiation was not able to be measured. The uniaxially aligned melt-electrospun fibers were obtained by using a rotating metal target. The surface velocity of the rotating target was set at 78.5 cm/s (100 rpm of rotating velocity). For comparison, some of the fibers were collected on a fixed flat target. The fibers prepared were annealed for 5 min at temperatures between 130 and 190°C keeping the fiber length constant.

2.3 Measurements and observation

2.3.1 Morphology

Morphology was observed by using a scanning electron microscope (SEM, VE-7800,

KEYENCE). The average diameter of 50 filaments was determined from the SEM image. Selected-area electron diffraction (SAED) measurements were carried out by a transmission electron microscope (TEM) (JEM-200CS, JEOL Ltd) and the diffraction patterns and the bright-field images were recorded on the Kodak® electron image film (SO-163, Kodak Ltd., Japan). Accelerating voltage was set up at 200 kV. The sample was fixed to copper grid by neoprene rubber bond (Bioden Mesh Cement, Okenshoji Co., Ltd.).

2.3.2 Differential scanning calorimetry (DSC)

Thermal analyses were carried out by using a DSC (DSC-50, Shimadzu) under a nitrogen atmosphere. About 2.0 mg amount of sample was sealed in an aluminum pan. The heating process was carried out to 250°C at a heating rate 10°C/min. Melting temperature and crystallization temperature were determined from the top of the endothermic and the exothermic peaks. Crystallinity was calculated by using 142 J/g of equilibrium fusion enthalpy reported by Loomis et al.[10]

2.3.3 Wide angle X-ray diffraction (WAXD)

WAXD patterns and spectra were obtained at room temperature using a nickel-filtered CuKα radiation of the wave-length 0.1542 nm, from a RAD2C (Rigaku) sealed beam X-ray generator operating at 40 kV and 20 mA. X-ray beam was irradiated to the uniaxailly aligned bundle of fibers in the direction to perpendicular to the fiber axis for 15 min and the pattern was recorded on the imaging plate.

3. Results and discussion

3.1 Fiber diameter

Fig. 2-1 shows the average diameter of the fibers collected on the rotating target at various irradiation laser outputs. Although there are some fiber diameter distributions, the fiber diameter tended to be thinner with increasing irradiation laser output. When the irradiation laser output was 20 W, the fiber of the diameter ranging from 3 to 4 μm was obtained. Although the minimum PLA fiber diameters obtained in the solution electrospinning have been reported to be in the range between 700 nm and 2 μm [5-6, 11-13], PLA fibers obtained by melt-electrospinning are much thicker. This may be because the viscosity of the melt rapidly increases as the temperature approaching to the glass transition temperature (Tg) and the fiber solidifies, while the viscosity of the solution gradually increases with the solvent

evaporation. Quench the melt to the room temperature prevented the sufficient extensional deformation, since the Tg of PLA is higher than the room temperature. Zhou et al.[11] pointed out that the high spinning temperature, small nozzle diameter, atmospherics temperature above Tg, and high voltage are necessary to obtained the PLA fibers with sub-micron diameter. However, the melt-electrospun fibers obtained in this study have much thinner diameter as compared with those of the PLA stereocomplex fibers (~ 20 μm) obtained by the conventional melt-spinning process.[14-15] The distribution of the fiber diameter shown in Fig. 2-2 shifted to the smaller diameter direction and tended to be sharper with increasing irradiation laser outputs. The diameter of the melt-electrospun fibers is considered to be affected by the melt viscosity, similarly to the solution-electrospinning process. Increase in the laser output increases the melt temperature and decreases the melt viscosity, and accordingly decreases the fiber diameter. SEM images of PLLA/PDLA blend fibers obtained on the rotating target at various irradiation laser outputs are shown in Fig. 2-3. The fibers of circular cross-section were obtained irrespective of irradiation laser outputs.

Our previous study on the PLLA melt-electrospun fiber showed the similar shift of the fiber diameter to smaller diameter with increasing laser output.[8] Although the PLLA ribbon-like fibers were obtained in the previous study, only the fibers with a circular cross-section were observed in this study.

3.2 Thermal property

DSC curves of the fibers taken-up on the rotating target at various laser outputs are shown in Fig. 2-4. Fig. 2-4 includes the curve of the annealed film for comparison. The film annealed at 130°C did not show a crystallization peak because it was well crystallized in the annealing process. Instead it showed a large melting peak of α-form HC around 175°C and a small melting peak of SC around 220°C, respectively. On the other hand, all the fibers showed a crystallization peak around 95°C, which tended to be larger with increasing laser output. The melting peaks of HC and SC were observed around 170°C and around 220°C, respectively. The melting peak of α-form HC tended to be smaller and that of SC tended to be larger with increasing laser output. However, these melting peaks include those of the crystal formed in the DSC heating process. This suggests that the as-spun fiber has a pre-structure which easily transformed to SC rather than HC and the fibers are considered to have more pre-structure as the laser output increases. In order to confirm this, the thermal property of the annealed fiber was determined.

Fig. 2-5 shows the DSC curves of the fibers annealed at 150°C keeping the fiber length constant. Crystallization peak around 95°C observed before annealing was disappeared. The melting peak of HC was observed around 170°C and the peak area decreased with the laser output. On the other hand, the melting peak of SC was observed around 220°C and it increased with the laser output. Melting peak area is in proportion to the crystallinity, and the crystallinity of SC reached as high as 42 % and that of HC was suppressed to 6 % when the laser output was 20 W.

Fig. 2-6 shows the DSC curves of the fibers obtained on the fixed target and annealed at 150°C keeping the fiber length constant. The tendency is very similar to that shown in Fig. 2-5. Therefore, the extension of the fiber by the mechanical take-up at the velocity applied in this study did not affect the higher-order structure significantly.

3.3 Higher-order structure

WAXD patterns of as-spun fibers did not show any trace of the crystalline reflections and only the amorphous halo was observed regardless of the laser output.

Generally PLLA is melt-spun into amorphous fibers. Similarly the melt-electrospun PLLA fibers are also amorphous as shown in the previous report.[8] WAXD patterns of the fibers annealed at various temperatures were shown in Figs. 2-7 ~ 2-10. Further the equatorial WAXD spectra obtained from these patterns are shown in Fig. 2-11. Annealed fibers showed a diffraction at 2θ value around 16.5^{o} indexed as (110)/(200) of HC [3] and the diffractions at 2θ values around 12° and 22° indexed as (100)/(010)/(-110) and (110)/(-120)/(-210) of SC [16]. The tendency of the reflection from α-form HC to slightly concentrate on the equator indicates the slight crystalline orientation of HC. On the other hand, the reflections from SC were observed as rings although the intensity on the equator is slightly high. The intensity of ring-like SC shown in Figs. 2-7 ~ 2-10 increase with the laser output and are higher than the ark-like α-form HC regardless of the annealing temperature. Especially the fibers annealed at elevated temperatures (150°C and 170°C) show a much stronger SC reflection than those of α-form HC. The ratio of the intensity of SC at 2θ = 12° to that of α-form HC at 2θ = 16.5^{o} was given to the Fig. 2-11. The ratio SC/HC increases with the laser output and annealing temperature. It should be noted that the reflection from α-form HC was completely disappeared when the fiber was annealed at 190°C.

The stereocomplexation in PLLA/PDLA blend fiber has been known to be promoted by applying the drawing and annealing processes[14-15]. In this study, the molecular or crystalline

orientation was not significantly given to the fiber, although the crystallization of SC improved by the increase in the laser output. The melt viscosity of PLA decreases with increasing laser output and the melt can be highly extended by the electrostatic force. This large extensional deformation may increase the interfacial eare between PLLA and PDLA phases and promoted the stereocomplexation.

For comparison, PLLA and PDLA were melt-blended according to the method reported by Masaki et al.[9] PLLA/PDLA blend prepared in this method only forms SC without forming any trace of HC. Melt-electrospun fiber was obtained from this blend and annealed at 150°C. Although as-spun fiber was in an amorphous state, the orientation of the amorphous chains to the fiber direction was confirmed by using a polarizing optical microscope. WAXD patterns of these fibers obtained at various laser output show only ring-like reflection from SC (Fig. 2-12). Therefore, it may be concluded that the molecular or crystalline orientation of SC cannot be given to the melt-electrospun fibers obtained even from the PLLA/PDLA blend which only forms SC. This may suggest that the orientation of SC relaxes in the crystallization process although HC may crystallize without relaxing the orientation.

Among the fibers obtained at a laser output of 20 W and annealed at 150°C, two fibers with average fiber diameters of 400 nm and 900 nm were selected and TEM bright-field images (Fig. 2-13 (a) and (c)) and SAED patterns (Fig. 2-13 (b) and (d)) were obtained. The fiber with an average diameter of 400 nm ((a) and (b)) showed both reflections of α-form HC indexed as (110)/(200) and of SC indexed as (100)/(010)/(-110), (110)/(-120)/(-210), and (200)/(020)/(-220). The reflections from both of HC and SC are arc-like suggesting the fiber has more or less oriented. On the other hand, the fiber with an average diameter of 900 nm ((c) and (d)) showed only ring-like reflection from SC indexed as (110)/(-120)/(-210). In general, the fibers obtained by electrospinning have a broad diameter distribution. Yoshioka et al.[17] reported that the electrospun polyethylene fibers have different degree of orientation depending on the fiber diameter, and revealed by TEM observation that the thinner fiber, the higher the orientation.

TEM patterns shown in Fig. 2-13 show that only the fiber with an average fiber diameter of 400 nm shows the crystalline orientation. However the fiber diameter distribution shown in Fig. 2-3 indicates the majority of the fibers have an average diameter ranging from 1 to 4 μm and only a small fraction of the fibers has a diameter around 400 nm. Therefore, it may be concluded that the WAXD ring-like SC reflection shown in Fig. 2-7 are from SC in the fibers with the diameters larger than 1 μm.

4. Conclusion

The blend of poly(L-lactic acid) (PLLA) and poly(D-lactic acid) (PDLA) were laser heated melt-electrospun into fibers with average diameters ranging from 3 ~ 6 μm. These fibers have crystalline forms of both α-form homo-chiral crystal (HC) and the stereocomplex (SC). WAXD measurements of annealed fibers revealed that the fibers have coexistence of more or less uniaxially oriented α-form HC and almost unoriented SC. The α-form HC was almost completely disappeared after annealing at 190°C and the fiber with SC as a unique crystalline component was obtained. Further, it was found that both α-form HC and SC in the thinner fibers with a diameter around 400 nm are uniaxially orientated to the fiber direction. Therefore, the orientation of SC was more strongly affected by the fiber diameter than α-form HC.

References

1. Y. Ikada, K. Jamshidi, H. Tsuji, and S. H. Hyon, *Macromolecules*, **20**, 904 (1987).
2. P. De Santis and A. J. Kovac, *Biopolymer*, **6**, 299 (1968).
3. W.Hoogsteen, A. R. Postema, A. J. Pennings, G. ten Brinke, and P. Zgenmaier, *Macromolecules*, **23**, 634 (1990).
4. T. Okihara, M. Tsuji, A. Kawaguchi, K. Katayama, *Journal of Macromolecular Science: Physics*, **B30(1&2)**, 119 (1991). / H. Tsuji, *Macromolecules Bioscience*, **5**, 569 (2005).
5. J. Lyons, C. Li, and F. Ko, *Polymer*, **45**, 7597 (2004).
6. D. H. Reneker, H. Hou, R. Rangkupan, and J. D. Lennhoff , *Polymer Preprints*, **44**(2), 68 (2003).
7. Japan Patent Kokai 2008-115503 (2008).
8. G. Nishikawa, M. Yamamoto, A. M. Afifi, Y. Kawahara and H. Yamane, *Sen'i Gakkaishi*, **66**, 124 (2010).
9. D. Masaki, Y. Fukui, K. Toyohara, M. Ikegami, B. Nagasaka, and H. Yamane, *Sen'i Gakkaishi*, **64**, 212 (2008).
10. G. L. Loomis, J. R. Murdoch and K. H. Gardner, *Polymer Preprints*, **31(2)**, 55 (1990).
11. H. Zhou, T. B. Green, and Y. L. Joo , *Polymer*, **45**, 7597 (2004).
12. P. D. Dalton, K. Klinkhammer, J. Salber, D. Klee, and M. Möller, *Biomacromolecules*, **7**, 686(2006).
13. N. Ogata, S. Yamaguchi, N. Shimada, G. Lu, T. Iwata, K. Nakane, and T. Ogihara, *Journal of Applied Polymer Science*, **104**, 1640 (2007).
14. Y. Furuhashi, Y. Kimura, N. Yoshie, and H. Yamane , *Polymer*, **47**, 5963 (2006).
15. M. Takasaki, H. Ito, and T. Kikutani, *Polymer Journal of Macromolecular Science*, **B42**, 403 (2003).
16. D. Brizzolara, H. -H. Cantow, K. Diederichs, E. Keller, A. J. Domb, *Macromolecules*, **29**, 191 (1996).
17. T. Yoshioka, R. Dersch, M. Tsuji, and A. K. Schaper, *Polymer*, **51**, 2383 (2010).

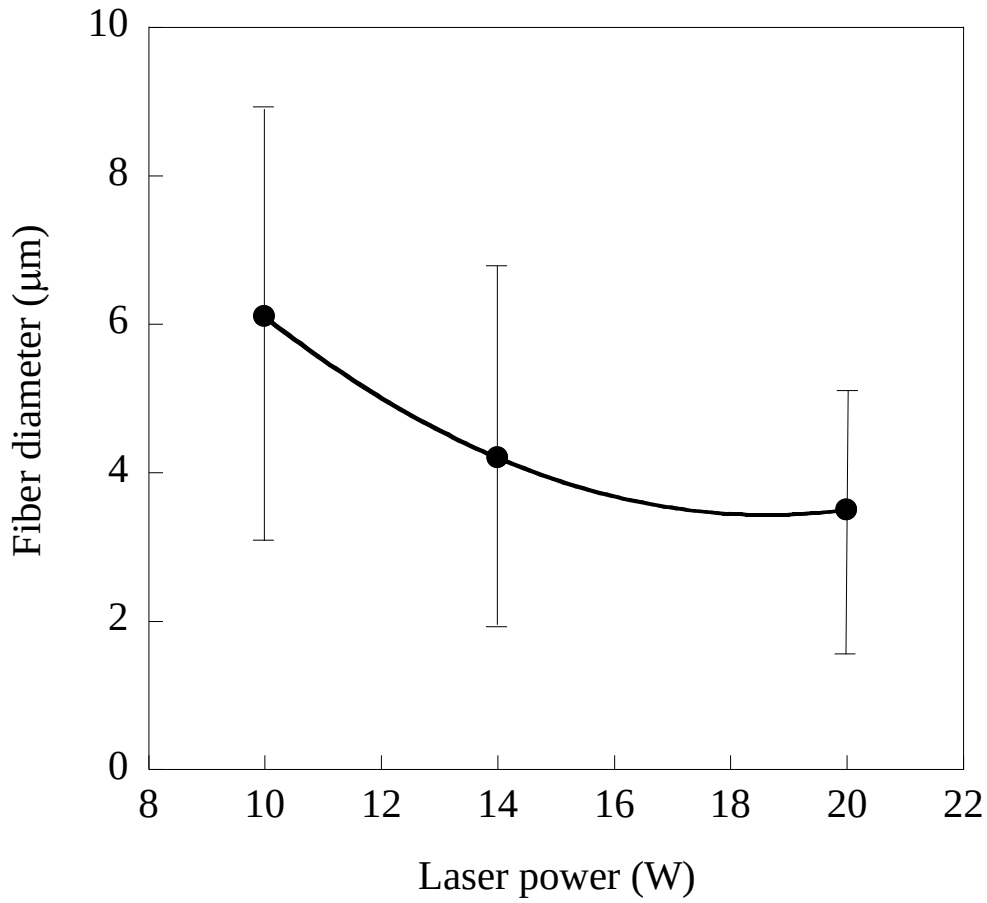

Fig. 2-1 Diameters of PLLA/PDLA blend melt-electrospun fibers obtained at various applied laser power.

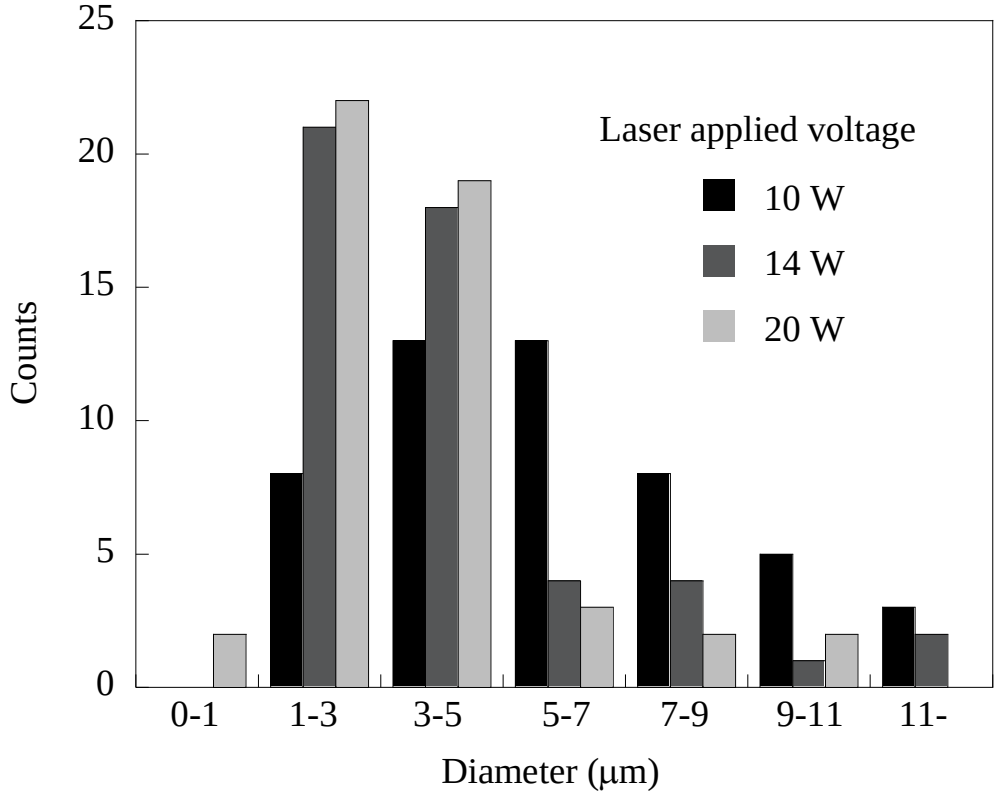

Fig. 2-2 Diameter distribution of PLLA/PDLA blend melt-electrospun fibers collected on the rotating collectors.

(a) 10 W

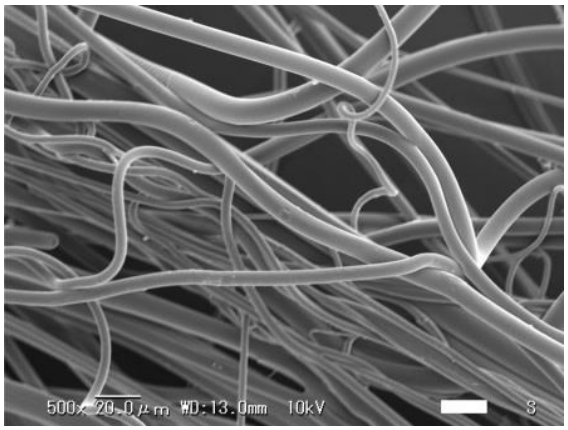

(b) 14 W

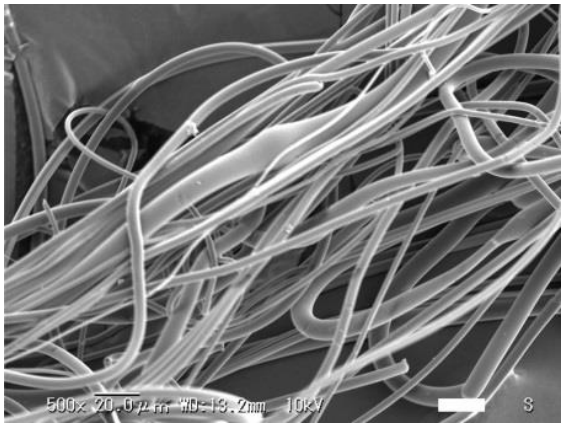

(c) 20 W

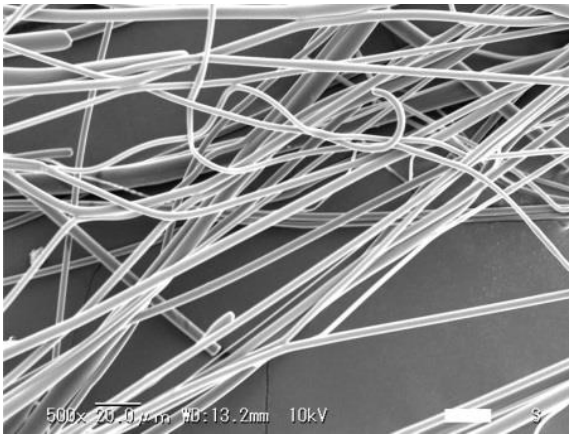

Fig. 2-3 SEM images of PLLA/PDLA blend melt-electrospun fibers collected on the rotating metallic collector. Scale bar indicates 20 μm.

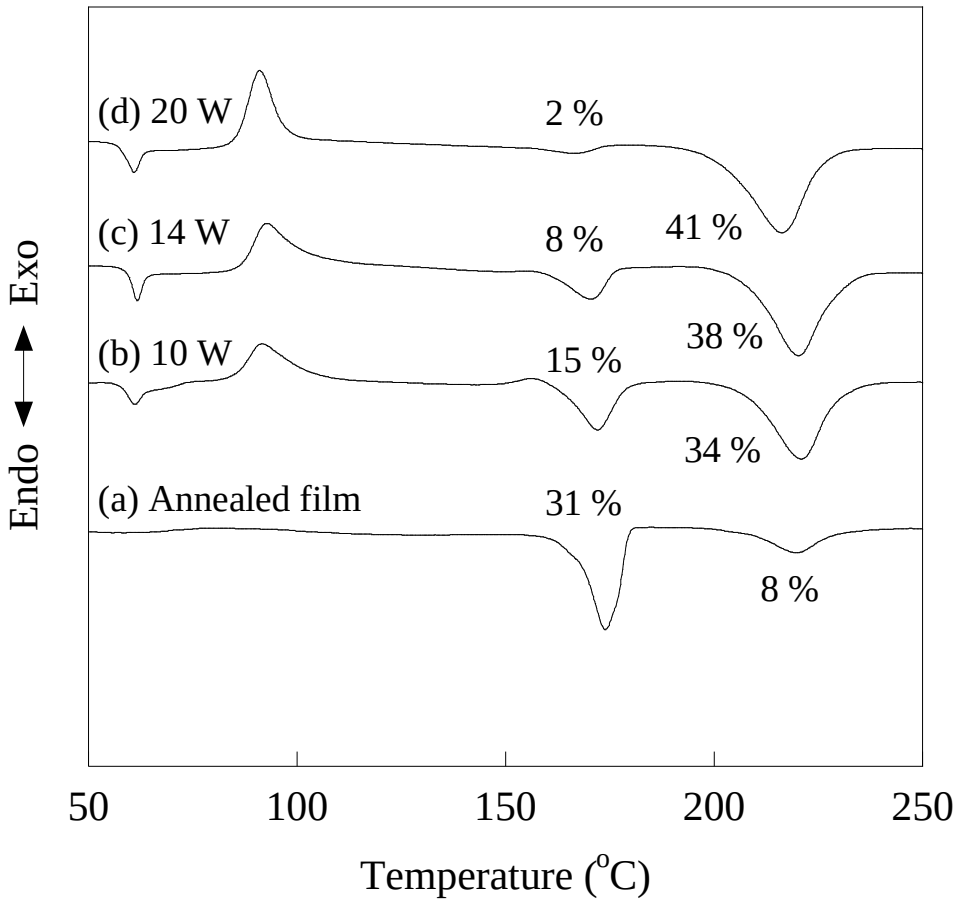

Fig. 2-4 DSC curves of the PLLA/PDLA blend melt-electrospun fibers collected on the rotating target.

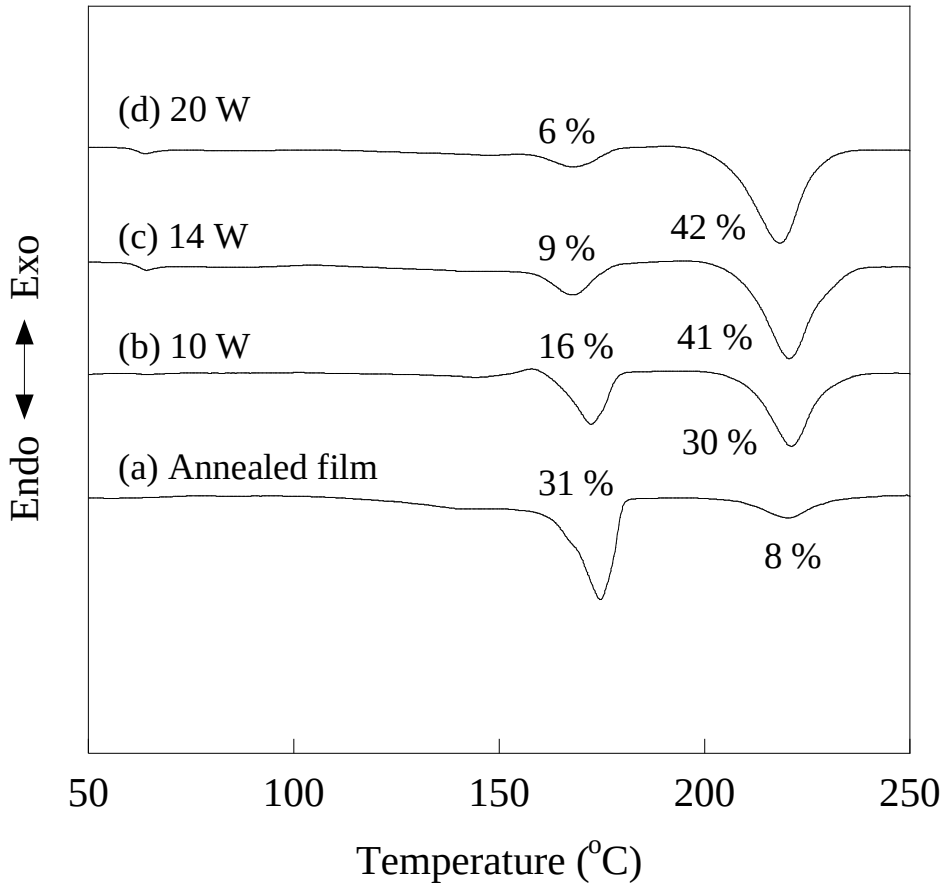

Fig. 2-5 DSC curves of PLLA/PDLA blend fiber melt-electrospun on the rotating target and annealed at 150°C.

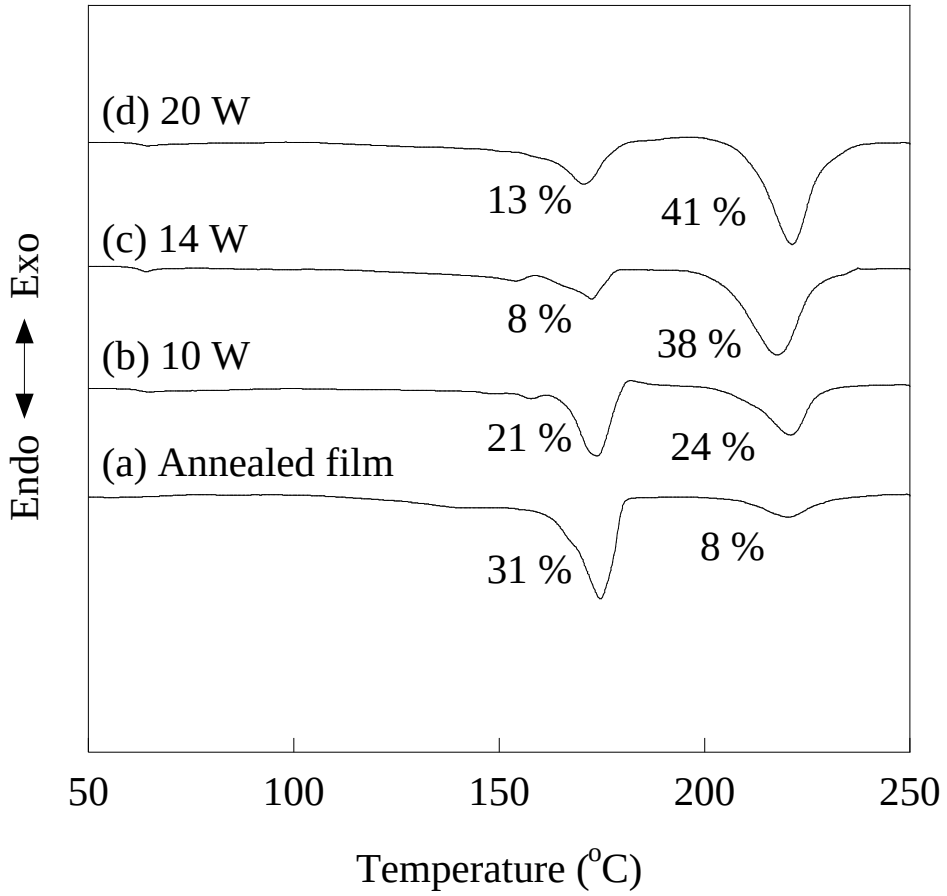

Fig. 2-6 DSC curves of PLLA/PDLA blend fiber melt-electrospun on the flat target and annealed at 150°C.

(a) 10 W

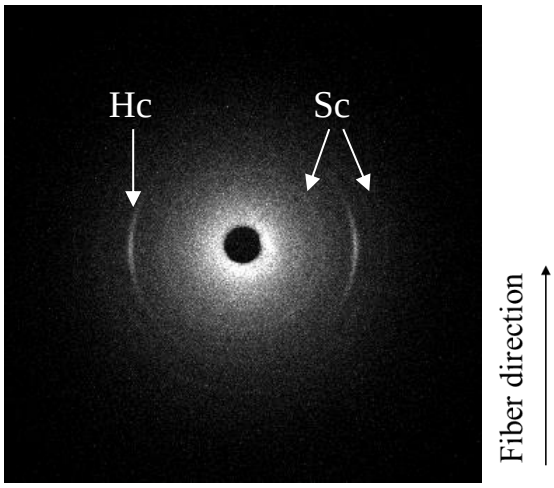

(b) 14 W

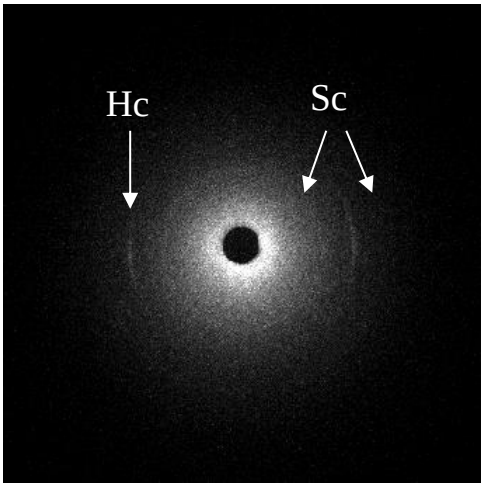

(c) 20 W

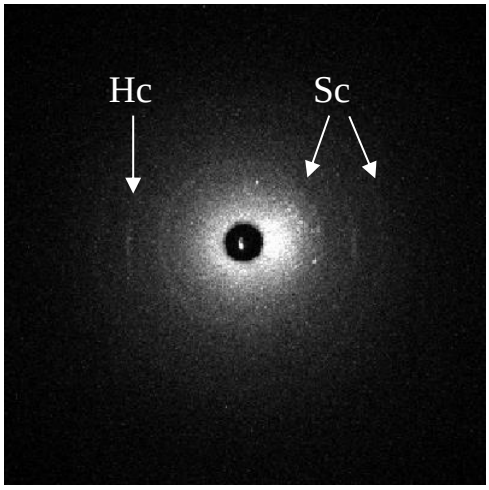

Fig. 2-7 WAXD patterns of PLLA/PDLA blend fibers melt-electrospun on the rotating target and annealed at 130°C.

(a) 10 W

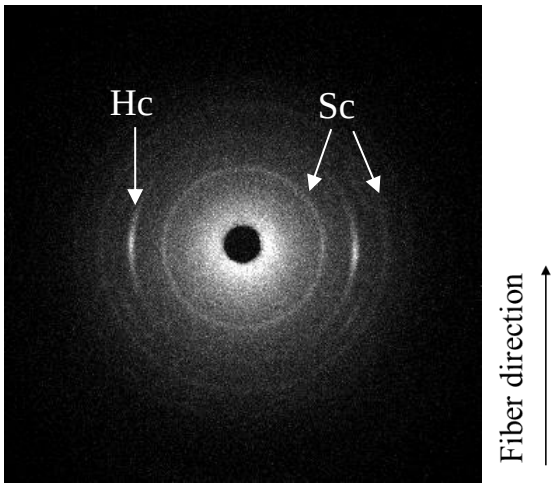

(b) 14 W

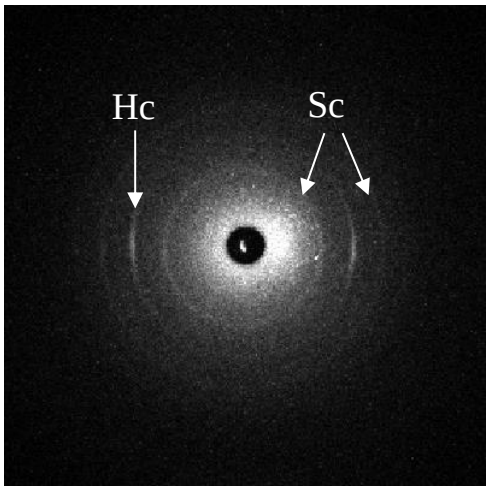

(c) 20 W

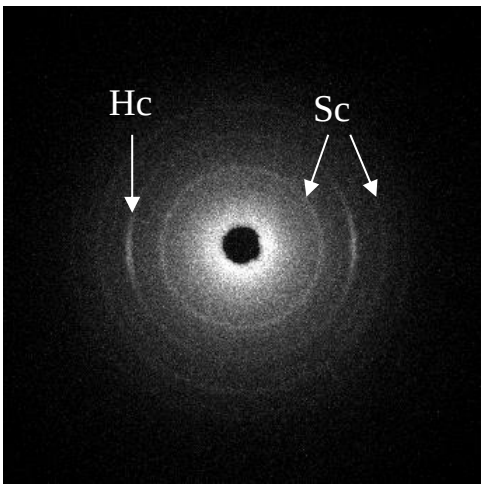

Fig. 2-8 WAXD patterns of PLLA/PDLA blend fibers melt-electrospun on the rotating target and annealed at 150°C.

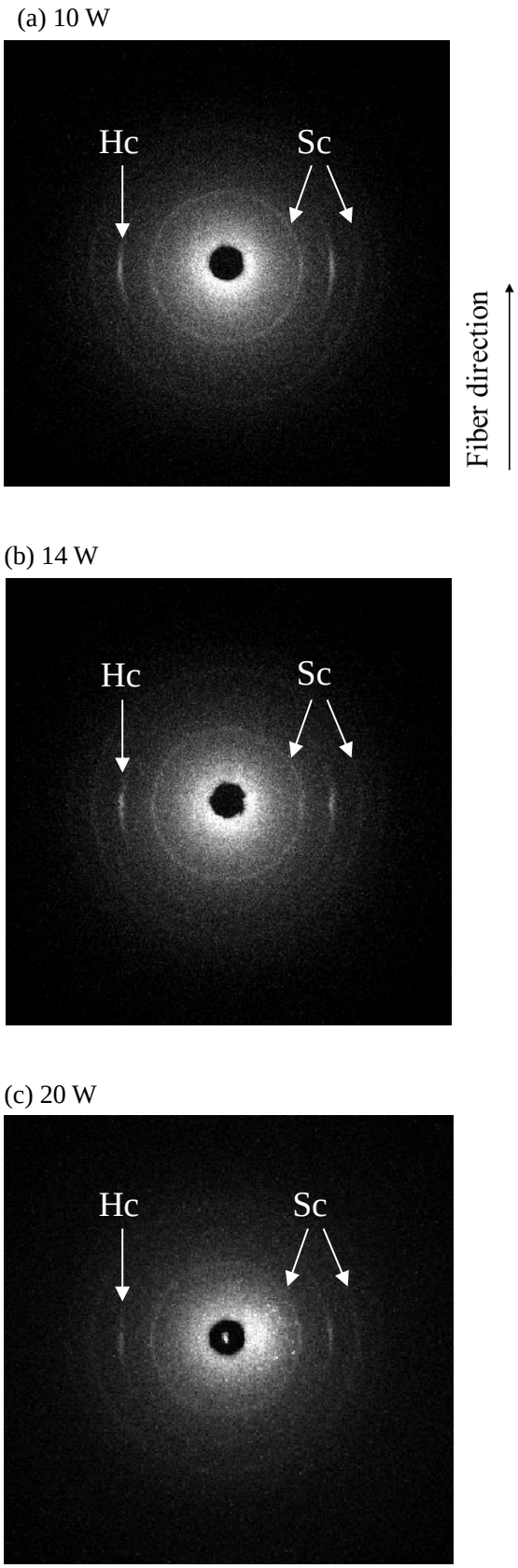

Fig. 2-9 WAXD patterns of PLLA/PDLA blend fibers melt-electrospun on the rotating target and annealed at 170°C.

(a) 10 W

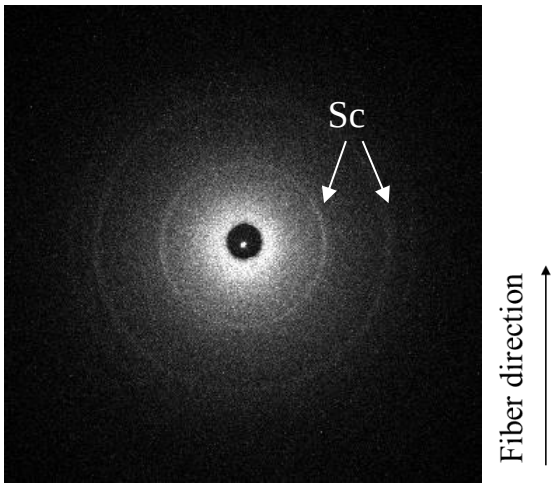

(b) 14 W

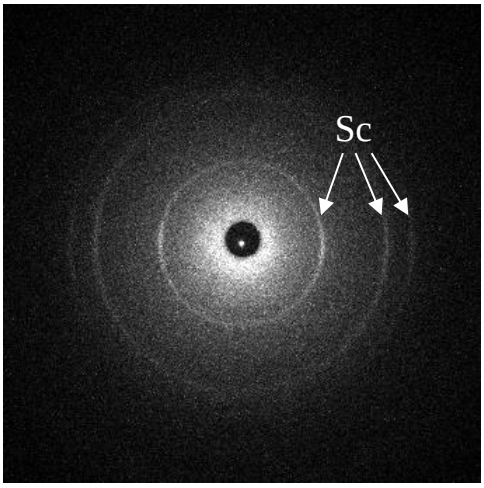

(c) 20 W

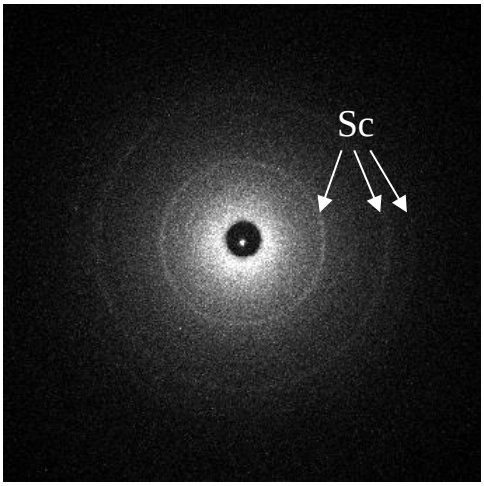

Fig. 2-10 WAXD patterns of PLLA/PDLA blend fibers melt-electrospun on the rotating target and annealed at 190°C.

(a) Annealed at 130°C

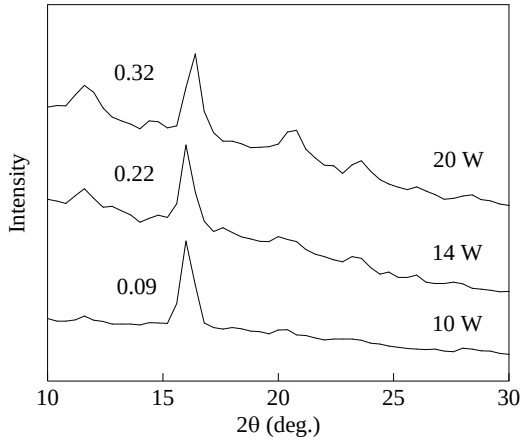

(b) Annealed at 150°C

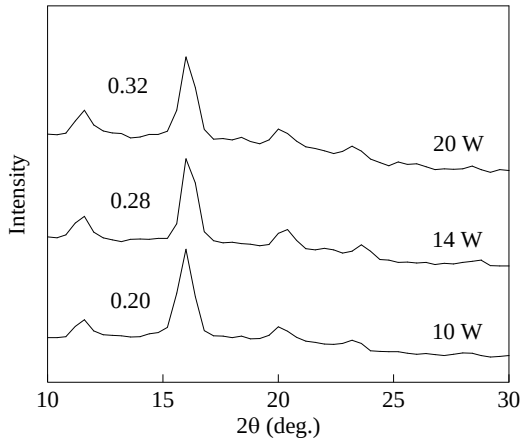

(c) Annealed at 170°C

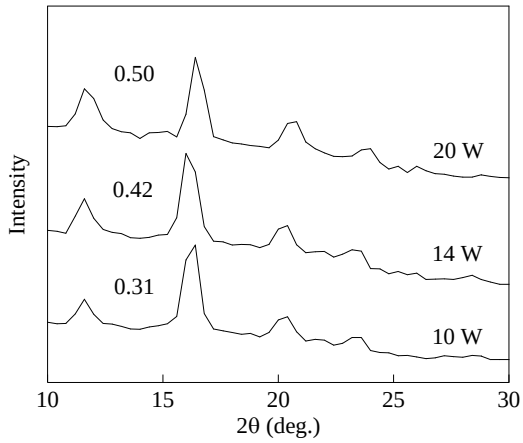

Fig. 2-11 WAXD equatorial spectra of PLLA/PDLA blend melt-electrospun fibers annealed at various temperatures. Numbers in the figures are the applied laser powers and Sc/Hc ratios.

(a) 10 W

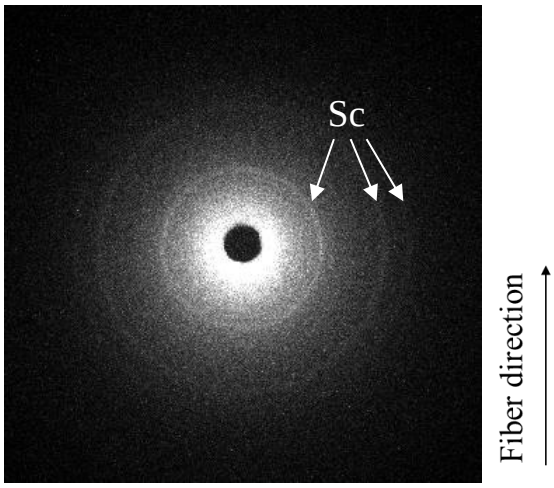

(b) 14 W

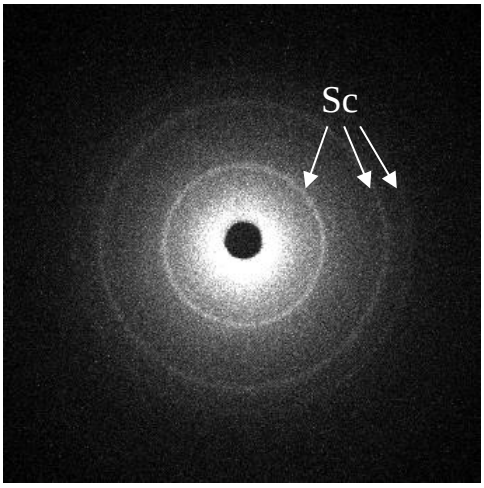

(c) 20 W

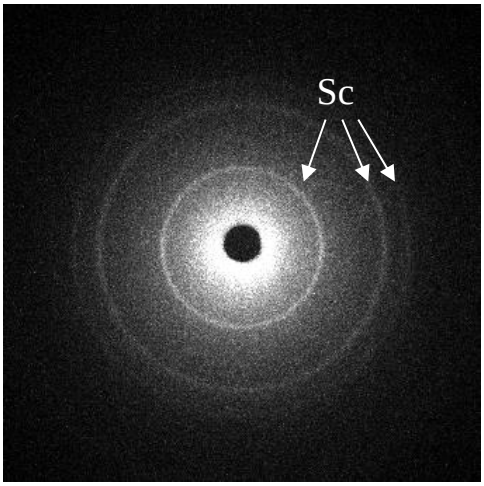

Fig. 2-12 WAXD patterns of melt-electrospun fibers annealed at 150°C prepared from melt blended PLLA/PDLA according to Masaki et al.[10]

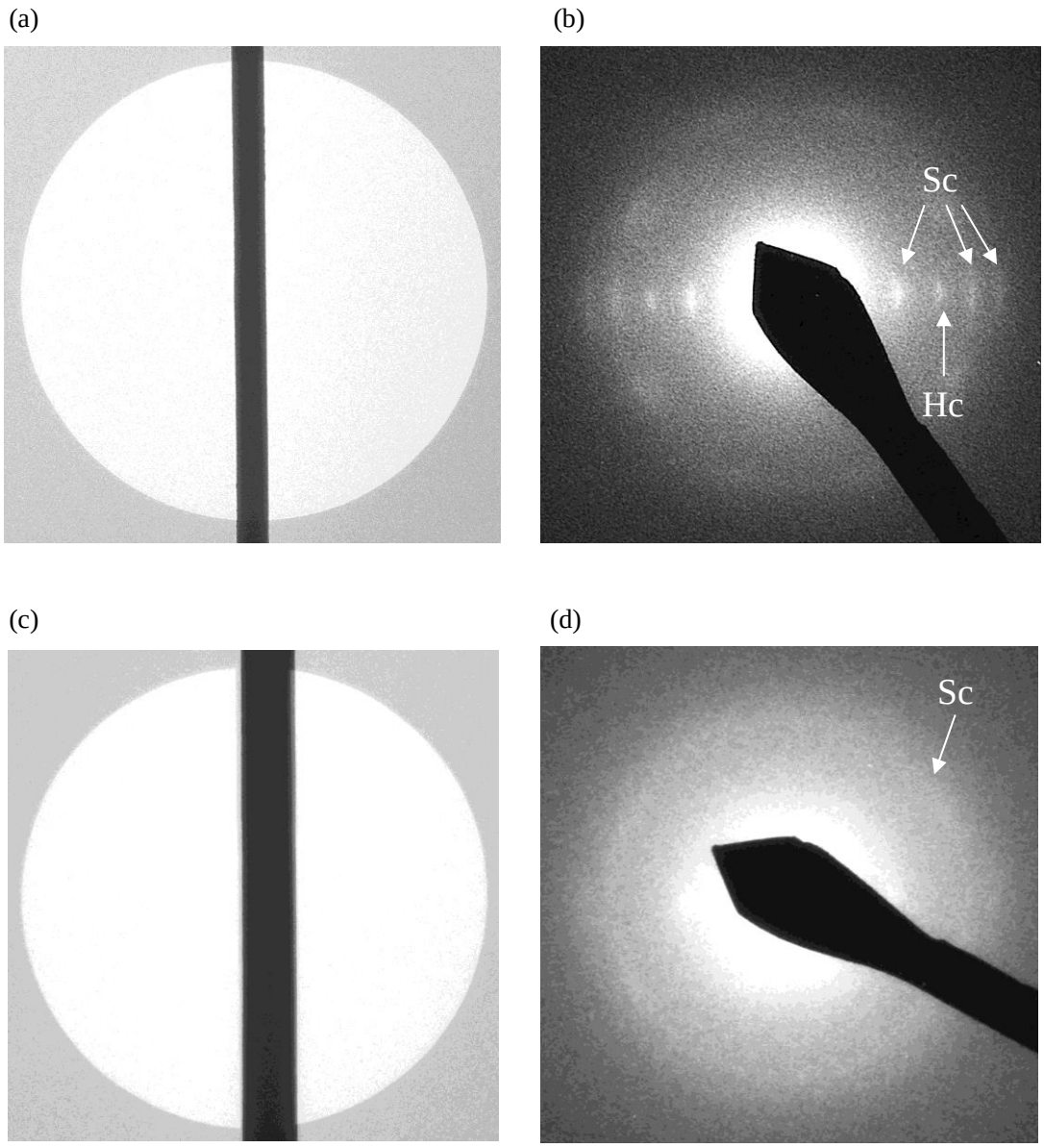

Fig. 2-13 TEM defocus contrast images ((a) and (c)) and corresponding SAED patterns ((b) and (d)) for the PLLA/PDLA blend monofilaments melt-electrospun at a laser power of 20W and annealed at150°C. The diameter of selected-area aperture on the object plane (i.e., at the sample position) is approximately 8 μm in (a) and (c): Circles in (a) and (c) indicate the size and shape of the aperture. Fiber diameters are about 400 nm for (a) and (b), and about 900 nm for (c) and (d).

CHAPTER 3

Effect of the take-up velocity on the higher-order structure of the melt-electrospun PLLA/PDLA blend fibers

1. Introduction

Poly(lactic acid) (PLA), one of the typical bio-based materials has been applied in the medical and agriculture fields. In addition, PLA is expected as an alternative to the petroleum-based plastics because of its fairly high melting point among various aliphatic polyesters and a good mechanical property. However the application has been restricted due to the insufficient thermal resistance in comparison to the other synthetic polymers used for the textile fibers. One of the way to solve this problem is to utilize the stereocomplex crystal (SC) which forms in the equal blend of poly(L-lactic acid) (PLLA) and poly(D-lactic) (PDLA), first reported by Ikada et al.[1] It has been known that SC has a melting point about 235°C higher than that of the homo-chiral crystal (HC) of PLLA.

The HC is crystallized in a pseudo-orthorhombic unit cell with parameters for a = 1.07 nm, b = 0.595 nm, c (fiber axis) = 2.78 nm, and $\alpha = \beta = \gamma = 90^{o}$ reported by De Santis et al.[2] Two 10_3 helices are contained in the unit cell of HC. On the other hand, the SC shows different crystal structure from that of HC. The SC system is triclinic ($P1$) with cell dimensions: a = 0.916 nm, b = 0.916 nm, c (chain axis) = 0.870 nm, α = 109.2º, β = 109.2º, γ = 109.8º reported by Okihara et al.[3] In the unit cell, PLLA and PDLA segments are contained as a pair and packed laterally in parallel fashion. The SC takes a 3_1 helical conformation, which is extended a little from a 10_3 helix in the HC. Several reports[4-7] have indicated that both SC and HC of each component co-exist in the PLLA/PDLA prepared by the simple blending. Takasaki et al.[6] reported on the development of SC of PLLA/PDLA blend by high-speed melt spinning process. They showed that the PLLA/PDLA blend fibers taken-up at high velocities indicated highly oriented and highly crystallized structure containing both α-form of HC and SC. However the fiber contained mainly SC after drawing and subsequent annealing at 190°C. Masaki et al.[8] took a special blending technique and prepared the PLLA/PDLA blend in which only SC form. They reported that the melt-spun fibers drawn and annealed at an optimum condition have SC as a unique crystalline component and show an excellent thermal stability.

Various trials have been made to produce thermally resistant PLA fibers obtained by the

melt-spinning and the solution-spinning methods.[6-9] Recently, the studies on the production of PLLA/PDLA blend electrospun nanofibers have been reported.[10-12] Electrospinning is a facile method of producing fibers of nano-order diameters from polymer solution. Electrospinning system consists of the extrusion device, high voltage generator, and the metal target. A high voltage is applied between the polymeric liquids and the metal target. When electrostatic force exceeds the surface tension of the polymeric liquid, the liquid jets are drawn from the spinneret and carried to the metal target.

Present authors[13] have investigated the effects of the electrospinning condition on the higher-order structure and the stereocomplex (SC) formation of the nanofibers from the PLLA/PDLA blend solution taken-up on the rotating target. The fibers collected on the fixed target have almost no crystalline orientation to any particular direction. However the crystalline orientation increased significantly with the take-up velocity. Although the amount of SC in the fiber showed a linear correlation to the crystalline orientation, there was a fairly large variation. The fiber diameter showed a more apparent correlation to the amount of SC.

Recently, the researches on the melt-electrospinning have attracted the attention. Although the fibers with nano-order scale may not be obtained in this process, its solvent free process is considered to be environmentally friendly. Nishikawa et al.[14] reported the structure of the PLLA/PDLA melt-electrospun nanofibers collecting on a flat target and a target rotating at a fairly low velocity. They showed that the melting endotherm of SC became larger and sharper while that of HC became smaller with increasing laser output power. The X-ray diffraction patterns of the annealed fibers indicated the coexistence of an oriented Hc and a randomly oriented Sc. However the selected-area electron diffraction pattern revealed that Sc in the annealed very fine fiber has higher degree of orientations of Hc and Sc to the fiber direction than those in the fiber with a larger diameter.

It is a purpose of this chapter to investigate the higher-order structure of the melt-electrospun fibers of PLLA/PDLA blends taken-up on a target rotating setting the other melt-electrospinning conditions to the same as those taken by Nishikawa et al.[14]

2. Experimental

2.1 Materials

The materials used were PLLA (Mw = 2.90 x 10^5, and Mn = 1.18 x 10^5) and PDLA (Mw = 2.83 x 10^5, and Mn = 1.17 x 10^5). Equal amounts of PLLA and PDLA were dissolved in $CHCL_3$ and 1,1,1,3,3,3-hexafluoro-2-propanol (HFIP) (9:1) mixed solvent at a concentration

of 5 wt%. Cast films with a thickness of 0.2 mm were prepared from the solution and were annealed at 130°C for 5 min. The films were cut into long rectangular rods with a width of 1 mm.

2.2 Melt-electrospinning

Fig. 3-1 shows a melt-electrospinning set-up used in this study. The melt-electrospinning system consists of a CO_2 layzer system equipped with a feeding device (PIN-30R, Onizuca Glass Co. Ltd), a high voltage supply (Model-600F, Pulse Electronic Engineering), and a take-up device. The rod-shaped sample was fed at a constant rate of 0.1 mm/s from a metallic pipe. The laser beam from the emitter was split into 4 beams and radiated to the sample from 4 directions, and the sample was melted instantaneously. Meanwhile the high voltage was applied between the melt and the target. The jets from the nozzle were carried to the target rotating at the velocities ranging from 100 m/min to 1,130 m/min. The melt-electrospinning condition was set at the applied voltages of 20 kV, the distances between the nozzle and the metal target of 5 cm, and the irradiation laser of 20W. The uniaxially aligned melt-electrospun fibers were obtained on a rotating metal target. For comparison, some of the fibers were collected on a fixed flat target.

2.3 Measurements and observations

Morphology was observed by using a scanning electron microscope (SEM) (VE-7800, KEYENCE). The samples were coated with gold prior to the observation. Thermal analyses were carried out by using a DSC (DSC3100SA, Bruker axs) under a nitrogen atmosphere. The heating rate was set at 10°C/min. Wide-angle X-ray diffraction (WAXD) patterns and spectra were obtained at room temperature using a nickel-filtered CuKα radiation of the wave-length 0.1542 nm, from a X-ray generater (CN4037A1, Rigaku) sealed beam X-ray generator operating at 40 kV and 20 mA. The distance between sample and camera was 63 mm.

3. Results and discussion

3.1 Morphology

SEM images and the average fiber diameter of the fibers taken-up at various velocities are shown in Figs. 3-2 and 3-3, respectively. The diameter distributions were added to Fig. 3-3.

As spun fibers collected on the fixed target and the rotating target at velocities up to 100

m/min were randomly accumulated without showing almost no orientation to any particular directions and the diameter distribution was broad. The fibers obtained on the target rotating at velocities higher than 300 m/min were more or less aligned. The diameter distribution tended to be much narrower with increasing take-up velocity. This may suggest that the velocity of the jet stretched by the electrostatic force may be lower than 300 m/min so that the fibers were further extended when the take-up velocity was higher than 300 m/min.

The average fiber diameter of the fiber taken-up at 1,130 m/min, the maximum take-up velocity, is close to 1 μm. Unfortunately, any fibers with nano-order scale diameter were obtained. This diameter is about 10 times larger than that of the electrospun fibers taken-up at the same velocity obtained from the PLLA/PDLA solution.[13]

3.2 Thermal Analyses

DSC thrmograms of the fibers taken-up at various velocities are shown in Fig. 3-4. The fibers collected on the fixed target and on the target rotating at low velocities showed a crystallization peak around 95°C and the melting peak of HC and SC around 172°C and 222°C, respectively. When the take-up velocity exceeded 600 m/min, the crystallization peak at 95°C turned to be smaller and another exothermic peak appeared around 75°C. The melting peak of HC observed around 172°C became smaller and that of SC observed around 222°C became larger with increasing take-up velocity.

It has been known that the randomly oriented PLLA crystallizes into HC very slowly while the mixture of PLLA and PDLA crystallizes into SC at a much higher rate than HC.[8] PLLA and PDLA chains in the fibers collected on a fixed target and a target rotating at a low velocity stayed almost in an amorphous state and could not crystallize into HC in the DSC heating process. However those chains well mixed rapidly crystallized into SC when they were heated in the DSC process. This may be a reason why DSC curves of these fibers showed a crystallization peak around 95°C without showing any exothermic peaks around 75°C. When the fibers were taken-up at higher velocities, PLLA and PDLA chains were stretched rapidly, oriented to the fiber direction and crystallized into SC in the electrospinning process. However some of the oriented chains which could not crystallize into SC in the spinning process stayed in an amorphous state. Since these chains were highly oriented, they can crystallize into HC in the DSC heating process.

The melting peak areas of SC and HC were plotted in Figs. 3-5(a) and (b) as functions of the take-up velocity and the fiber diameter, respectively. It is clear that the SC and HC

formations were dependent on the take-up velocity, hence on the fiber diameter. The peak area of SC increased and that of HC decreased with the decreasing fiber diameter. Tsuji et al.[10] reported that the orientation caused by high voltage or electrically induced high extensional force during electrospinning enhances the formation and growth of SC suppressing the formation of HC. In our study, an additional extensional force was given to the spinline by the rotating target. The fibers tended to have a higher molecular orientation and more promoted the SC formation with increasing take-up velocity. Promotion of SC formation and the reduction of the fiber diameter further reduced the residual space for HC.

3.3 Higher-order structure

3.3.1 Crystalline forms

Since the fibers obtained in this study were in an amorphous state, WAXD analyses were carried out for the fibers annealed at 150°C for 5 min keeping the fiber length constant. Fig. 3-6 shows the WAXD patterns and the equatorial spectra of the annealed fibers taken-up at various velocities.

Oriented PLLA fibers generally show strong equatorial reflections at a 2θ value around 17°, and 19°, identified as the α-form of PLLA crystallized in a pseudo-orthorhombic unit cell of dimensions a = 1.07 nm, b = 0.595 nm, and c = 2.78 nm, $\alpha = \beta = \gamma = 90^{o}$, which contains two 10_3 helices.[2] These two reflections are indexed as (110)/(200), and (203) of HC.[15] On the other hand, the oriented stereocomplex fibers show three equatorial reflections at 2θ values around 12°, 21°, and 24° for the PLA stereocomplex crystallized in a triclinic unit cell of dimensions a = 0.916 nm, b = 0.916 nm, c = 0.870 nm, $\alpha = 109.2^{o}$, $\beta = 109.2^{o}$, and $\gamma = 109.8^{o}$, in which L-lactide and D-lactide segments are packed parallel taking a 3_1 helical conformation.[3] These three reflections are indexed as (100)/(010)/(-110), (110)/(-120)/(-210), and (200)/(020)/(-220) of SC.[3,16]

The fibers collected on the fixed target show a ring-like reflection of HC at 2θ = 16.7^{o} and also ring-like reflections of SC at 2θ = 11.8^{o}, 20.5^{o}, and 23.8^{o}. The fibers obtained on the target rotating at 100 m/min showed arc-like reflections of HC at 16.7^{o}, and 19° while those of SC were still ring-like suggesting the HC has much higher crystalline orientation than SC. The reflections of HC changed from being arc-like to spot-like and reduced their intensity with increasing take-up velocity. The reflection of HC almost disappeared when the fiber was taken-up at 1,130 m/min. Figs. 3-7(a) and (b) show the equatorial WAXD spectra of the as-spun and annealed fibers taken-up at various velocities, respectively. When the fibers were

collected on a fixed target and on a target rotating at a velocity lower than 300 m/min, the fibers are amorphous. However when the fibers were taken-up at velocities higher than 600 m/min, a very broad peak appears at $2\theta = 17^{o}$. Masaki et al.[8] speculated that this broad peak is from a smectic structure which can be considered as a pre-structure of SC and this structure immediately transforms to SC upon annealing. Similar phenomenon was also reported by Hyun et al.[17] for the melt-spun fibers of the block copolymer of L- and D-lactic acids.

After annealing the fiber keeping its length constant, more clear crystalline structure was observed. The reflections from SC at $2\theta = 11.8^{o}$, 20.5^{o}, and 23.8^{o} gradually increase their intensity as the take-up velocity increased. However that of HC observed at $2\theta = 16.7^{o}$ once increased with the take-up velocity and then decreased at higher velocities. Similar results have been reported by Takasaki et al.[6] for the high-speed spun PLLA/PDLA blend fibers. They observed that the formation of SC was promoted with the increase in the take-up velocity suppressing the formation of HC in the fiber. On the other hand, the reflections of SC changed from being ring-like to arc-like with increasing take-up velocity.

3.3.2 Crystalline Orientation

Figs. 3-8(a) and (b) show the c-axis orientation factor of the fibers as functions of the take-up velocity and the fiber diameter, respectively. The fibers collected at lower take-up velocities were manually aligned. Unfortunately, the fibers on the fixed target were completely randomly accumulated so that the determination of the orientation factor was not possible. The reflection of HC at 2θ around 19° indexed as (203) was not observed from the fibers taken-up at the velocity higher than 600 m/min and the orientation factor of HC could not be calculated. It should be noted that the orientation factor was determined form the reflections of HC and SC in the annealed fibers and reflects the orientation of the molecules which can be easily transformed into HC or SC.

The orientation factors of both SC and HC are almost zero when the fiber was collected on a fixed target and gradually increases with the increasing take-up velocity, hence with the decreasing fiber diameter. This result indicates that the stretching of the fiber only by the electro-static force did not give much molecular orientation. Similar results were observed for the electrospun PLLA/PDLA blend nanofibers from the solution.[8] However large increases in the orientation factor of HC and SC occurred after taking-up by the target rotating even at a low velocity. The orientation factor of HC was higher than SC comparing at a constant fiber diameter. Although the orientation factor of HC still showed an increasing tendency at a

higher take-up velocities, that of SC leveled off around f_c = 0.6 at the take-up velocity higher than 600 m/min.

Now the relation between the molecular and crystalline orientation and the extents of the SC and HC formations has to be examined. The peak areas of SC and HC determined by using the DSC are plotted against the orientation factor of each crystalline form as shown in Fig. 3-9. It is clear that the SC formation was promoted with the increase in the orientation factor of SC. On the other hand, the peak area of HC linearly decreased this the orientation factor of HC. The latter does not mean that the molecular orientation suppresses the formation of HC. As the take-up velocity increases, the formation of SC is promoted and the diameter of the fiber decreases. Both of these factors may reduce the space to form HC in the fiber.

The solution contains the equal amount of PLLA and PDLA chains. However the mixing state of these two chains may not be homogeneous at a molecular level. It is natural that there are some fluctuations of the content of each chain so that both HC of PLLA and PDLA and SC coexist in the fibers obtained on the fixed target. When the solution jet was stretched further by the rotating target, the molecular chains are more stretched and oriented to the fiber direction resulting in the promotion of the SC formation. Once the stereocomplexation occurs, the amorphous region surrounding the SC crystallites contains almost equal amount of PLLA and PDLA chains and this state further promote the SC formation. As the stereocomplexation takes place and the fiber diameter decreases, the space for the HC reduces and the formation of such crystal is suppressed.

4. Conclusion

The effect of the take-up velocity on the higher-order structure and the formations of SC and HC of the PLLA/PDLA blend melt-electrospun fibers were investigated. The fiber collected on the fixed target was amorphous and showed almost no molecular orientation to any particular directions indicating that the stretching of the fiber by the electrostatic force did not give much molecular orientation to the fiber. The fibers collected on the target rotating at low velocities were also amorphous. However the molecular orientation was given to the fiber even after taking-up at lower velocities.

The formation of the SC seems to be promoted by applying taking-up force. The increase in the take-up velocity resulted in the reduction of the diameter and the increase in the molecular orientation. On the other hand, the formation of the HC was suppressed by applying taking-up force. This may be due to the promotion of SC and the reduction of the

fiber diameter which result in the reduction of the space for HC as the take-up velocity increases.

References

1. Y. Ikada, K. Jamshidi, H. Tsuji, and S. H. Hyon, *Macromolecules*, **20**, 904 (1987).
2. P. De Santis and A. J. Kovac, *Biopolymer*, **6**, 299 (1968).
3. T. Okihara, M. Tsuji, A. Kawaguchi, K. Katayama, *Journal of Macromolecular Science: Physics*, **B30(1&2)**, 119 (1991).
4. H. Tsuji, S. -H. Hyon, Y. Ikada, *Macromolecules*, **24**, 5651 (1991).
5. H. Tsuji, Y. Ikada, *Macromolecules*, **26**, 6918 (1993).
6. M. Takasaki, H. Ito, T. Kikutani, *Journal of Macromolecular Science, Part B Physics*, **42**, 403 (2003).
7. J. Zhang, K. Tashiro, H. Tsuji, A. J. Domb, *Macromolecules*., **40**, 1049 (2007).
8. D. Masaki, Y. Fukui, K. Toyohara, M. Ikegame, B. Nagasaka, and H. Yamane, *Sen'i Gakkaishi*, **64**(8), 212 (2008).
9. H. Tsuji, Y. Ikada, S. -H. Hyon, Y. Kimura, T. Kitao, *Journal of Applied Polymer Science*, **51**, 337 (1994).
10. H. Tsuji, M. Nakano, M. Hashimoto, K. Takashima, S. Katsura, A. Mizuno, *Biomacromolecules*, **7**, 3316 (2006).
11. D. Ishii, T. H. Ying, A. Mahara, S. Murakami, T. Yamaoka, W. -K. Lee, T. Iwata, *Biomacromolecules*, **10**, 237 (2009).
12. O. Monticelli, M. Putti, L. Gardella, D. Cavallo, A. Basso, M. Prato, S. Nitti, *Macromolecules*, **47**, 4718 (2014).
13. M. Yamamoto, G. Nishikawa, A. M. Afifi, I. Wataoka, J.-C. Lee, H. Yamane, *American Journal of Macromolecular Science*, submitted.
14. G. Nishikawa, M. Yamamoto, H. Yamane, A. M. Afifi, J. -C. Lee, Y. Kawahara, M. Tsuji, *Sen'i Gakkaishi*, **69**, 118 (2013).
15. W. Hoogsteen, A. R. Postema, A. J. Pennings, G. ten Brinke, *Macromolecules*, **23**, 634 (1990).
16. D. Brizzolara, H. -H. Cantow, K. Diederichs, E. Keller, A. J. Domb, *Macromolecules*, **29**, 191 (1996).
17. J.-Y. Hyun, J.-C. Lee, H. Yamane, Y. Kimuya, The International Textile Conference 2013, Daegu, Korea (2013).

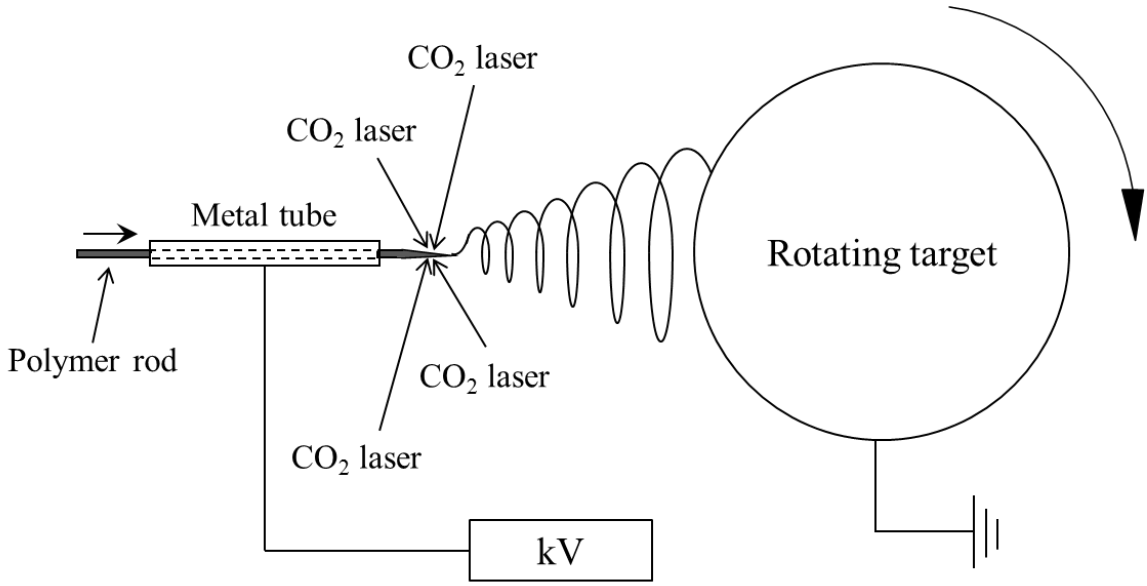

Fig. 3-1 Melt-electrospinning set-up used in this study.

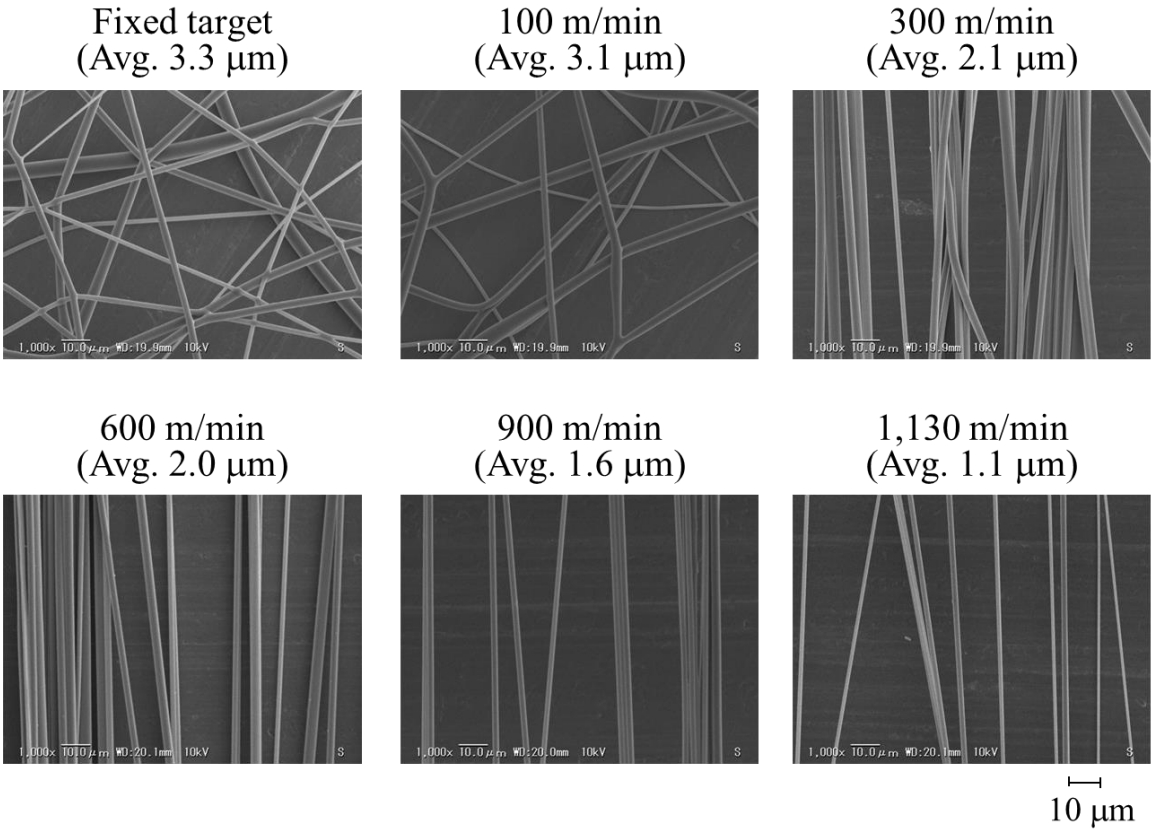

Fig. 3-2 SEM images of the fibers taken-up at various velocities.

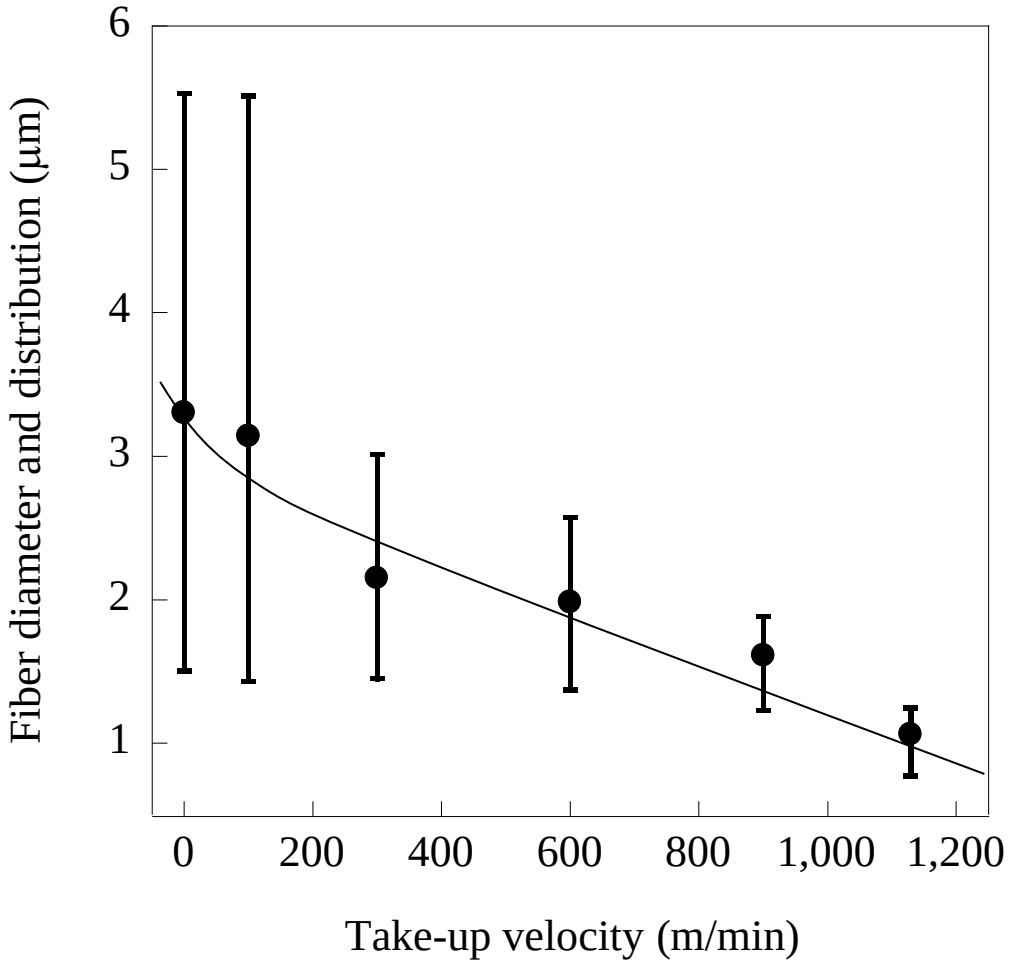

Fig. 3-3 Average fiber diameter and its distribution of the fibers taken-up at various velocities.

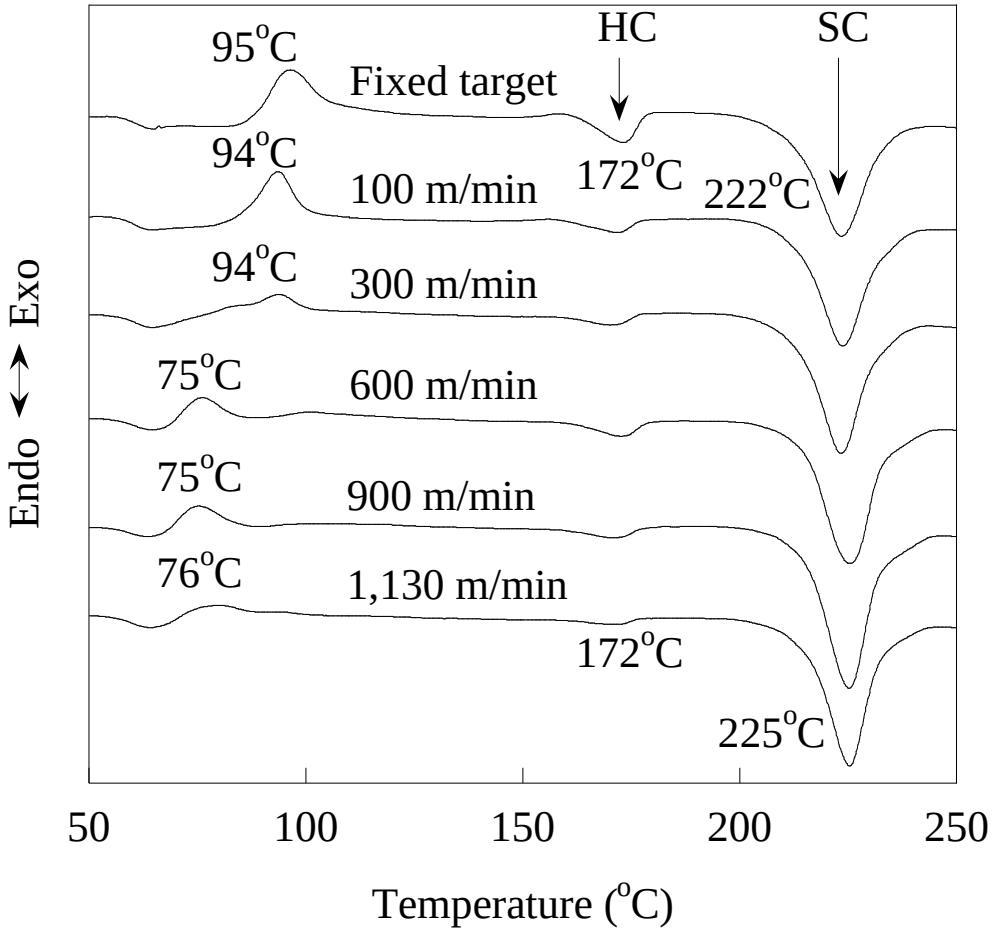

Fig. 3-4 DSC thermograms of the fibers taken-up at various velocities.

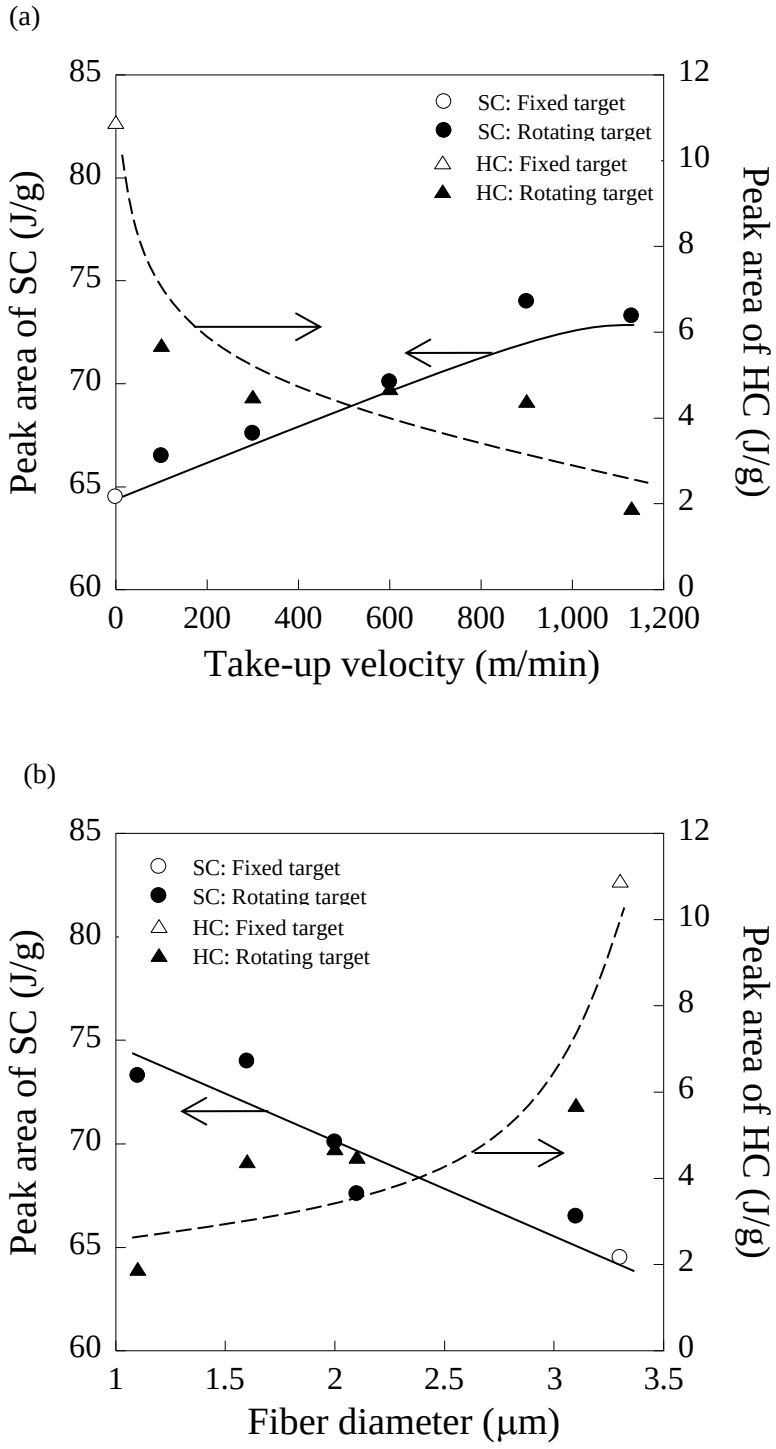

Fig. 3-5 Melting peak area of SC and HC as functions of (a) the take-up velocity and (b) the fiber diameter.

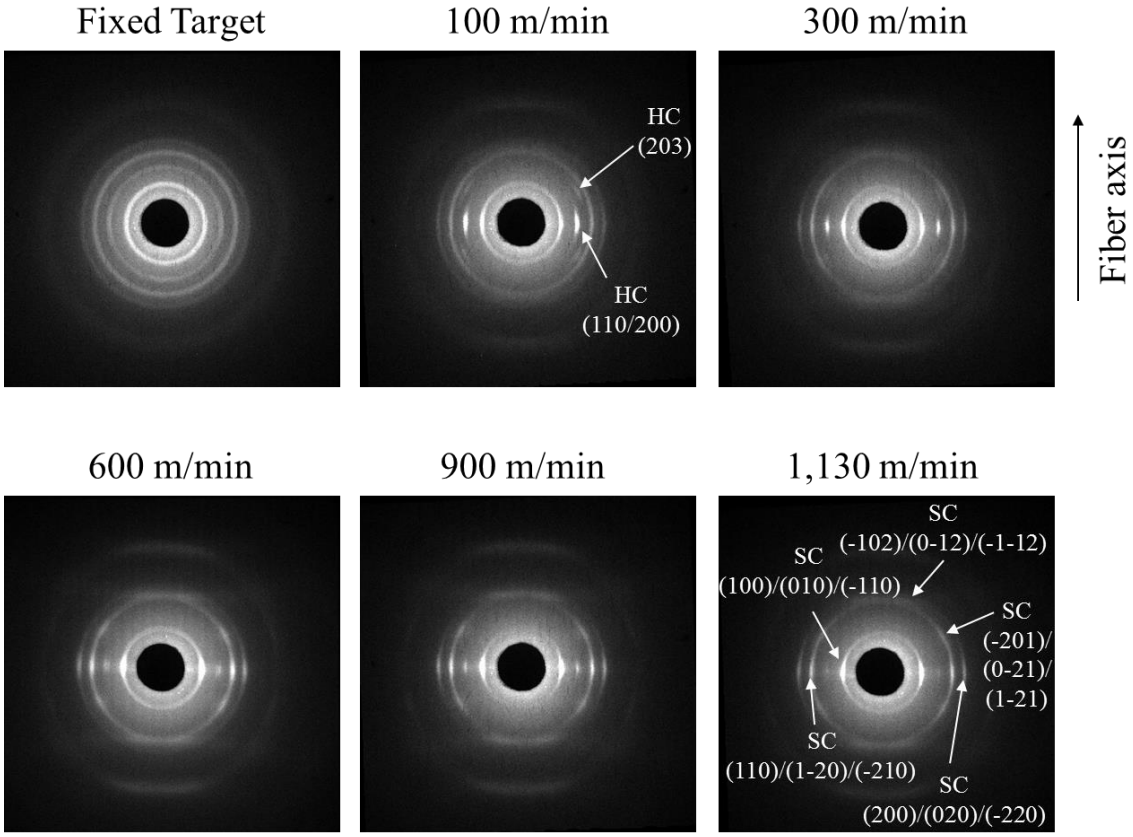

Fig. 3-6 WAXD patterns of the annealed fibers taken-up at various velocities.

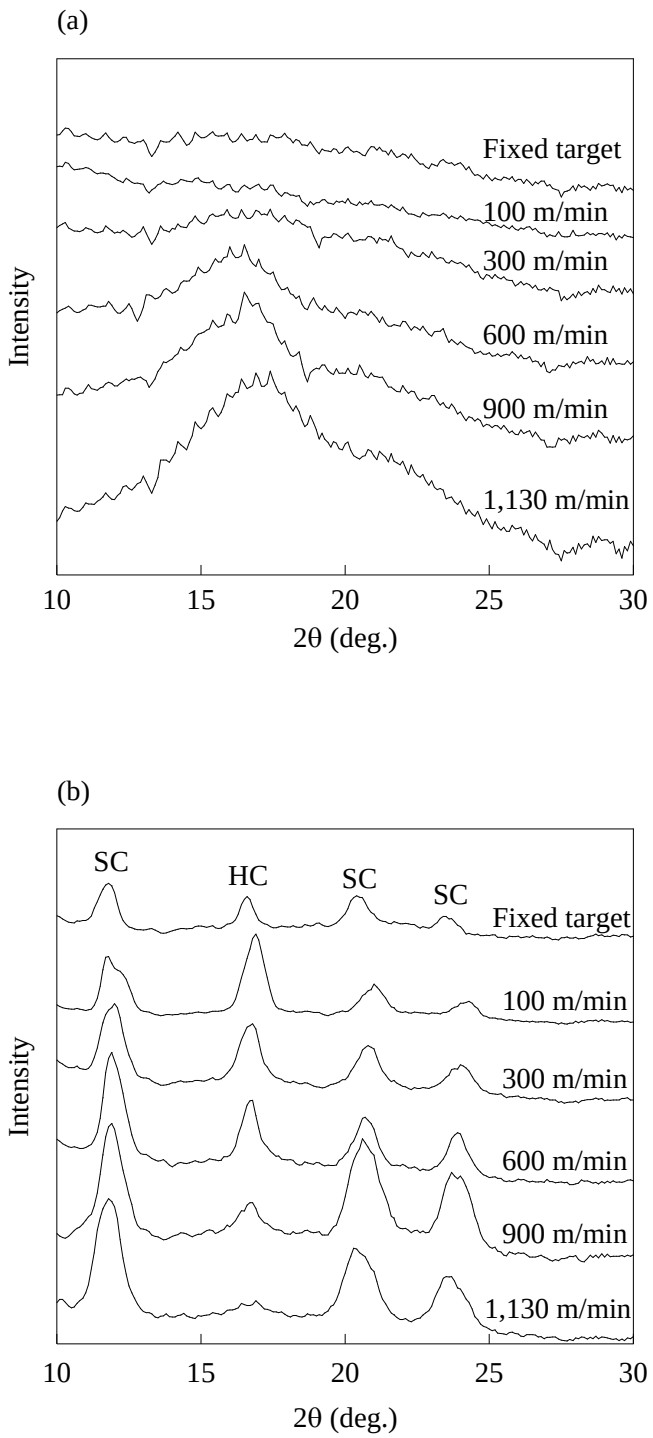

Fig. 3-7 Equatorial WAXD spectra of the as-spun (a) and annealed (b) fibers taken-up at various velocities.

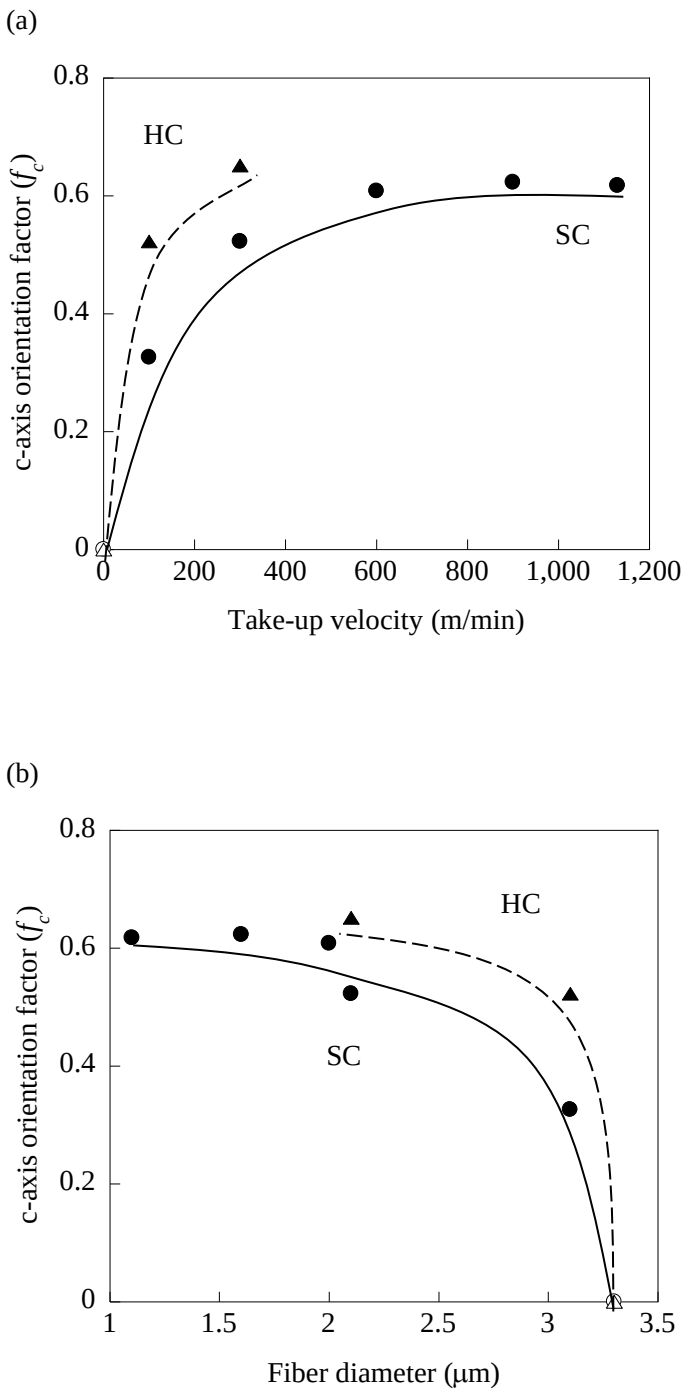

Fig. 3-8 C-axis orientation factor of the fibers as functions of (a) the take-up velocity and (b) the fiber diameter.

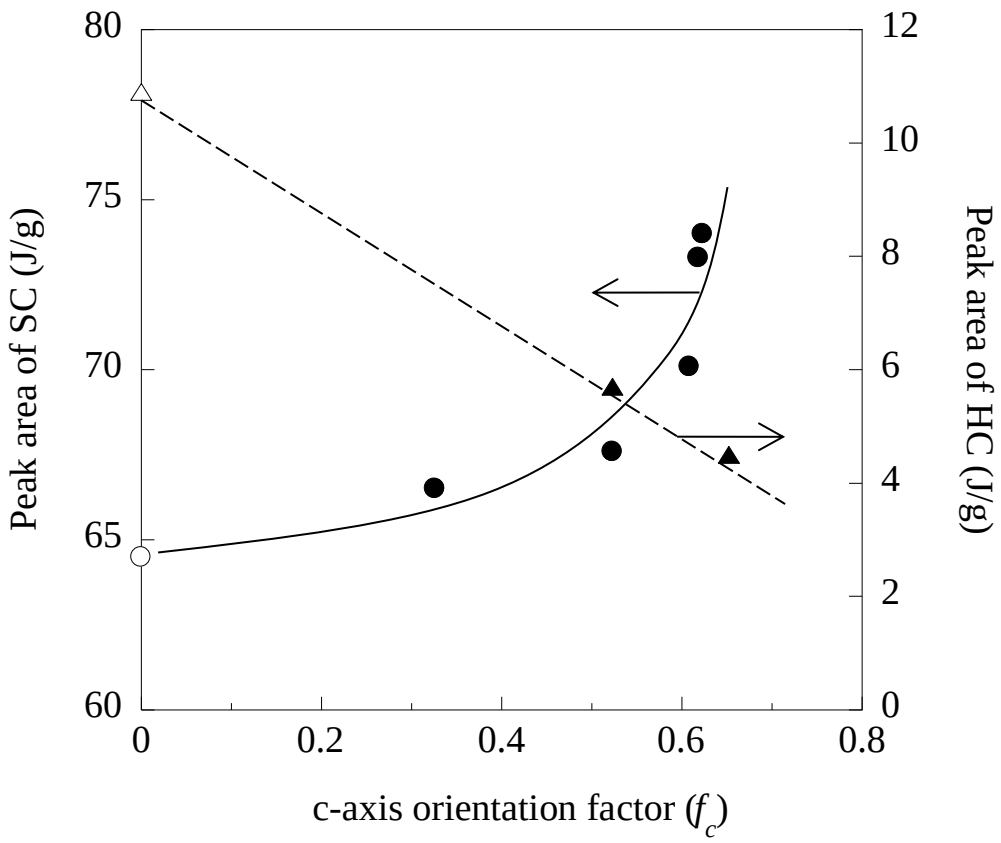

Fig. 3-9 Peak areas of SC and HC against the orientation factor of each crystalline form.

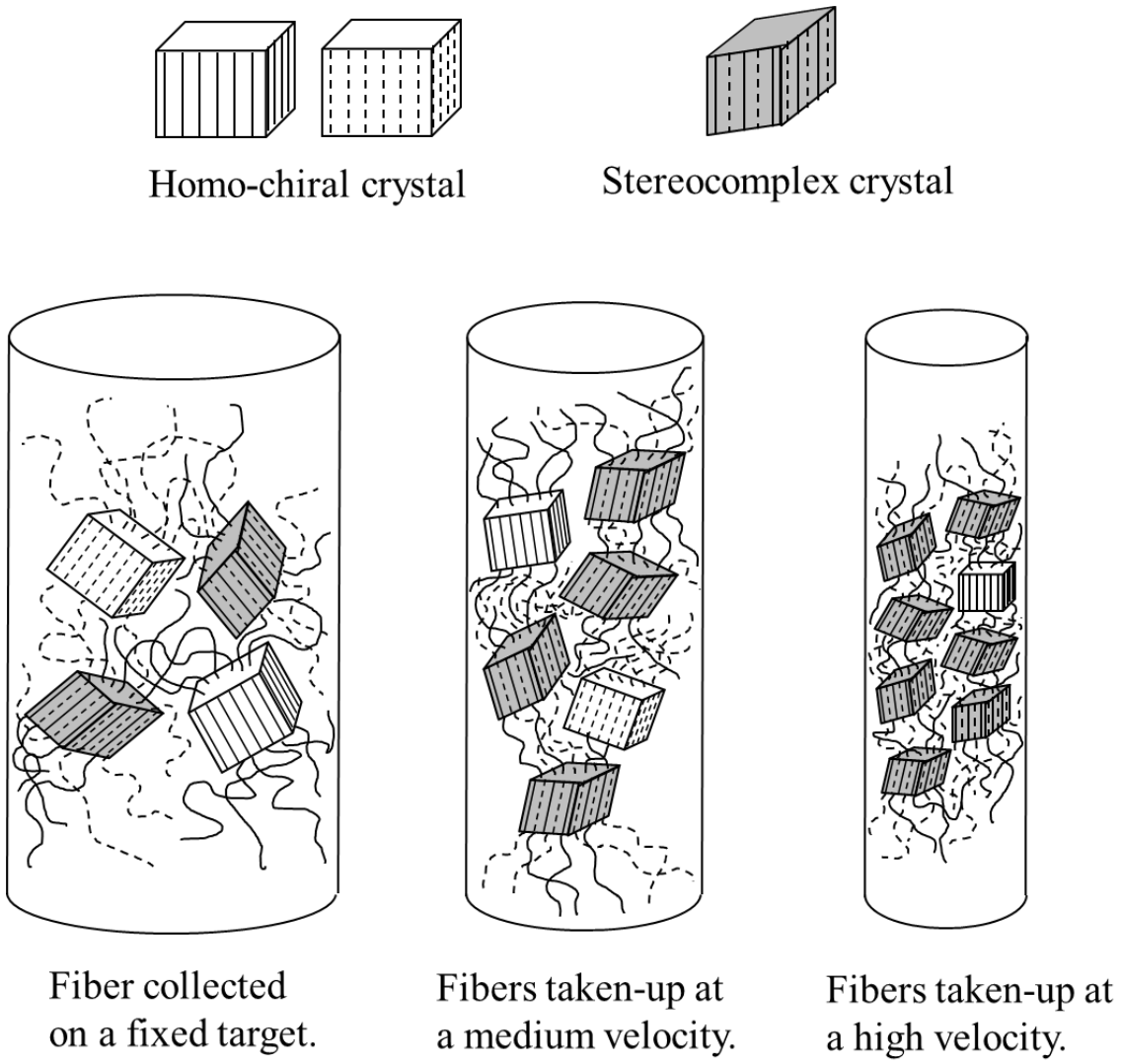

Fig. 3-10 Speculated mechanism of the promotion of the stereocomplexation.

SUMMARY

The higher-order structure and the formation of the stereocomplex crystal (SC) in poly(L-lactic acid) (PLLA) and poly(D-lactic acid) (PDLA) blend electrsospun nanofibers were investigated. Electrospinning was carried out by two methods, one the solution-type and the other the melt-type by using CO_2 laser heating. PLLA/PDLA blend nanofibers obtained by these electrospinning methods were collected on the fixed and the rotating targets. Results obtained in each chapter are summarized as follows.

In the chapter 1, the effects of the condition of the solution-type electrospinning on the higher-order structure and the SC formation of the PLLA/PDLA blend nanofibers were investigated. The fiber diameter decreased with increasing the applied voltage and the nozzle-target distance. In addition, the fiber diameter further decreased to as low as 100 nm with the take-up velocity. The solution jet launched from the solution extrudate was just carried to the target by the electrostatic force and the jet is not stretched between the nozzle and target. On the other hand, the solution jet was uniaxailly stretched by the mechanical taking-up force. These differences in the spinning mechanism reflect the molecular orientation in the nanofiber. The fibers obtained on a fixed target did not show a significant molecular orientation to the fiber direction, while those taken-up on a rotating target showed various degree of the molecular orientation depending on the take-up velocity. The formation of SC was promoted with the degree of orientation as well as with the decrease in the fiber diameter. As the take-up velocity increased, the fiber diameter significantly decreased to the size comparable to the crystal lamella thickness. In the small space of the nanofibers, only the stereocomplex can exist as a lamellar crystal decreasing its thickness due to its higher enthalpy of fusion. However the homo-chiral crystal (HC) was not able to grow and tended to disappear as the space in the nanofibers getting smaller. Another explanation may be possible. As the fiber diameter becomes extremely small, crystal has to reduce its size and hence the melting temperature may drop to lower than annealing temperature.

In the chapter 2, the structure of melt-electrospun PLLA/PDLA blend fibers was investigated. The blend of PLLA and PDLA were laser heated melt-electrospun into fibers with average diameters ranging from 3 ~ 6 μm. The average fiber diameter decreased and the diameter distribution got to be narrower with increasing laser output. The fibers obtained showed a coexistence of the oriented homo-chiral crystal and the unoriented SC and the amount of SC increased and that of HC decreased with increasing laser output. Although the

thick fiber showed the existence of unoriented SC, the existence of oriented SC and HC was observed in the thinner fibers. These results suggest that the molecular orientation of SC was significantly influenced by the fiber diameter as compared with that of HC.

In the chapter 3, the effects of the take-up velocity on the higher-order structure and the formations of SC and HC of the PLLA/PDLA blend melt-electrospun fibers were investigated. The fiber collected on the fixed target was amorphous and showed almost no molecular orientation to any particular directions indicating that the stretching of the fiber by the electrostatic force did not give much molecular orientation to the fiber. The fibers collected on the target rotating at low velocities were also amorphous. However the molecular orientation was given to the fiber even after taking-up at lower velocities. The formation of the SC seems to be promoted by applying taking-up force. The increase in the take-up velocity resulted in the reduction of the diameter and the increase in the molecular orientation. On the other hand, the formation of the HC was suppressed by applying taking-up force. This may be due to the promotion of SC and the reduction of the fiber diameter which result in the reduction of the space for HC as the take-up velocity increases.

This study can be summarized as follows.

The electrospinning is a process which consists of drawing thin jet from the polymeric liquid and carrying the jet to the metallic target by the electrostatic force. The jet of the polymeric liquid is not stretched in this process, so that the filaments obtained do not show any particular molecular orientation. However the application of the mechanical taking-up by the rotating target causes an extensional flow of the jet and the resultant filaments show an molecular orientation of various levels.

The formation of SC seems to be promoted by the stretching of the molecular chains. Although the similar effect of the molecular stretching on the formation of HC can be expected, the size of the nanofiber limits the formation of HC and HC tends to disappear when the fiber diameter becomes comparable with the lamella thickness.

List of publications

Chapter 1

"Effect of the electrospinning conditions on the higher-order structure and the stereocomplex formation of the PLLA/PDLA blend nanofibers"

Masaki Yamamoto, Goro Nishikawa, Amalina M. Afifi, Isao Wataoka, Jae-chang Lee, and Hideki Yamane

American Journal of Macromolecular Science, in press.

Chapter 2

"溶融エレクトロスピニング法により調製したポリ **L-**乳酸/ポリ **D-**乳酸ブレンド繊維の構造"

西川午郎、山本真揮、山根秀樹、Amalina M. Afifi、Jae-Chang Lee、河原 豊、辻 正樹

繊維学会誌第 69 巻第 6 号 118 頁～124 頁（2013 年）

Chapter 3

"Effect of the take-up velocity on the higher-order structure of the melt-electrospun PLLA/PDLA blend fibers"

Masaki Yamamoto, Goro Nishikawa, Amalina M. Afifi, Jae-chang Lee, and Hideki Yamane

Sen-i Gakkaishi, in press.

Other publications

"溶融エレクトロスピニング法により製造したポリ乳酸繊維の構造"

西川午郎、山本真揮、Amalina M. Afifi、河原　豊、山根秀樹

繊維学会誌第 66 巻第 5 号 124 頁～130 頁（2010 年）

"Electrospinning and Characterization of Aligned Nanofibers from Chitosan/Polyvinyl Alcohol Mixtures: Comparison of Several Target Devices Newly Designed"

Amalina M. Afifi, Masaki Yamamoto, Hideki Yamane, Yoshiharu Kimura, Ahmed El Salmawy, and Shigeyuki Nakano

Sen'i Gakkaishi, **67**(5), 103-108 (2011)

List of presentations

1. Masaki Yamamoto, Amalina M. Afifi, and Hideki Yamane,
   "Stereocomplexation in the electro-spun PLLA/PDLA blend nano-fibers",
   Kyoto International Symposium on Biodegradable and Biobased Polymers (KISBP 2012),
   Kyoto Institute of Technology, December 9-10, 2012.

2. 山本真揮, 西川午郎, Amalina M. Afifi, 山根秀樹
   "ポリ(L-乳酸)/ポリ(D-乳酸)ブレンドの電界紡糸とナノファイバーのステレオコンプレックス形成"
   第 62 回高分子討論会, 金沢大学, 2013 年 9 月 11 ~ 13 日.

3. 山本真揮, 西川午郎, Amalina M. Afifi, 山根秀樹
   "電界紡糸された PLLA/PDLA ブレンドナノファイバーの高次構造に与える引取速度の影響"
   平成 26 年度繊維学会年次大会, 東京・タワーホール船堀, 2014 年 6 月 11 ~ 13 日.

4. Masaki Yamamoto, Goro Nishikawa, Amalina M. Afifi, and Hideki Yamane,
   "Effect of the take-up velocity on the higher-order structure of the electro-spun PLLA/PDLA blend nanofibers"
   International Symposium on Fiber Science and Technology (ISF2014), Big Sight Tokyo Fashion Town Hall, September 28 to October 1, 2014.

5. Masaki Yamamoto, Goro Nishikawa, Amalina M. Afifi, and Hideki Yamane,
   "Effect of the take-up velocity on the higher-order structure of the electro-spun PLLA/PDLA blend nanofibers"
   Kyoto International Symposium on Neo Fiber Technology 2014 (Post Symposium of ISF2014), Kyoto Institute of Technology, October 2-3, 2014.

Acknowledgements

The author would like to express his deepest and sincere gratitude to his supervisor, Professor Hideki Yamane at the Department of Bio‐based Materials Science, Kyoto Institute of Technology (KIT), for giving him the opportunity to do his study under his supervision. His wide knowledge has been a great value to him. His continuous support, understanding, encouraging and guidance have kept him motivated to do good research and writing.

The author would also like to thank Professor Shinichi Sakurai and Dr. Isao Wataoka at the Department of Bio‐based Materials Science, KIT, for their kindly help and teaching on the nanostructure of polymer.

The author owes his gratitude to Dr. Amalina Muhammad Afifi and Dr. Goro Nishikawa who have also helped him in many ways. Their willingness to teach him many things about electrospinning and fiber technology has been a very great help.

The author would like to offer his special thanks to Professor Thomas Gries and Mr. Pavan Kumar Manvi at the Institut für Textiltechnik, RWTH Aachen University, Germany, for giving him the opportunity to study abroad and helping him many things.

The author is deeply grateful to Dr. Shinichi Yagi, who has also guided him throughout his research work. His comments are very valuable for him to improve his research skills and knowledge.

The author is indebted to all the students in Professor Yamane's lab, without their support and help in many ways his research works could not have been easier. The author also owes deepest thanks to all people in his family for their moral support and warm encouragement.

December 25, 2014

Masaki Yamamoto